Hurricane Wave Characteristics and Performance Characteristics of Platform Pile Foundations in the Bay of Campeche, Mexico

by

Zhaohui Jin

Hurricane Wave Characteristics and Performance Characteristics of Platform Pile Foundations in the Bay of Campeche, Mexico

by

Zhaohui Jin

and

Professor Robert G. Bea

Marine Technology and Management Group

Department of Civil and Environmental Engineering

University of California at Berkeley

May, 1999

TABLE OF CONTENTS

LIST OF FIGURES

LIST OF TABLES

Summary

Since 1897 when the first recorded offshore oil well was drilled from a wooden pier offshore California, the offshore hydrocarbon recovery operations have grown steadily to an incredibly large industry. Nowadays, there are more than 10,000 offshore platforms around the world in operations such as exploration, production, and storage of oil and natural gas.

However, from the point of view of engineering, the more than 100-year history and more than 10,000 design samples of platforms still can not form a sufficiently large design database similar to the one that naval architects have developed in their field. The lack of such a database determines that the engineering practice of platform design and manufacture is still case-specific to some extent. Even though we have some general guidelines such as API RP 2A (American Petroleum Institute Recommended Practice For Planning, Designing and Constructing Fixed Offshore Platforms), they are not universally applicable because each platform has its own unique location-specific environmental characteristics and case-specific operating requirements. Also, these kinds of guidelines are continually being updated while the oil industry accumulates more and more knowledge about offshore engineering practices. One major research effort to get such knowledge is the postmortem studies of the cases of failures, near misses, or survivals of platforms exposed to extreme environmental loading. This is the reason why oil companies, governments, and research organizations initiated extensive research studies

after the destructive Hurricane Andrew swept across the Gulf of Mexico in September 1992, where nearly 4,000 platforms are located.

In October 1995, Hurricane Roxanne formed in the western Caribbean Sea, crossed the Yucatan Peninsula, and entered the Bay of Campeche. Due to a southward moving front, the Roxanne did not follow the normal north-direction path of most hurricanes. It was forced back into the Bay of Campeche and the eastern coast of Mexico where it did considerable damage. Roxanne was the most severe hurricane to affect the Bay of Campeche during this century. It generated environmental conditions of wind, wave and current that approximated those of a 100-year return period hurricane, to which the major body of the fleet of exploration and production platforms and vessels belonging to PEMEX (PETRÓLEOS MEXICANOS) were exposed.

This incident provides an excellent opportunity for research of the environmental conditions and platform behaviors in the Bay of Campeche. Marine Technology and Management Group at University of California at Berkeley performed an extensive study for PEMEX to build a reliability-based design and re-qualification criteria of the offshore platforms in this area. This report summarizes a part of these research efforts, with emphases on the wave attenuation, and pile loading and capacities.

CHAPTER 1
INTRODUCTION

1.1 General Problem Definition and Background

In 1997-1998, an extensive study was performed for PEMEX to build a reliability-based design and re-qualification criteria of the offshore platforms in the Bay of Campeche, using Hurricane Roxanne as a study case. This region has some special characteristics with respect to geographic and oceanographic conditions. The major cause of these specialties is that layers of soft soils extensively and uniformly cover this region, unlike the relatively rigid sea bottom conditions in other areas in the Gulf of Mexico.

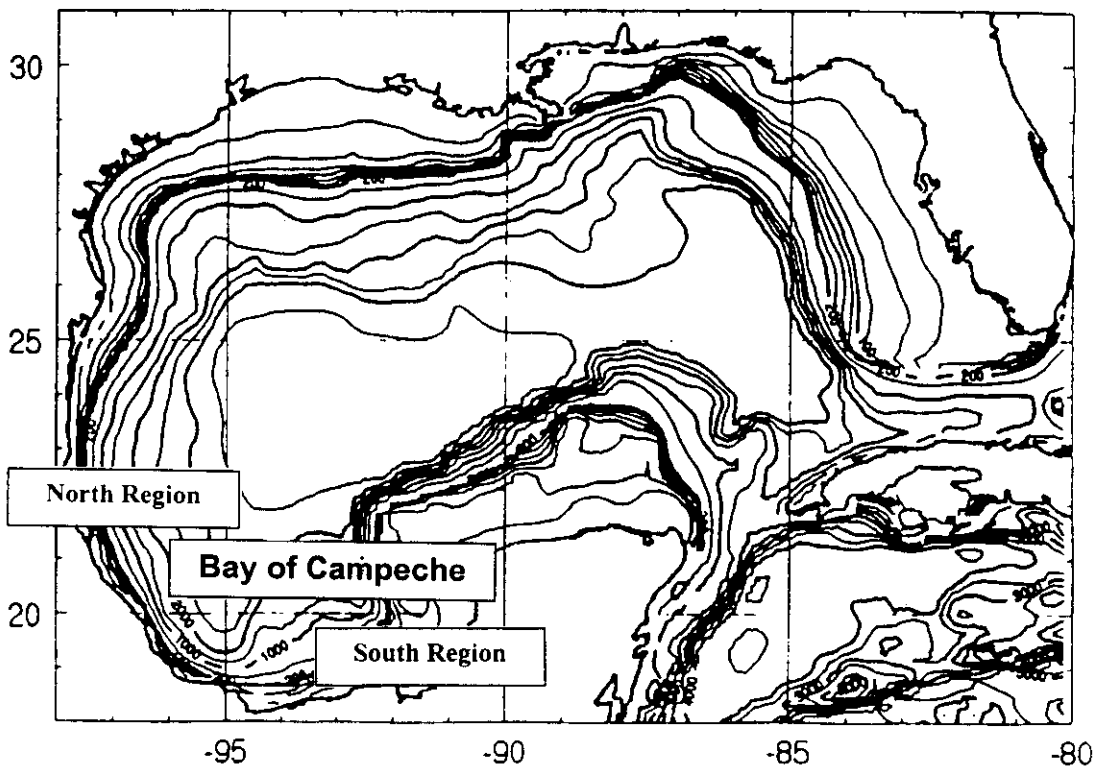

Figure 1.1 Bathymetry of the Bay of Campeche and Gulf of Mexico

This report focuses on the above specialties, its effects on hurricane wave heights and response of pile foundation to loading, and its implications on the reliability analyses of the offshore structures in this region. Figure 1.1 shows the bathymetry of the Bay of Campeche and the Gulf of Mexico, and the regions of concern in this study. Figure 1.2 shows the locations of platforms and pipelines in the Bay of Campeche. Figure 1.3 shows a typical pile-supported platform in this area.

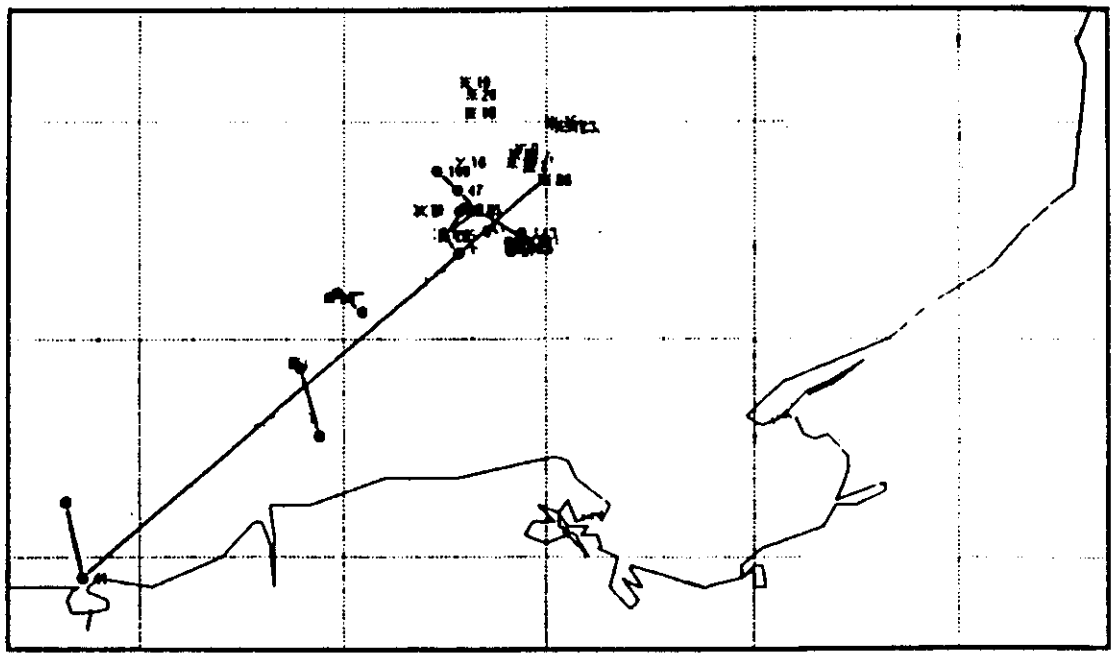

Figure 1.2 PEMEX platform and pipeline locations in Bay of Campeche (south region)

1.1.1 Wave Attenuation

There were several paradoxes in the information of Hurricane Roxanne furnisher by PEMEX. One was that the visual observation of the maximum wave heights during Hurricane Roxanne indicated that the observed wave heights were considerably lower than the hindcasted results obtained by the advanced ocean wave hindcast models

(Oceanweather, 1996). Another paradox was the reported damage to the lower deck portions of some platforms in the Bay of Campeche during Roxanne. The damage to light structures that extended below the platform cellar deck levels was sporadic. Examination of the photographs of this damage and photographs taken during the peak of the hurricane indicates that the damage was likely produced by the crests of highly directionally spread waves interacting with the very light sub-cellar structures that were in this area. There is no evidence of the crests of very forceful waves interacting with the lower deck portions of the platforms in the Bay of Campeche during hurricane Roxanne.

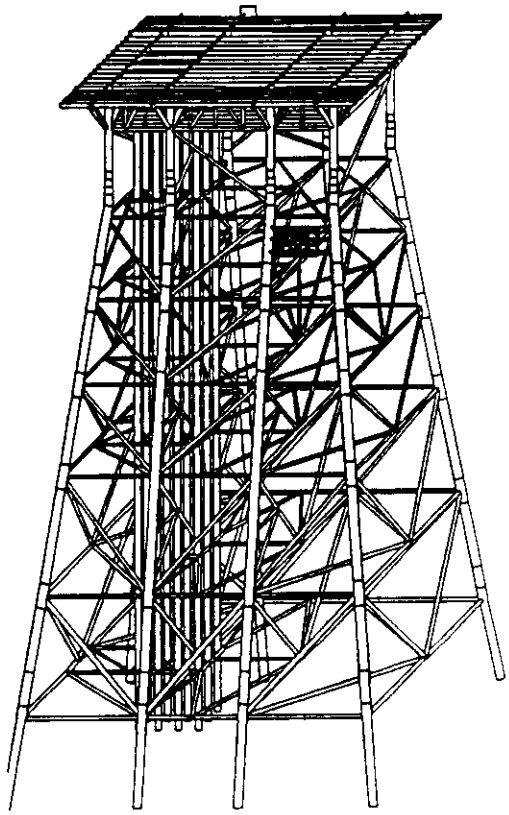

Figure 1.3 Typical pile-supported platforms in Bay of Campeche

These paradoxes were ultimately traced to the interactions of the hurricane waves with the soft sediments at the sea bottom. Simplified analysis (Bea, 1997) indicated there was substantial wave attenuation due to sea wave-soft bottom interaction in the Bay of Campeche. Figure 1.4 shows the differences between the hindcast and the observed data of wave heights. It also shows the possible correction to the wave height prediction, considering the effects of soft sea bottom. Given this background, detailed research was conducted to study the phenomenon of wave-sea bottom interaction. The meteorological and oceanographic conditions were developed to include the wave-sea bottom interactions for the risk based design and re-qualification criteria for offshore platforms in the Bay of Campeche.

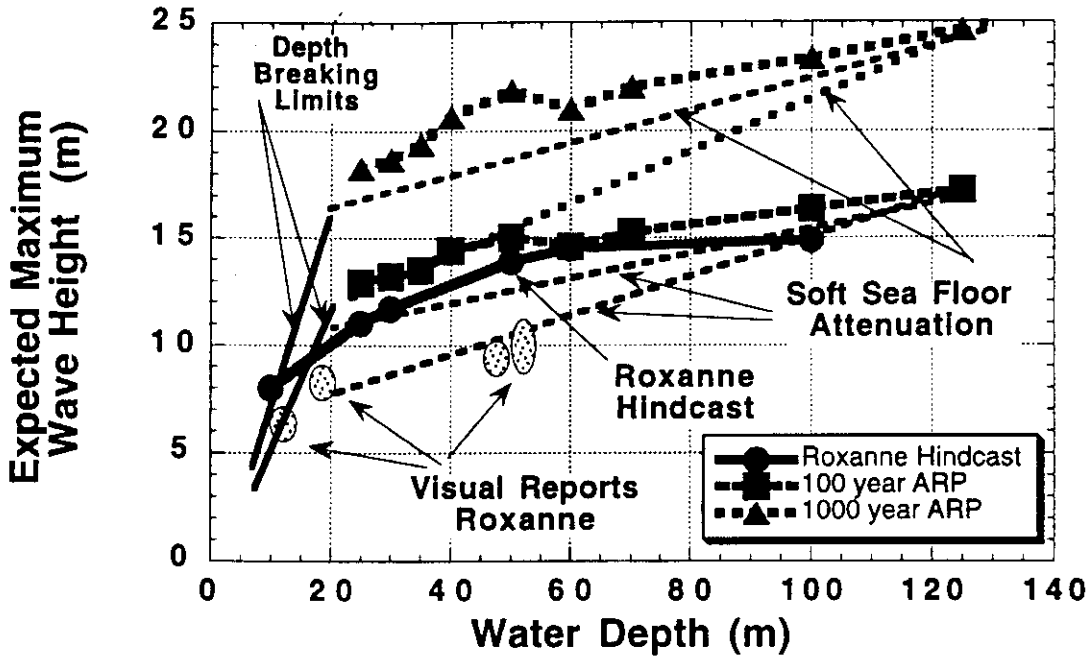

Figure 1.4 Different data of expected maximum wave heights at various water depths

The design of offshore platform systems in soft cohesive soils, subjected to large ocean waves has historically presented engineers with difficult challenges and at times harsh lessons. This soft, deformable sea bottom introduces a coupling interaction between incoming waves and sea bottom soils. This interaction has two effects: larger wave height decay at sea surface and large movement of the sea bottom. This phenomenon leads to lower wave loading on jacket and deck, and increased soil loading on piles and pipelines.

A large number of studies, both experimental and analytical, have confirmed this phenomenon. Experimental studies have shown that the loss of wave energy to the movement of mud can be quite large and can be the dominant factor in controlling wave heights in coastal waters, especially during storm conditions (Tubman and Suhayda, 1976; Forristall, Reece, Thro, Doyle, and Hamilton, 1980). Foristall conducted a classical experimental research program (SWAMP) in Mississippi Delta in 1979-1980. During the Hurricane Frederic (1979), a significant wave height of 28.2ft was observed in deep water (water depth = 1025ft), while near shore, a significant wave height of only 8.0 feet was observed in shallow water (water depth = 63 feet). Conventional wave height forecasting, which assume rigid sea bottom condition, indicated much less wave height decay than was observed. Also, the experimental measurement presented another important aspect in the sea wave-bottom interaction - directionality of the wave propagation. SWAMP measurements during Hurricane Allen produced different results than during Hurricane Frederic. The deep-water wave height was 12.9 feet in deep water while the shallow water wave height was surprisingly 9.3 feet. Although this difference in wave height decay may be due to different intensity of these hurricanes, study showed

that Frederic's path is along the highly disturbed soft soils, while Allen's path is mainly along stiff soils. This accounts for the difference between the two hurricanes. This directionality is important and will be addressed later. Figure 1.5 shows the wave attenuation phenomenon measured in the field. (Forristall, 1980). It shows measured energy spectra in deep and shallow water with respect to wave frequency. The maximum wave height is a function of the area under these spectra. The rigid (normal) attenuation for the wave components is also shown. It is obvious that the soft sea floor soils had a dramatic effect in reducing the wave amplitudes and energy.

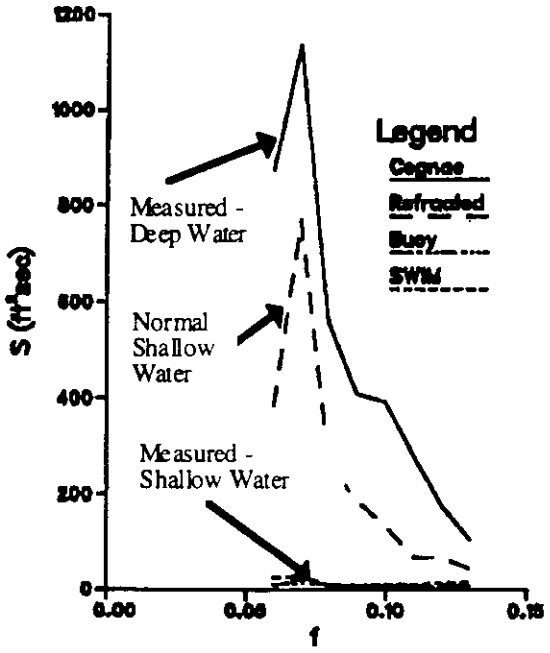

Figure 1.5 Measure wave attenuation of waves from deep to shall water in Mississippi Delta

A large number of sophisticated analytical models have also been developed to assist in the evaluation of the response of seafloor to wave loading. These models fall into three

general classes: (1) limit equilibrium, (2) finite element, (3) layered continua. All these models can correctly predict the wave attenuation and mud movement if the in situ soil characteristics, wave properties, wave traveling paths, and sea floor bathymetric conditions are interpreted properly as the inputs to these models. (Schapery and Dunlap, 1976, 1978; McClelland Engineers Inc., 1978; Wright 1976, 1983; Yamamoto, 1981; Farristall and Doule, 1987; Kraft and Suhayda, 1985, 1990; Hooper, 1994). Figure 1.6 shows the wave spectra in deep and shallow water assessed by Exxon for design of platform facilities in the Mississippi Delta (Clukey, et al, 1990). The significant wave attenuation due to soft sea floor soils was taken into account in the design of these facilities.

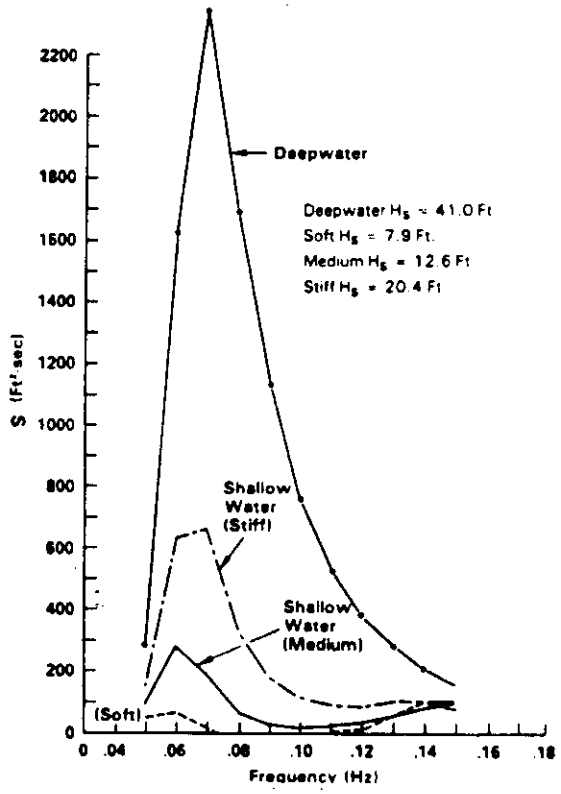

Figure 1.6 Exxon design wave spectra for deep and shallow water locations in Mississippi Delta

This complicated response of soft sea floor to storm waves is believed to be responsible for the puzzling behaviors of PEMEX platforms in the Bay of Campeche (Bea, 1997). During the Hurricane Roxanne (1996), which was nearly equivalent to a hurricane of 100-year return period and lasted for 7 days, there are no significant damages to these platforms but extensive failure of pipelines. As the first focus of this research and report, this wave attenuation problem was thoroughly investigated. The approach adopted was analytical, based on the computer program SWBI (Sea Wave Bottom Interaction) to simulate the wave attenuation and mud movement. The SWBI program adjusts the wave height prediction results in this area thus may greatly reduce wave loading on the platforms and warrantee the proposed modifications to the design and re-qualification criteria.

1.1.2 Dynamic Response of Pile Foundations to Loading

In the field of Offshore Engineering, foundation design is always an essential element for fixed platforms. In the Gulf of Mexico, most fixed platforms are pile-supported as are the PEMEX platforms. The response of the pile foundation of these platforms to the external loading, both dynamic and static, is a classical subject for offshore engineers. With the extension of offshore operations into deeper water and more hostile environments, concerns with implications of foundation design on overall platform costs, and the need to incorporate more realistic foundation response characterizations into the re-qualification analyses of existing structures have brought a recent focus to the dynamic response of marine foundations. The general engineering guidelines for treatment of such

problems are still under development. High quality experimental and analytical research needs are highlighted.

Almost all the fixed platforms of the PEMEX in the Bay of Campeche, Mexico are supported by piles. Pile foundations of these platforms are the key components for the whole drilling and production systems, which determine the safety, serviceability, durability and compatibility of such systems. It is desired that the pile foundations be designed in a safe and economic manner. Building up proper design criteria and keeping them up to date is an essential and important challenge for engineers.

The second focus of this report is on the dynamic response of platform foundation piles. As stated above, Bay of Campeche presents special geotechnic conditions. This region is uniformly covered with a layer of soft clays having a thickness of 25m to 30m and sea floor strengths in the range of 50 pounds per square foot to 100 pounds per square foot (Bea, 1997). Besides causing wave attenuation, there is increased loading on piles and pipelines. The soft soils may also experience notable cyclic degrading or load rate effects. Very complicated interaction takes place between platforms' pile foundation and the supporting soils. This is particularly the case for dynamic responses. This is due to the non-linearity of soil material, degradation of soil under cyclic loading, viscous and hysteretic damping of soils, etc. Although under intensive study for decades, a lot of unknowns remain concerning these soil behaviors. Both state of art and state of practice techniques in this field are basically founded on a semi-empirical approach. This warrants

a special investigation of pile foundation, on which the risk-based design and re-qualification criteria were based.

This report follows the similar approach. The response of pile foundation to loading is analytically simulated by numerical tools. The computer programs SPASM, TOPCAT/ULSLEA, and Drain3D were used. The input parameters such as soil strength profiles, degradation patterns, and soil resistance characteristics were based on laboratory tests, empirical formulae, and proper engineering judgment. The results of these provided important information about the biases and uncertainties associated with loading, ultimate limit state capacities of this key platform component.

1.2 Work Scope and Research Objectives

As an aftermath of Hurricane Roxxane, an extensive research project of Risk Based Criteria for Design and Re-qualification of Offshore Platforms for PEMEX and IMP was initiated in June 1997. This report covers two parts of this research project: the hurricane criteria with emphasis on wave attenuation and dynamic pile response.

The research work on wave attenuation includes:

- Study of bathymetric characteristics in the Bay of Campeche, including the determination of different wave travel paths from deep water to shallow water;
- Collection and study of the geotechnic information, including soil boring data, soil non-linearity, soil cyclic degradation properties;

- Collection and study of oceanographic data in the region, including observed wave height data in field, wave height hindcast of Roxxane, and long-term wave height prediction obtained by assuming rigid sea bottom;
- Modifying the general computer program SWBI (Sea Wave Bottom Interaction) for the purpose of analyzing the wave attenuation in the Bay of Campeche;
- Building analytical models of wave attenuation along different paths, under different soil conditions, and for the cases of hurricanes of different ARP's (average return periods);
- Running extensive sensitive analyses for calibration and verification

The research work on the topic of dynamic pile response includes:

- Study and determination of soil conditions and important parameters under different cases of static, cyclic and fast loading;
- Determining typical loading patterns representing hurricane wave loading and earthquake loading;
- Developing and modifying computer analysis tools such as SPASM, Drain3D and TOPCAT for the special analysis dynamic response of laterally or axially loaded platform piles;
- With the support of the above computer analysis codes, building analytical models to simulate the dynamic response of the piles in field under different loading patterns, that are capable of handling both the nonlinear piles and nonlinear-hysteretic soil resistance;

- With the models developed, performing analysis of the behaviors of pile-soil system beyond the elastic range up to final collapse to find the system's ultimate capacities;
- Comparing and calibrating the analysis results to define the unique characteristics of pile foundation behaviors in the Bay of Campeche

The objectives of the above research works are to provide essential information on which the development and verification of the risk-based hurricane and earthquake criteria and guidelines for the platforms of PEMEX in the Bay of Campeche could be based. This essential information includes the biases and uncertainties of environmental loading and ultimate capacities of platforms, which are applied in the reliability analysis.

The wave attenuation study improved the understanding of the special wave decay patterns in the area. The study builds an applicable model quantifying how the soft sea bottom soils influence hurricane wave heights as the waves propagate across the continental shelf. The results indicate considerable correction to the maximum wave heights used in the reliability analysis that is the basis of the design and re-qualification criteria. The results also have important implications on the adoption of a truncated wave height spectrum in the long-term reliability analysis.

The study of dynamic response of pile foundation improved the understanding of the behaviors of the pile-soil system in the Bay of Campeche. The correlation of the results from different analytical models of the piles under different loading patterns provided

essential analysis parameters of biases and uncertainties in the reliability analysis of the platform foundations.

1.3 Organization of the Report

This report is divided into 5 chapters. Following a summary, chapter 1 is an introduction of the problem definition, research background, work scope and research objectives.

Chapter 2 focuses on the topic of special wave decay patterns in the Bay of Campeche. First the chapter gives an account of the mechanism of the wave attenuation phenomenon. Then it describes the basic approach of the wave height prediction tool – SWBI, the analysis models and SWBI program. Chapter 2 also explains the process of building a wave attenuation analysis model, putting the soil profiles, bathymatric information and oceanographic data all together. Chapter 2 has a detailed summary of the analysis results along different wave propagating paths, under different soil conditions.

Chapter 3 first gives a review of the current research of the topic of pile response to dynamic loads. Then the chapter describes the basic assumptions and approaches in the study. It details the building-up process of the analysis models in the research, with an emphasis on the new DRAIN3D numerical model. Then, it talks about the lateral response of a single pile, including the first yielding capacity, ultimate capacity. The analysis address pile-soil systems behaviors under static loading, cyclic loading and fast loading. The lateral responses are predicted by SPASM, DRAIN3D, ULSLEA3.0 and TOPCAT. Following this, another section summarizes the analysis of the axial response

of a single pile. The basic approach is the same as lateral response. The behaviors under static, fast and cyclic loading are studied. The calculating code is DRAIN3D and TOPCAT. A calculation is also performed according to the API RP2A guideline.

Chapter 2

Analyses of Hurricane Wave Decay Characteristics

2.1 Analysis Model: SWBI

The Bay of Campeche is uniformly covered with a layer of soft clays having a thickness of 25m to 30m and sea floor strengths in the range of 50 pounds per square foot to 100 pounds per square foot (Bea, 1997). Interactions of this soft clay layer with the surface storms could have reduced wave heights by 10% in a travel distance of 2,000 feet to 5,000 feet depending on the water depths, wave heights and periods. An analysis tool was needed to quantifying this interaction.

2.1.1 Basic Approach of SWBI

There are basically two approaches to analyze the sea-bottom-wave-interaction effects: experimental and analytical. Both have provided a lot of important information, interpretation and prediction of this complicated phenomenon. To address the wave height decay patterns in the Bay of Campeche, this report takes an analytical approach; using a computer program to forecast the wave height decay. The analysis model is SWBI (sea wave bottom interactions). SWBI is a modification of the identical computer program WASBIN developed by Schapery and Dunlap (1978) of Texas A&M University. This program has been under continuing development since the 1970's.

Wave height in coastal areas with normal sea bottom sediments is affected by processes such as diffraction, refraction, reflection, shoaling, wind generation, and bottom friction. Usually, these factors account for the major parts of wave height decay for normal rigid sea bottom soil. For soft sea bottom, the energy absorption by the movement of soft sea bottom sediments is another notable factor. So, as a complete shallow-water wave height forecasting tool considering the soft sea bottom effect, the general stepwise wave forecasting formula for a discrete analysis model is:

$$H_{n+1} = H_n \bullet K_s \bullet K_f \bullet K_r \bullet K_d \bullet K_{re} \bullet K_w \bullet K_m \qquad 2.1$$

Where, n represents the (n)th wave height forecasting station along the wave propagating path; H_{n+1} is the forecasted wave height at the ($n+1$)th station; H_n is the wave height at the (n)th station; K_s is the wave attenuation coefficient for shoaling; K_f is the attenuation coefficient for bottom friction; K_r is the coefficient for refraction; K_d is the coefficient for diffraction; K_{re} is the coefficient for reflection; K_w is the coefficient for wind generation effect; K_m is the coefficient for energy absorption of the soft sea bottom soils.

To simplify the analysis, two attenuation coefficients are introduced:

- K_m is introduced to account for the effects due to soft soil bottom only, and
- K_{rb} is developed to include all other effects, which can be solved by the normal rigid bottom wave prediction method, such as the computer model used by Oceanweather Inc. (1996a, b, c).

Therefore, the wave height forecasting formula becomes:

$$H_{n+1} = H_n \bullet K_{rb} \bullet K_m \qquad 2.2$$

K_m resulted from soft-bottom effects depends on the absolute wave height at a site; the wave period; and the shear resistance, shear modulus and damping properties of the soils. This stepwise formula is used in the discrete SWBI wave height forecast model.

2.1.2 SWBI Model

The SWBI analytical model couples the wave and sea bottom interactions. It takes water as an inviscous, incompressible fluid. Linear wave theory is applied in the model. The soil is assumed to be a layered, incompressible, visco-elastic material. The nonlinear response of the soil is accounted for by a hyperbolic stress-strain relationship. A linear dynamic theory is used through an interaction technique to solve the non-linear response of the soils.

The SWBI analysis is an iterative procedure, in which the secant modulus of the soil stress-strain curve is solved based on the computed stress condition and compared with the tolerance requirement. These stress conditions are determined by the secant modulus of the soil stress-strain curve in the previous analysis. Therefore, the complex sea-bottom interaction problem is reduced to an elastic analysis of a layered half-space in every iteration. Schapely and Dunlap detailed the analytical model (1978). The algorithm to solve this elastic-viscous problem of wave-sea bottom interaction is the linear dynamic

theory developed by Biot (1965). This program has been under constant update since the 1970's and has been verified extensively with field data (Schapery and Dunlap, 1976,1978; Kraft et al, 1985, 1990; Suhayda 1994, 1997).

The sea bottom soils are represented in the SWBI model as visco-elastic materials. The mechanics behavior of these materials can be represented by a complex shear modulus, G^*, which consists of a real part, G', and an imaginary part, G''. The shear modulus is thus expressed as:

$$G^* = G' + iG'' \qquad 2.3$$

The phase angle, θ, between the stress and the strain is given by:

$$\theta = \tan^{-1}(G''/G') \qquad 2.4$$

The relationship between the amplitudes of the shear stress and the shear strain is given by:

$$|\tau| = |G|\,|\gamma| \qquad 2.5$$

where τ is the shear stress, γ is the shear strain and,

$$|G| = [(G')^2 + (G'')^2]^{1/2} \qquad 2.6$$

The soils shear modulus is described with a power law relationship:

$$G(t) = G_1 t^{-n} \qquad 2.7$$

Where G_1 is the shear modulus corresponding to time t=1 sec and n is a constant reflecting the sensitivity of the soils to the strain rate effects. Laboratory tests were conducted to measure G_1 and n, and to correlate these parameters with routine available geotechnic variables such as shear strength and liquidity index.

If the soils are very soft, i.e., a small shear modulus G, notable stress and strain of soils may be resulted under external stress. The soils behavior more like liquid than like solid. For the case in the Bay of Campeche, the soft visco-elastic soils interact with the inviscous-incompressible water as hurricane waves travel from deep water to shallow water. There is a coupling of movement between the water and the viscous soils due to the varying water pressure produced by waves on the sea bottom. Large stress and strain are induced in the viscous soils. A large portion of wave energy is dissipated into this induced soil movement. This water wave energy loss can be figured out by summing the energy of the soil "waves" under the mud line. The energy of the soil movements can be easily obtained by integration over the soil "wave" field using the above stress-strain and shear modulus relationships. This soil movement adds the seventh factor into the wave height prediction model, the parameter K_m in Equation 2.1.

SWBI program quantifies the parameter K_m. This sea bottom wave attenuation coefficient is defined by:

$$K_m = \exp\left(\frac{-3.14 \cdot X \cdot M_s \cdot \sin\phi \cdot C_p^2}{T \cdot C_g}\right) \qquad 2.8$$

Where M_s is a bottom movement parameter, X is the horizontal distance, ϕ is the phase angle between the surface wave and the sea bottom soil wave, C_p is the bottom pressure coefficient, T is the wave period and C_g is the wave component group speed.

The sea bottom pressure coefficient is based on a modified linear wave theory formula given by:

$$C_p = \frac{0.84 + (h/L_0)^2}{\cosh(6.28 \cdot h/L)} \qquad 2.9$$

Where L_0 is the deepwater wavelength and L is the wavelength at the water depth h.

The sea bottom soil movement parameter M_s and phase angle ϕ depend on the wavelength and the soil shear strength S_u, shear modulus G_s and the soil viscosity M_u. Formulas for M_s and ϕ are:

$$M_s = \frac{5.09 \cdot L \cdot T^2}{\sqrt{G_s^2 + (6.28 \cdot M_u)^2}} \qquad 2.10$$

$$\phi = \arctan(0.12 \cdot (1 + \frac{G_m \gamma}{S_u})\sqrt{h/L}) \qquad 2.11$$

Where G_m is the initial shear modulus, G_s is the shear modulus at a shear strain of γ. The values of G_m, G_s and M_u are given by:

$$G_m = R_a \cdot S_u \qquad 2.12$$

$$G_s = \frac{G_m}{1 + R_a \gamma} \qquad 2.13$$

$$M_u = \frac{G_s \cdot T}{6.28} \cdot 0.12 \cdot L_d \cdot (1 + R_a \gamma) \qquad 2.14$$

R_a is an empirical constant. It is determined by resonant column tests and has a range of 100 to 400. L_d is the liquidity index of soil. The shear strain γ is given by:

$$\gamma = \frac{T_w}{G_e} \qquad 2.15$$

Where T_w is the wave induced soil shear stress. G_e is the equivalent soil shear modulus. They can be determined by:

$$T_w = 6.28 \cdot P_a \cdot \frac{Z}{L} \cdot e^{\frac{-6.28 \cdot Z}{L}} \qquad 2.16$$

$$G_e = \sqrt{G_s^2 + (\frac{6.28 \cdot M_u}{T})^2} \qquad 2.17$$

Where P_a is the amplitude of the wave induced sea bottom pressure. Z is the distance below sea bottom line.

In SWBI program, the degree of soil non-linearity is modeled by the ratio of the secant modulus to the initial shear modulus, G / G_{max}. The secant shear modulus is determined using a hyperbolic stress-strain relationship to reflect the stress-strain behavior of the soils:

$$\tau = \frac{G_{max}\gamma}{1 + \frac{G_{max}}{S_u}\gamma} \qquad 2.18$$

where G_{max} is the initial shear modulus at zero strain; τ is the shear stress; γ is the shear strain; and S_u is the shear strength. The secant shear modulus G can be determined from the above equation:

$$\frac{G}{G_{max}} = 1 - \frac{\tau}{S_u} \qquad 2.19$$

The use of this secant modulus assumes that the maximum stress and strain values for cyclic loading coincide with the hyperbolic curve, which is representative of a single loading condition.

It is assumed that Equation 2.18 provides a reasonable approximation of the variation in the modulus with increasing stress up to initial soil failure. Cyclic degradation and strain effect, however, can result in moduli that differ from the linear variation suggested by Equation 2.9. In addition, actual soil response does not exactly follow a hyperbolic curve over the full stress level range. Therefore, using the hyperbolic relationship requires a varying initial shear modulus ratio Gmax/Su with increasing strain to keep the stress-strain curve correct.

The stress-strain behavior of soils is a complex phenomenon and most stress-strain behavior relationships provide only an approximate representation of the real soil behavior. Although the stress-strain model given by SWBI is not perfect, comparison of experimental and analysis results indicate that it is reasonable and can provide realistic estimation of the sea wave-bottom interaction if appropriate input parameters are used to describe the in situ soil characteristics. (Kraft, et al, 1985, Forristall and Reece, 1980, 1985).

It should be noted that the soil modulus (a secant modulus at a specified stress level) measured in the laboratory may be less than the in-situ modulus, due to sample disturbance caused by drilling, sampling, sample preservation, transportation, and specimen preparation, and due to higher temperatures of the laboratory specimen than in-situ conditions. On the other hand, higher rates of strain in the laboratory test experienced in situ can result in the laboratory-measured modulus being greater than the in situ values. All these incorporate a large amount of natural uncertainties into the analytical

model that should be carefully considered in the preparation of input data and interpretation of the output results.

On the other hand, cyclic loading from storm waves can result in lower moduli than those obtained from monotonic loading. The cyclic action of the waves can reduce the shear resistance and the modulus of the soils near the surface. This reduction can increase the wave degeneration, but the soil movement can also increase. Therefore, cyclic degradation to the soil properties is included in the wave attenuation analyses. Some parametric studies and expert judgements should be conducted to determine an appropriate shear modulus profile considering the cyclic degradation effects.

Besides the soil conditions, the soil response at a site is sensitive to both the period and height of the storm wave. The wave conditions shall be carefully reviewed to represent the field oceanographic environments loading. A calibration of hurricane Roxanne can provide reasonable environmental conditions. In this report, the oceanographic conditions are interpreted from the reports of Oceanweather Inc.

2.1.3 SWBI Program Operation

For each run of SWBI program, a wave transect is set up based on the sea floor bathymetry information. The transect consists of a proper number of distance intervals from deep water where the wave attenuation starts. Each interval is regarded as a uniform segment. The sizes of these intervals, more exactly the distance between two successive stations along the wave-propagating path, can be varied to properly reflect the nonlinear

behavior of coupling of sea waves and soil bottoms to ensure the numerical stability and accuracy.

The main input for the SWBI model contains oceanographic and geotechnic information along the specific wave transect. The oceanographic information includes deepwater wave period, wind speed, and wave height along the wave transects. The geotechnic information include the soil types along transect, varying water depth, average sea floor slope, and bottom friction drag coefficient.

Each interval along the wave transect is assigned a soil type, which is typically a soil input file contains the soil properties such as submerged unit weight, liquidity index, soil layer thickness, ratio of initial shear modulus to undrained shear strength, and shear strength for each vertical soil layer.

As described in the basic approach, the stepwise wave height forecasting calculation is performed in the SWBI to predict mud movement and wave heights from one station (n) to the next station ($n+1$) over the specific wave transect. The source code of the program is modified to incorporate the Oceanweather (1996a, b, c) rigid bottom wave forecasting into the specific wave attenuation analysis for the Bay of Campeche.

The output of SWBI is to emphasize the factors of interest in the wave attenuation forecasting procedure. It shows the stepwise wave height calculation results and the coefficient K_m at each station along the wave propagating transect. It also shows the ratio

of shear stress induced by wave loading to the shear strength, τ/S_u, at each soil layers in each wave propagating intervals. Because wave attenuation is quite sensitive to the shear stress level in the soil layers, these shear stress information is valuable to gradually modify the input soil files and main input files to get satisfied calculation accuracy and reduce calculation time and iteration number.

The output also gives a correction factor - R_m, which can be applied to the forecasted rigid bottom wave height to get the reasonable estimate of in situ wave height with the wave-soft bottom interaction effect. This is a key input parameter to the reliability analysis.

2.2 Development of Wave Attenuation Analysis Model

Wave attenuation analysis requires extensive data collection of oceanographic, bathymetric and geotechnic information, especially in a vast region such as Bay of Campeche. The PEMEX platforms are mainly located in two areas in the bay – North Region and South Region, which are illustrated in Figure 1.1. As stated before, the soil sea floor in the south region is very soft. The layers of soft clay are very thick. The situation in the north region is a little different. The sea floor there is overlain by a thin top layer of very soft clay followed by thick layers of relatively stiff clay. It is expected that the wave attenuation effects from soft sea bottom will be different in these regions. To quantify the sea-bottom interaction effects along the different wave propagating paths, SWBI models are built respectively for both regions. The input files and soil files for SWBI models contain all the location-specific information stated above for each region.

2.2.1 Bathymetric Information

2.2.1.1 General

Bathymetric characteristics have very important impacts on wave decay patterns along coastlines. PEMEX and IMP provided very useful bathymetric information of the Bay of Campeche. It covers the concerned regions of the bay where most PEMEX platforms are located. The wave propagating transects in SWBI model are built on the basis of this information. Figure 2.1 shows the bathymetry along the coastline in the north region.

The wave propagating path should be carefully studied in the wave attenuation analysis. The bathymetric characteristics greatly affect the shoaling effects along the path. The soil conditions over the path of wave travel determine the effects of the soft sea bottom wave attenuation. Also, as discussed above, directionality, i.e. the wave propagating path, is crucial to wave attenuation. The wave characteristics at a site are controlled by the soil conditions over the path of wave travel. Therefore, the regional soil conditions around the wave propagation paths are as important as the site condition to accurately forecast of wave height at a site.

Usually, there are many different ways to set up the wave propagating path in the area of interest. One is to set one path which is considered the most conservative one: the wave travel distance is shortest, and generalized least disturbed soil types are assumed along the path (Kraft and Suhayda, 1990; Clukey et al, 1988). It is appropriate for a study

concerning a special field site. However, it may be not sufficient to form a solid foundation for design and re-qualification criteria.

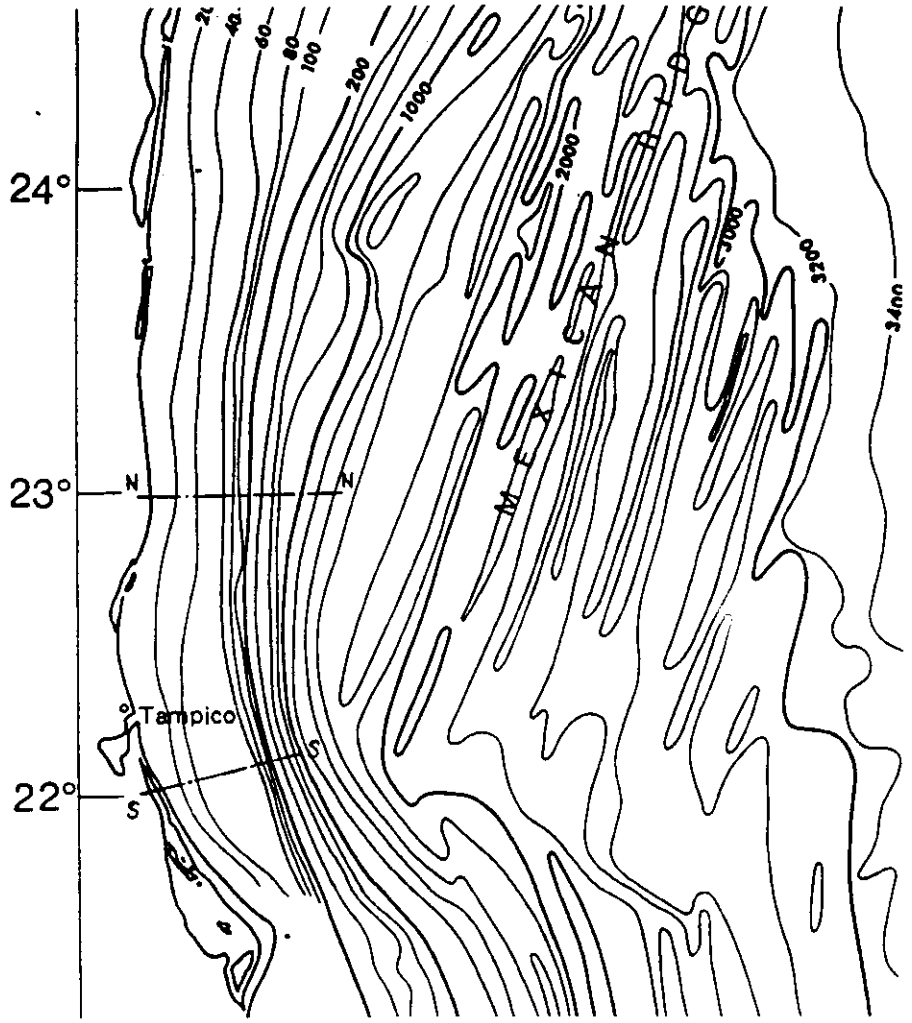

Figure 2.1 Bathymetry of the north region and the wave transects

2.2.1.2 South Region

In the analysis of south region, three wave propagating paths are considered extending from the north to the south: A-A transect, C-C transect and B-B transect (Figure 2.2-2.5).

the longest one. They were chosen also because they have quite different sea bottom slope. Compared with the situations in the south region, bathymetric characteristics have more notable effects on the attenuation in the North Region. This kind of set-up of wave propagating paths is intended to capture the lower bound of wave attenuation in the North Region.

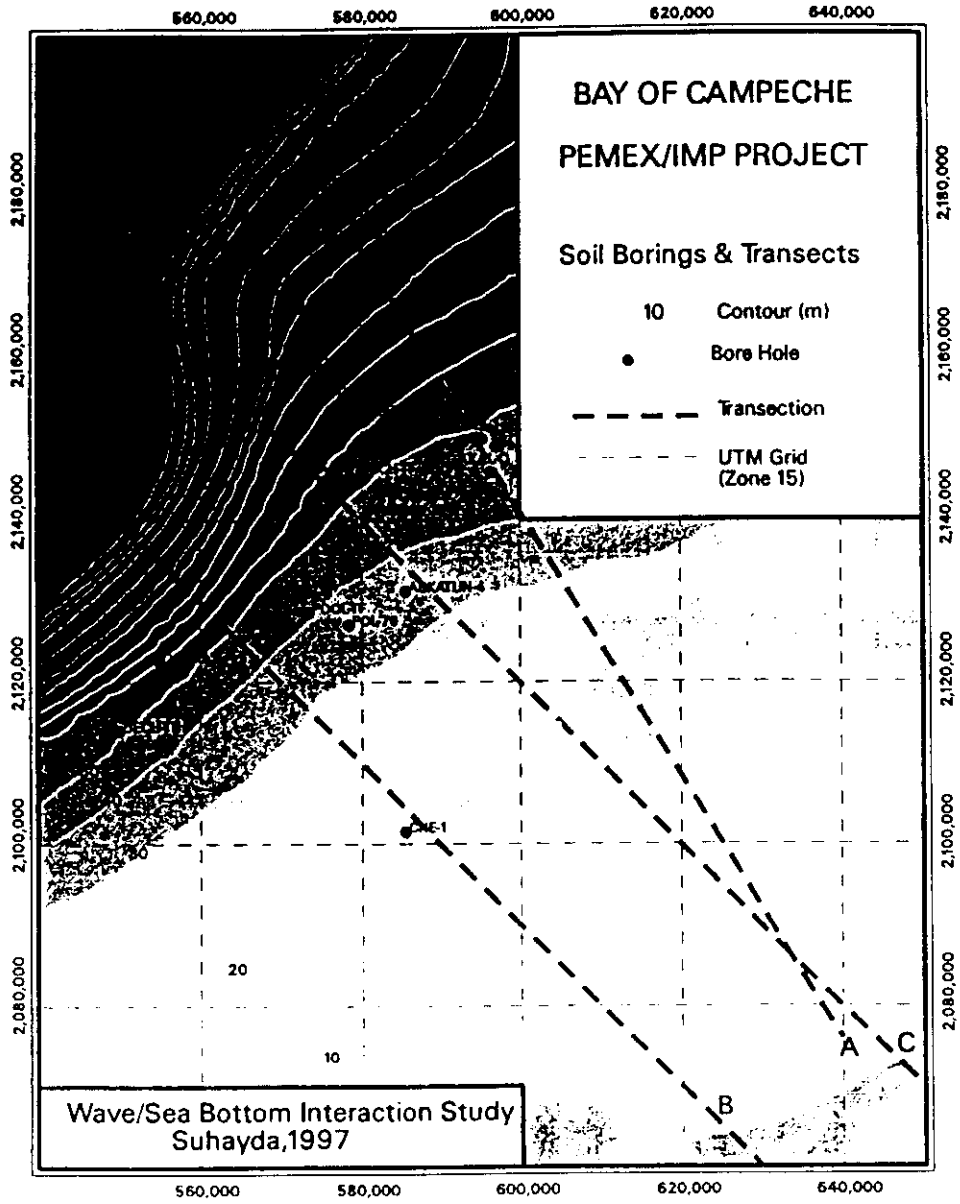

Figure 2.2 Wave transects and soil borings in the south region

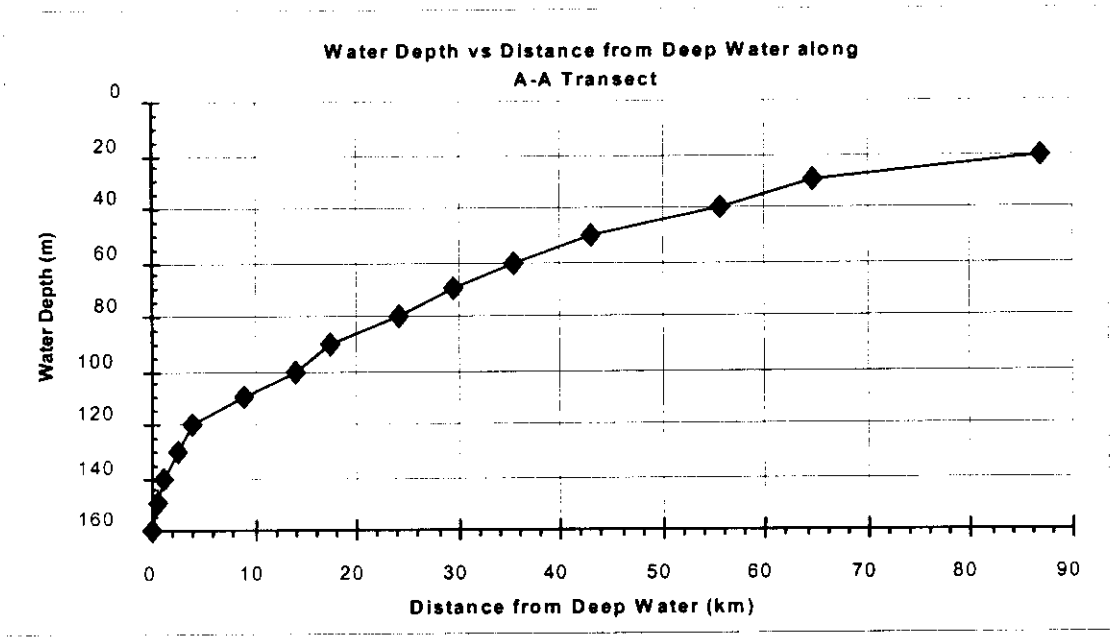

Figure 2.3 Wave Transect A-A

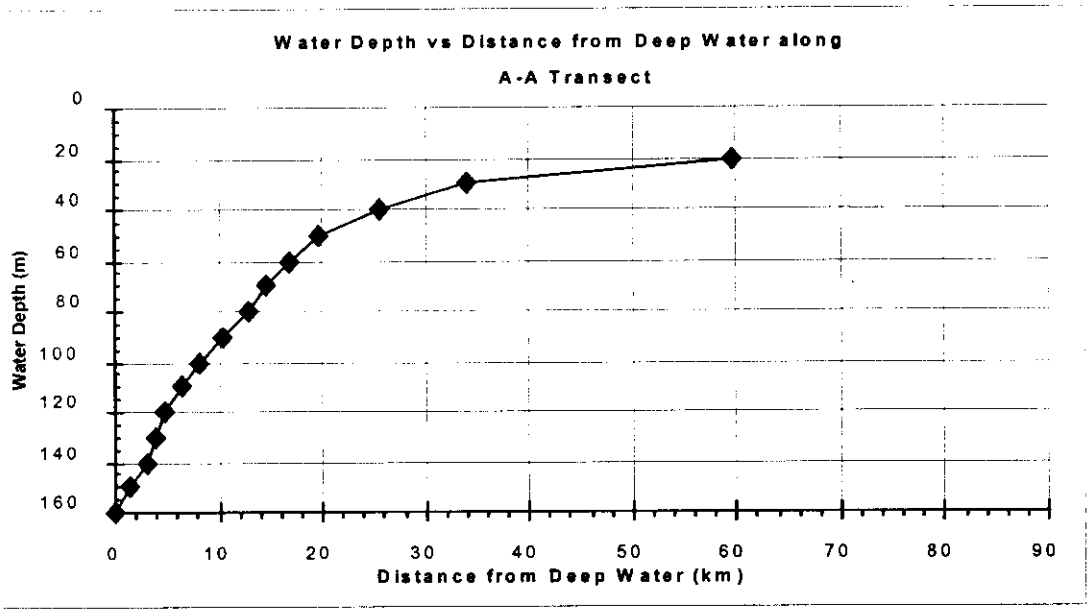

Figure 2.4 Wave Transect B-B

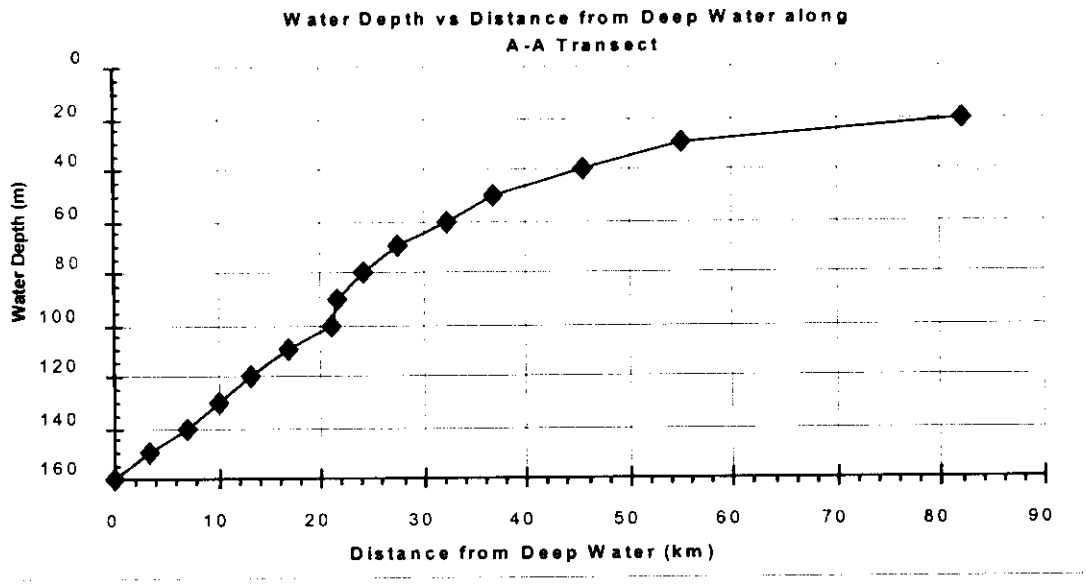

Figure 2.5 Wave Transect C-C

The bathymetric characteristics along N-N and S-S transects are shown in Figure 2.6 and Figure 2.7. It can be seen that the shallow range is far away from the coastline for the S-S transect. The distance between the 60m and 40m contours is very long, almost 25000 meters. In this segment of S-S transect, the shoaling effect shall be not obvious. But the energy loss by sea floor friction is large because of the long distance. And such a long range of smooth sea floor in the shallow water is also ideal for development of strong interaction between waves and soft sea floor. This is the reason why the wave height decay faster in the S-S transect than N-N transect, no matter whether the soft sea floor effect is considered or not.

Another thing should be noted is that both transects are much shorter than those studied in the south region. The lengths are less than half of the shortest one in the south region.

This is another implication that the wave attenuation due soft sea floor shall be less intensive that that in the south region in Bay of Campeche.

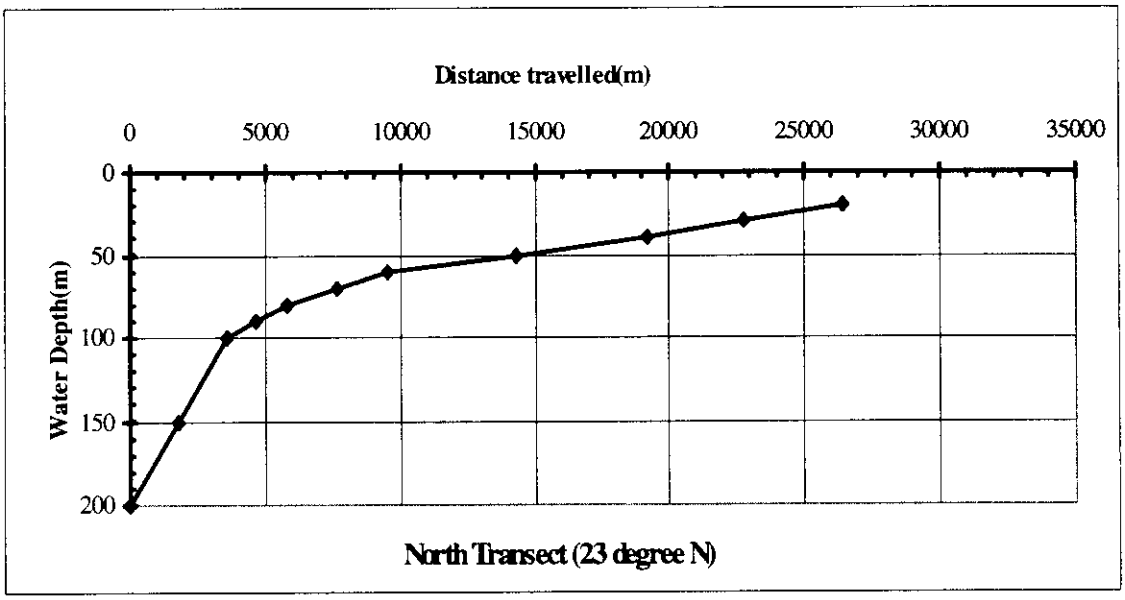

Figure 2.6 Wave transect N-N in the north region

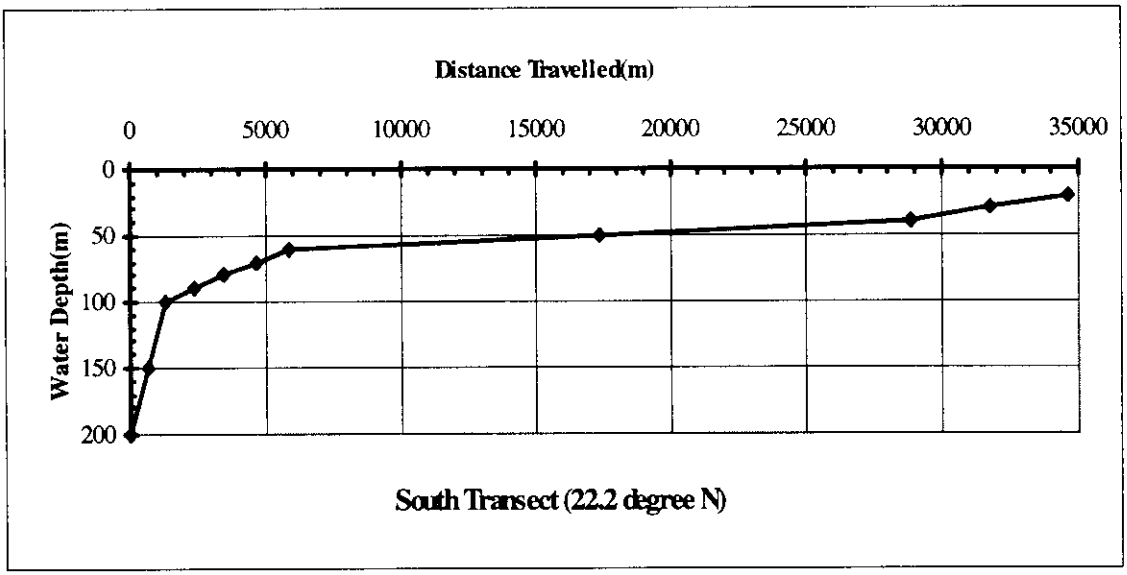

Figure 2.7 Wave transect S-S in the north region

2.2.2 Oceanographic Data

Like the notably different bathymetric characteristics, oceanographic data in both regions are also significantly different.

2.2.2.1 South Region

Oceanographic data in the south region were obtained mainly from two reports by Oceanweather Inc. (1996a, 1996b, 1996c) and A. H. Glen (1996a, 1996b). These reports were extensively studied and useful information was extracted as the basis for the wave attenuation analysis for the south region. The extreme ocean wave conditions are summarized in Table 2.1.

Table 2.1 Extreme Ocean Environmental Conditions in the South Region

Average Return Period (ARP)	Wave Period(s)	Deep Water Wave Height(m)
100-yr ARP Hurricane	13.0	16.0
1000-yr ARP Hurricane	15.0	23.0
10000-yr ARP Hurricane(met)	16.0	27.0
10000-yr ARP Hurricane(ext)	16.0	32.0
Hurricane Roxanne	13.0	15.9

In Oceanweather report, the wave heights were forecasted at different grid points and different water depths. Hurricanes with different average return periods were forecasted. A hindcast of Hurricane Roxanne was also given. Based on this information, the generalized rigid sea bottom wave height decay patterns were interpreted for hurricanes with different returned periods and for Hurricane Roxanne. The wave height decay

curves were summarized in Figure 2.8. These decay curves reflect all the other wave attenuation factors except soft bottom effect.

It shall be noted that the case of 10000-year return period hurricane is not available directly from the Oceanweather data. Statistic extrapolation was conducted to yield a wave height of 32m for 10000-year hurricane, which does not seem likely. An analysis of meteorology in this region predicts that the maximum "credible" hurricane in this region has a wave height of 27m. As parts of a systematic study, both cases were thoroughly evaluated.

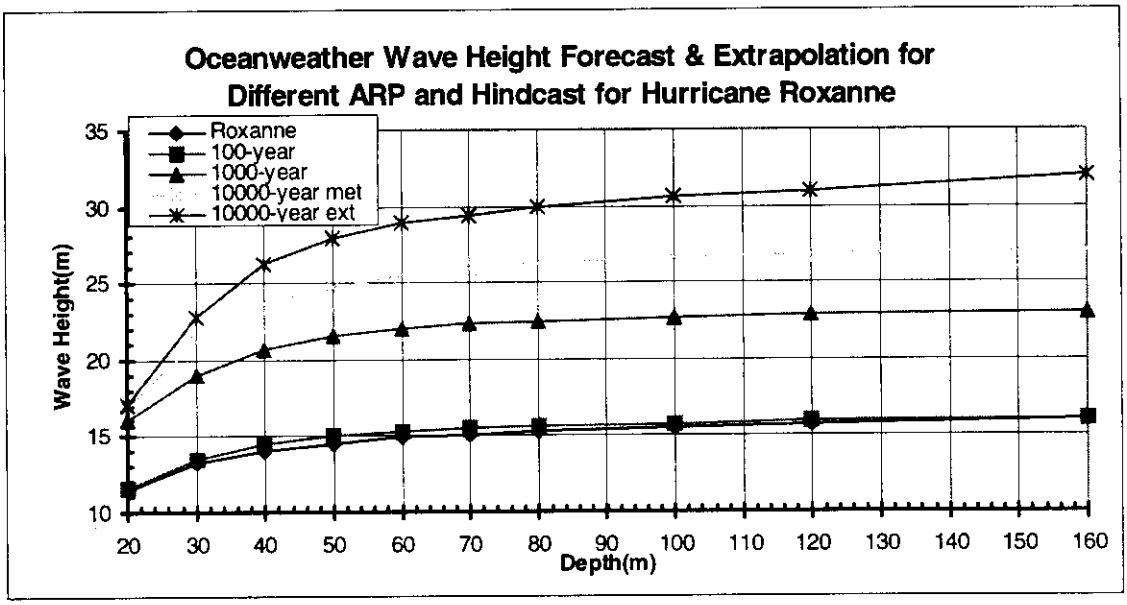

Fig. 2.8 Oceanweather rigid bottom wave height forecast and hindcast in the South Region

2.2.2.2 North Region

The deepwater oceanographic data in the North Region was also obtained mainly from the reports by Oceanweather Inc (1996a, b, c). The extreme deep water ocean wave

conditions are summarized in Table 2.2. But the general rigid sea bottom wave decay patterns are not extracted from the reports.

In Oceanweather report, the wave heights in the south region are forecasted at different grid points and different water depths. These points are scarcely distributed in the large area. Not like in the south region, the generalized rigid sea bottom wave height decay patterns are difficult to interpret from the roughly scattered grid points.

Table 2.2 Extreme Ocean Environmental Conditions in the North Region

Wave Return Period	Wave Period(s)	Deep Water Wave Height(m)
10-yr ARP Hurricane	10.0	11.6
100-yr ARP Hurricane	11.0	16.5
1000-yr ARP Hurricane	13.0	22.0
10000-yr ARP Hurricane	14.0	26.8

As an alternative, a small modification was made in the SWBI program to solve this problem. It assumes that the effects of reflection and diffraction are negligible. So the values of K_{re} and K_d are 1 in Equation 2.1. This assumption is reasonable for the study in north region and has been confirmed by the study in the south region. It is also assumed that there is no refraction along the transects. This is true because the coastline here is straight and open to the sea, not like the coastline with larger curvature in the south region. A more important reason is that the bathymetric contours are smooth and almost parallel to each other. For an incident wave with a direction vertical to these contours,

there should be little refraction. So K_r has a value of 1. The remaining K_s, K_f, K_w can be calculated by SWBI program. The rigid bottom soil properties can be obtained by specifying very large shear strength and Gmax/Su in the soil input files for the SWBI. The K_m for this soil condition is also 1.

So the rigid bottom wave height prediction has involved all the factors that influence the wave decay pattern except soft sea floor effects. These factors' effects are reflected in the coefficient K_{rb} in Equation 2.2. Then, the results of the rigid bottom wave height prediction can be taken as the input to the same SWBI model used to perform the analysis in the south region of Bay of Campeche. The generalized rigid bottom wave decay patterns are summarized in Figure 2.9 and 2.10.

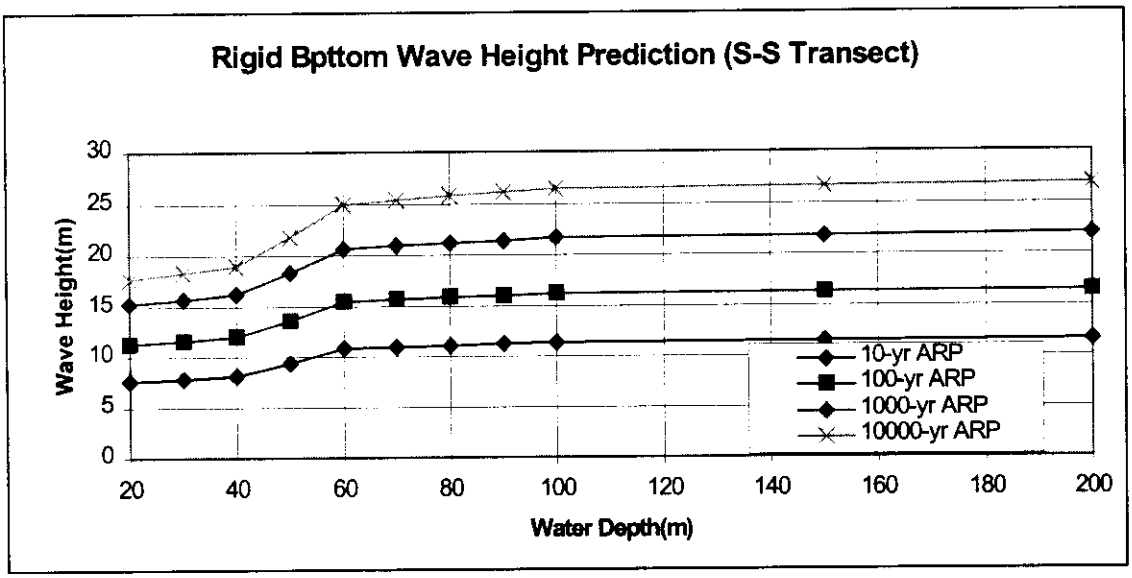

Figure 2.9 Rigid bottom wave height forecast along S-S transect in the north region

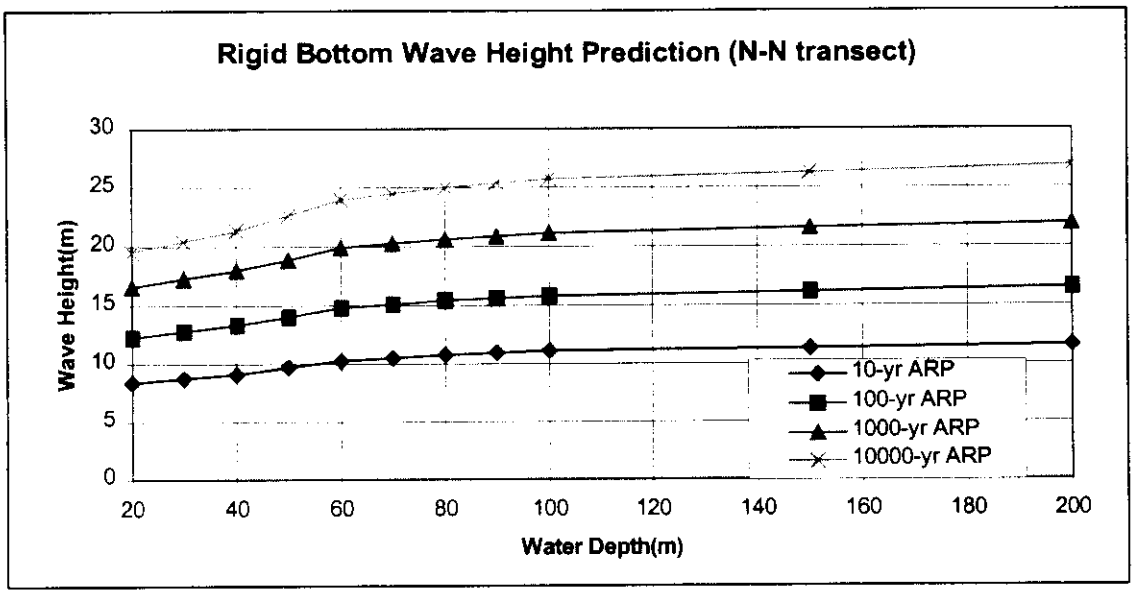

Fig. 2.10 Rigid bottom wave prediction along the N-N transect in the north region

2.2.3 Soil Conditions

Besides the sea bottom bathymetry information, a more important factor is the soil conditions along the transects. As stated before, the in situ and laboratory soil sampling and test have involved natural uncertainties, and the interpretation of the test data involve model uncertainties. Engineering judgment based on expertise and experience in synthesizing soil properties is the key element to evaluate these uncertainties. The in-situ soil conditions must be correctly interpreted from the raw data of borings along the transects. This information has a critical influence on the wave attenuation analysis. Figure 2.2 shows the locations of the borings along the three transects in the south region. Table 2.3 is the list of the borings used in the wave attenuation analysis. Figure 2.11 is a typical soil boring log and soil testing results in the Bay of Campeche.

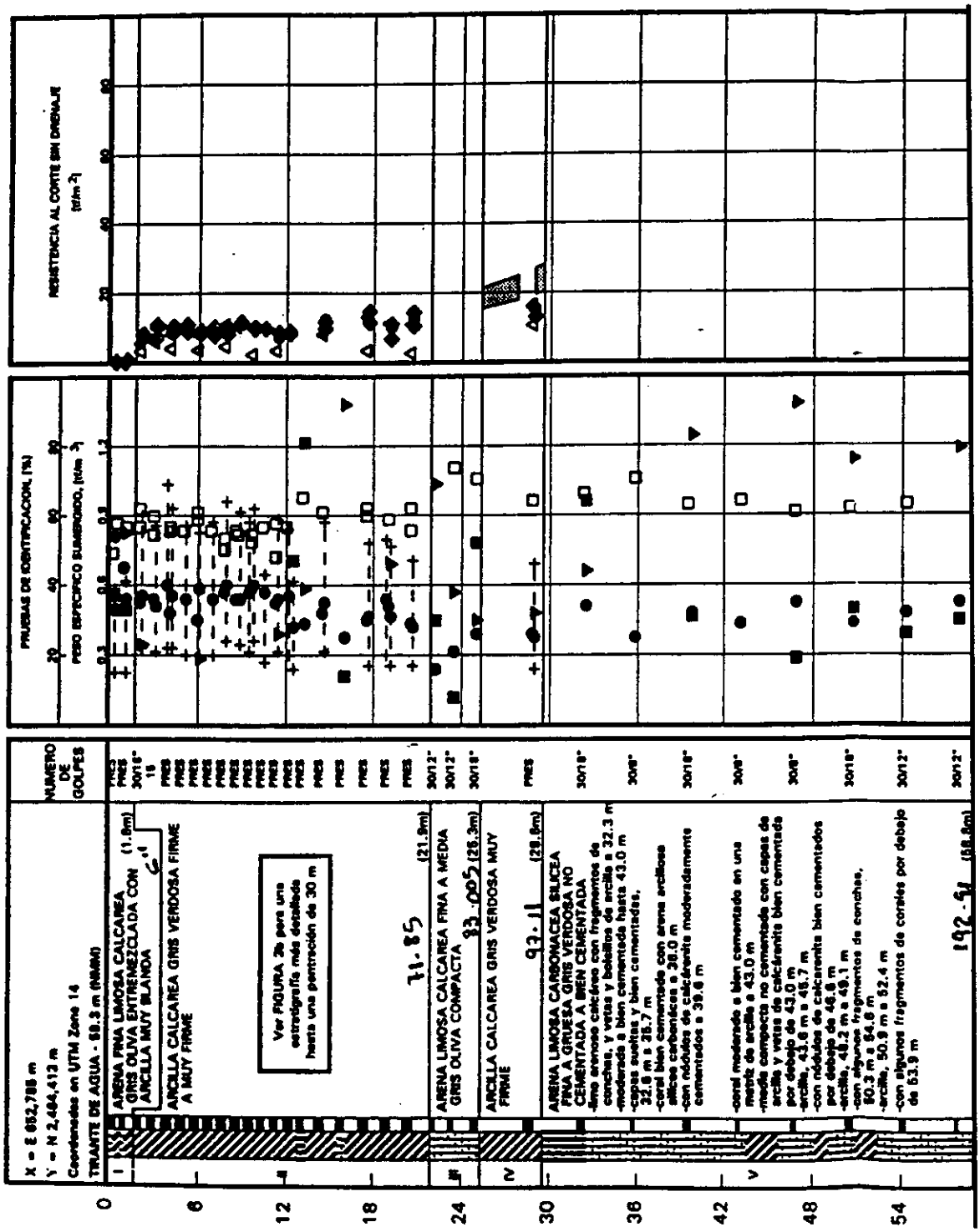

Figure 2.11 Typical soil boring log and soil testing results

Table 2.3 Borings used in Analysis of Wave/Bottom Interaction

Boring Name	Location(UMT)		Water Depth
	X	Y	ft (m)
POL-79	578,377	2,127,023	111 (33.8)
KU-57	586,782	2,161,192	217 (66.2)
ABKATUN-4	585,573	2,131,178	113 (34.4)
AKAL-O	596,476	2,145,814	148 (45.1)
AKAL-T-J	595,303	2,149,901	161 (49.1)
CEEH-101	576,301	2,174.714	335 (101.9)
TABAY-1	573,774	2,188,115	413 (125.9)
POOL—TF	573,393	2,128,598	131 (39.9)
CHE-1	585,500	2,101,500	72 (22.0)
CHA-1	547,256	2,156,397	486 (148.3)
OCH-TA	554,836	2,122,573	198 (60.5)
TARATUNICH-TF	573,626	2,145,748	205 (62.4)

In the analysis, the soil is modeled as a layered system (8 or 9 or 10 layers) with uniform properties of shear strength, shear modulus, damping and density within each layer. For each layer, the unit thickness is determined based on the parametric studies. The soil density were taken from the boring logs and averaged to fit into the chosen layers. Liquidity indexes are interpreted from the boring log. The Liquidity Index is used to model visico-elastic stress-strain behavior. The initial shear modulus (G_{max}) is normalized to shear strength (S_u) in the form of Gmax/Su. The above soil information is stored in soil

files for the SWBI analysis model. Table 2.4 lists a typical input soil file. This analysis uses around 100 such soil files to reflect the location-specific soil conditions and to do systematic sensitivity studies.

Table 2.4 Typical input soil file for SWBI model

```
Soil82  North Region  upper strength profile and expected Gmax/Su
   8      10      5
   1      1       2       2       0
   1      0       100
 1000.     99.     99.0     999.      .02     1.128      0.   .90   1
  46.    1.65      0.      3.      .015     100.     100.
  46.    .80       0.      4.      .015     100.     200.
  53.    .38       0.      3.      .015     200.     1000.
  51.    .45       0.      30.     .015     300.     2000.
  51.    .43       0.      28.     .015     500.     2000.
  61.    .41       0.      30.     .015     500.     2000.
  60.    .28       0.      50.     .015     500.     2000.
  60.    .35       0.      50.     .015     1000.    2000.
  60.    .40       0.     10000.   .015     1000.    4000.
```

In the input files, both shear modulus and shear strength in the top soil layers subject to degradation due to cyclic wave loading and large strain rate. The degraded strengths are typically 25-50% of the undisturbed strengths, and the degraded moduli are 20-30% of the undisturbed moduli (Kraft, 1985). Another important parameter is Gmax/Su. As discussed before, the hyperbolic stress-strain curve is used in the analysis. However, actual soil response may not follow a hyperbolic curve over the full stress level range. Based on the experience in the sea-bottom intersection analysis in the Mississippi Delta (Kraft and Suhayda 1990), the ratio Gmax/Su of 450-400 at small strains in a hyperbolic model often provides a good fit to the measured stress-strain response in the soft sediments when shear strains is less than 0.1%. For large strains, Gmax/Su should be

decreased (Kraft, et al, 1985). Based on this argument, the analysis is first performed using the Gmax/Su values from PEMEX's boring logs. Then, the Gmax/Su is decreased in the analyses, according to interpretation of the results, to reflect the soil degradation due to shear strain effects and cyclic strain effects. The history of deep-water waves, bathymetery, and soil properties over the path of wave travel are considered in establishing the soil degradation model. For the case of soils in the Bay of Campeche, the top greatly degraded soils are determined to have an expected value of 100 in the Gmax/Su, with a lower bound of 50 and an upper bound of 200. The variation is considered to be equivalent to ± 2 times standard deviation in the reliability model.

Undrained soil strength profiles, soil liquidity index profiles and submerged unit weight profiles are also needed to create the input soil files. The initial undisturbed profiles are easily extracted from boring logs. To reflect the inherent natural variation in the soil properties in a macro geotechnic structure and the variation in the interaction between the waves and the soft sea floor, three different soil undrained shear strength profiles were determined to be used in the SWBI model: weak, expected and strong. The expected soil strength profile represents the "best estimate" soil properties appropriate for the time of occurrence of extreme hurricanes with cyclic strength degradation. The upper and lower bound profiles are intended to reflect the possible variation of the degree and extent of such a cyclic degradation during hurricanes. The upper and lower bounds are also equivalent to ± 2 times the standard deviation in the reliability model. A typical soil profile of undrained shear strength is plotted in Figure 2.12. Typical soil profiles of submerged unit weight and liquidity index are shown in Figure 2.13.

Besides the variation in the soil properties, the sea floor slopes in soil files has different values along the wave transect. This is because the shoaling effects for the transects depends on the sea floor slope. It is expected that the shoaling effects in the north region have a more influence on the final wave decay pattern than in the south region.

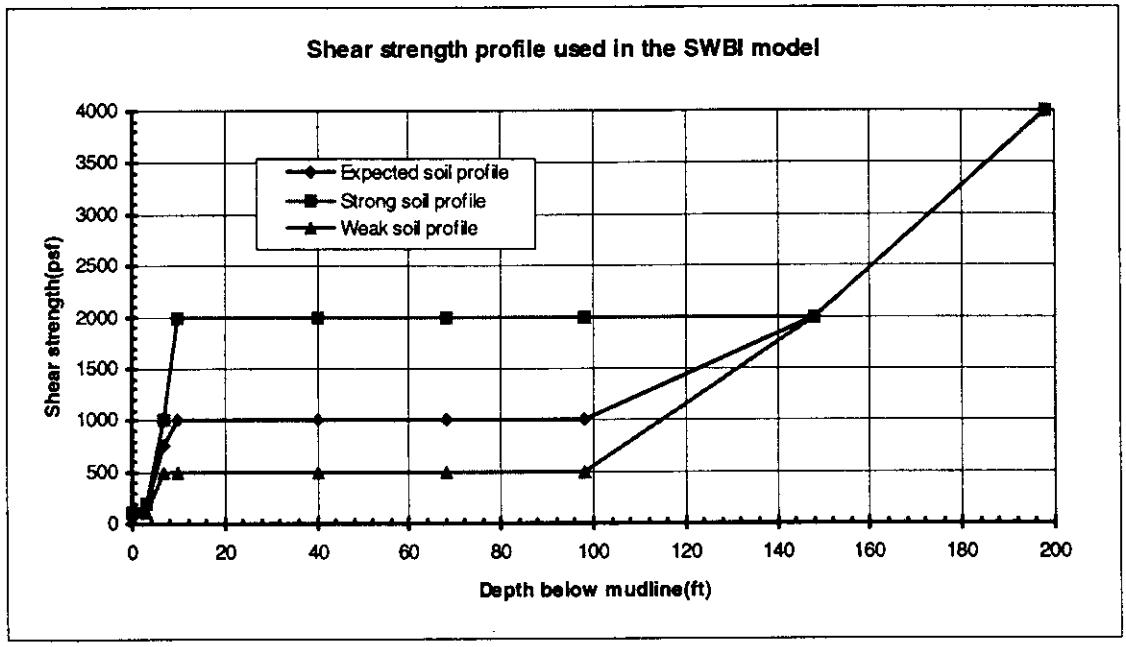

Figure 2.12 Generalized soil strength profiles used in the SWBI model in the North Region

2.2.4 Summary

In a short summary, the SWBI analysis model in this report considers the following conditions:

- 3 wave transects in the south region: A-A transect, B-B transect, and C-C transect; and 2 wave transects in the north region: N-N transect and S-S transect;

- 5 different extreme ocean wave conditions with different ARP's: 100 years, 1000 years, 10000 years (extrapolated), 10000 years (meteorological), and the hindcast of Hurricane Roxanne;
- 3 different values of Gmax/Su;
- 12 borings along the different transects;
- 3 versions of soil properties to recognize the inherent uncertainties and cyclic degradation effects in the north region;
- A systematic sensitivity analysis of wave attenuation to the soil characteristics with sets of soil file combination along different wave transects.

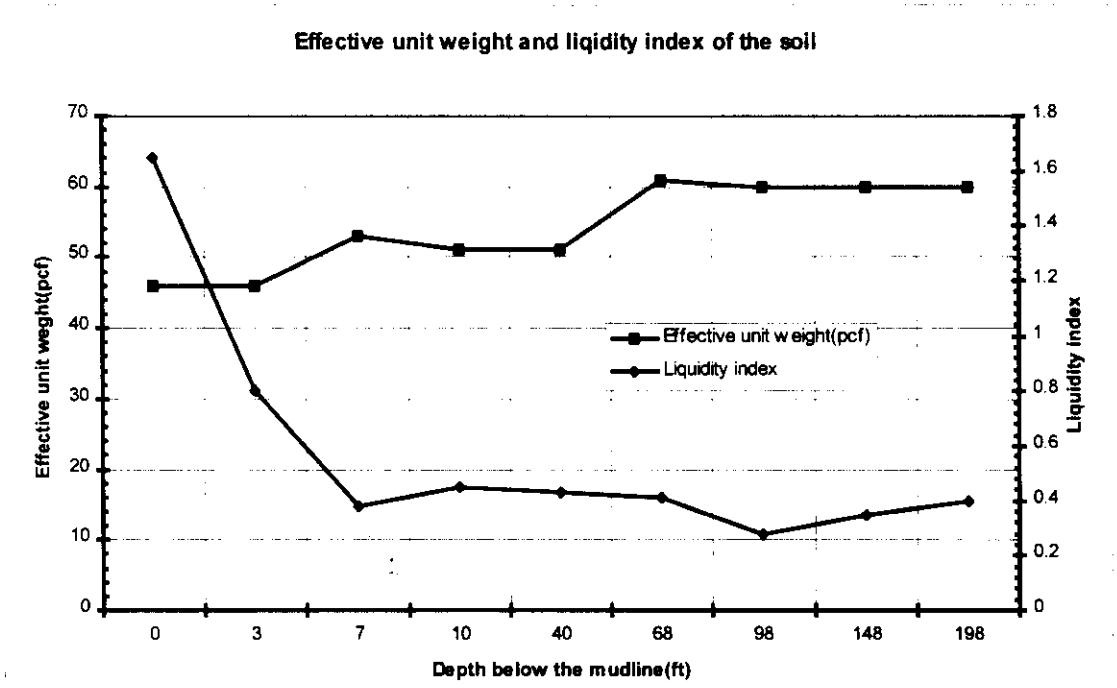

Figure 2.13 Profiles of submerged unit weight and liquidity index in the North Region

2.3 Wave Decay Characteristics in the Bay of Campeche

A systematic parametric analysis is conduct before the beginning of the detailed analysis to determine the appropriate parameters to enhance numerical stability, accuracy; and to properly simulate the nonlinear coupling behavior of wave and soft soils in vertical soil layers as well as in the horizontal transect intervals in the wave propagation paths. Then the detailed analysis of wave decay patterns in the north and south regions is performed. The analysis results are summarized in a series of graphs.

2.3.1 Wave Attenuation Analysis in the South Region

In the south region, there are a lot of soil boring logs available. The SWBI model can be built to reflect the location-specific soil condition along wave transects. Around 100 cases of wave attenuation were studied in this region.

2.3.1.1 Presentation of the Analysis Results

Figure 2.14 shows the analysis results for the A-A transect with a combination of different soil properties and different return period wave conditions. According to the results above, the wave attenuation along this transect is not very intensive in the water depth range of 40-80m, although this transect is the longest one. It suggests that there are stiffer soils along this transect. This argument is consistent with the input soil properties. It also appears that there is no abrupt change of soil properties along this transect because the wave height decay curves are rather smooth, even for the extrapolated 10,000-year return period hurricane. Figure 2.15 and 2.16 summarize the similar analysis results for

B-B and C-C transects. Note that the wave attenuation patterns, or the wave decay curve trends, are almost the same along these transects.

In order to show how the wave and bottom interaction changes the wave decay patterns for hurricanes of different intensity, the wave attenuation for different ARP waves were compared along each transect. The best estimate soil properties were used. Figure 2.17 shows these wave decay curves. As discussed before, SWBI gives a correction factor R_m as output, which can be applied to the Oceanweather rigid bottom wave height forecasts. Based on the analysis results, envelopes of R_m and the best-estimate values are given in Figure 2.18. For the sake of comparison, wave attenuation patterns along different transects were put together in Figure 2.19. Also, the results of expected maximum wave heights for different return periods and wave depths are summarized in Figure 2.20. As weather station Ixtoc A is very close to C-C transect, where the observed wave height data is reported during Hurricane Roxanne, a SWBI analysis model of Roxanne was built along this transect for the sake of calibration. The results are shown in Figure 2.21.

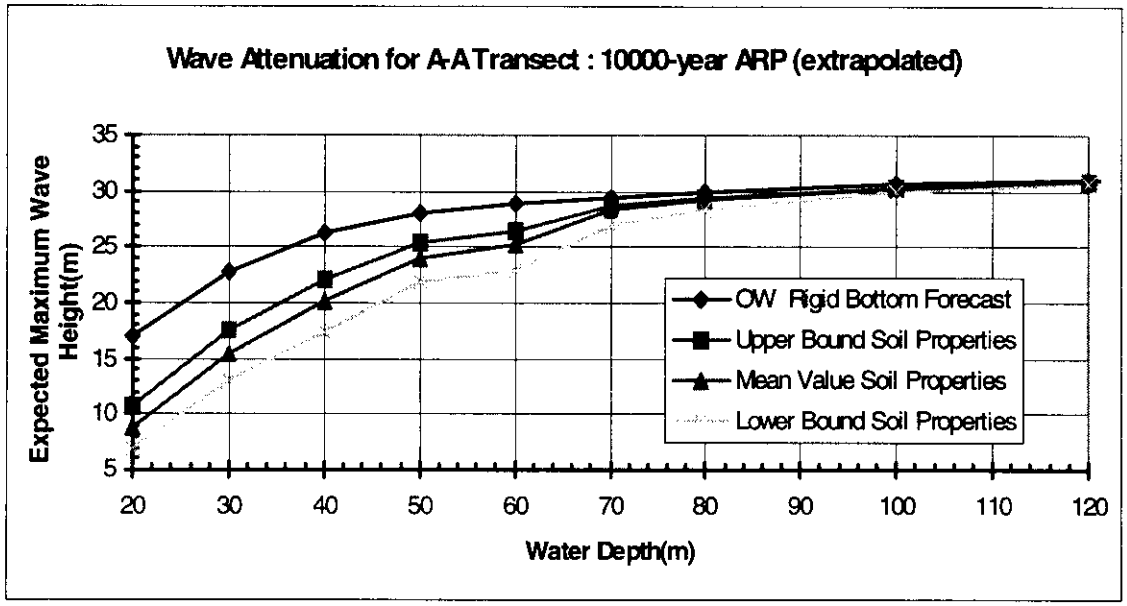

Fig 2.14a 10000-year ARP (extrapolated) expected maximum wave heights

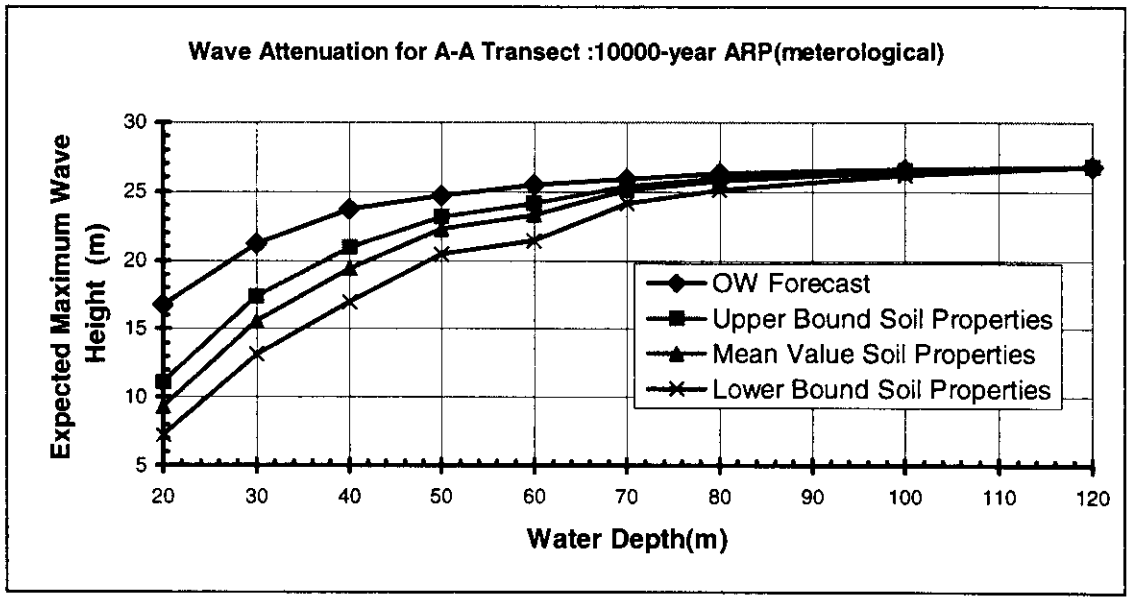

Fig 2.14b 10000-year ARP (meteorological) expected maximum wave heights

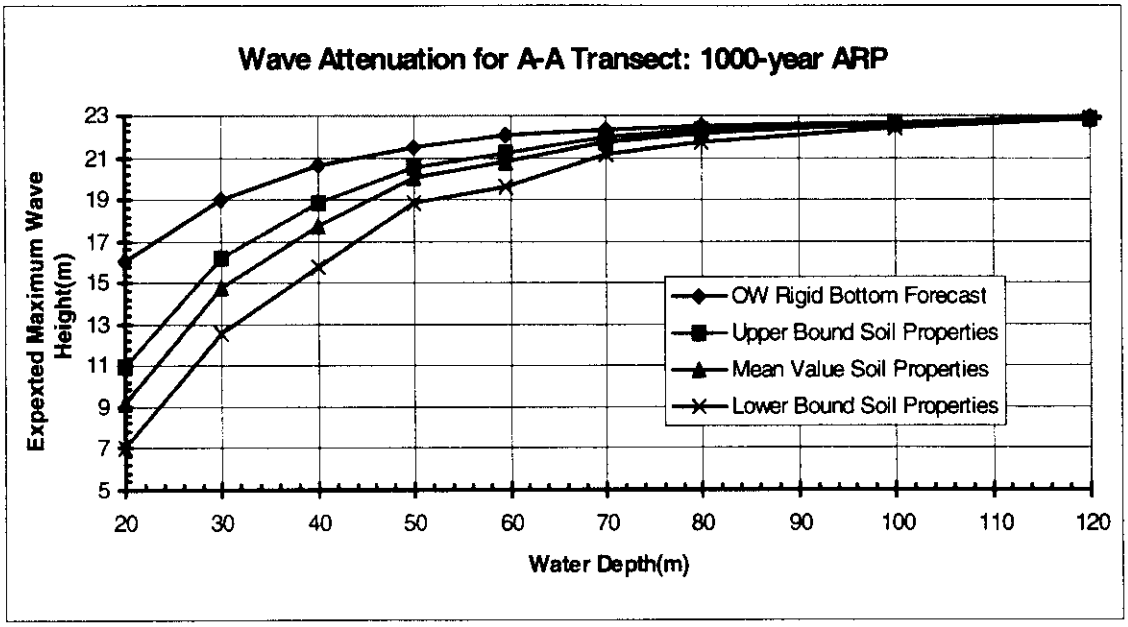

Fig 2.14c 1000-year ARP expected maximum wave heights

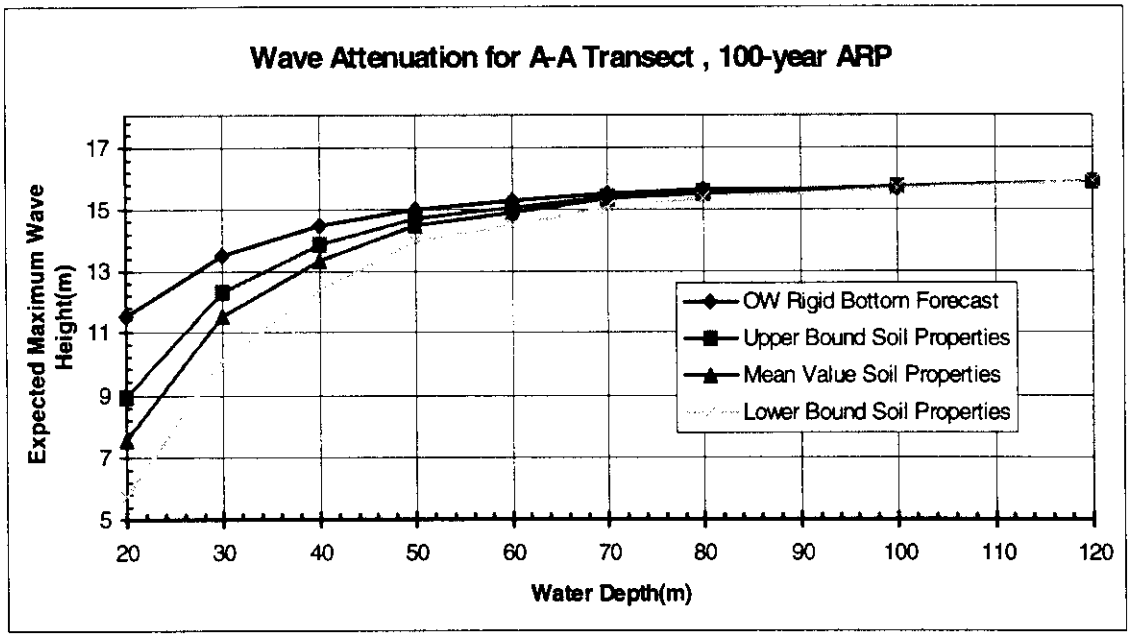

Fig 2.14d 100-year ARP expected maximum wave heights

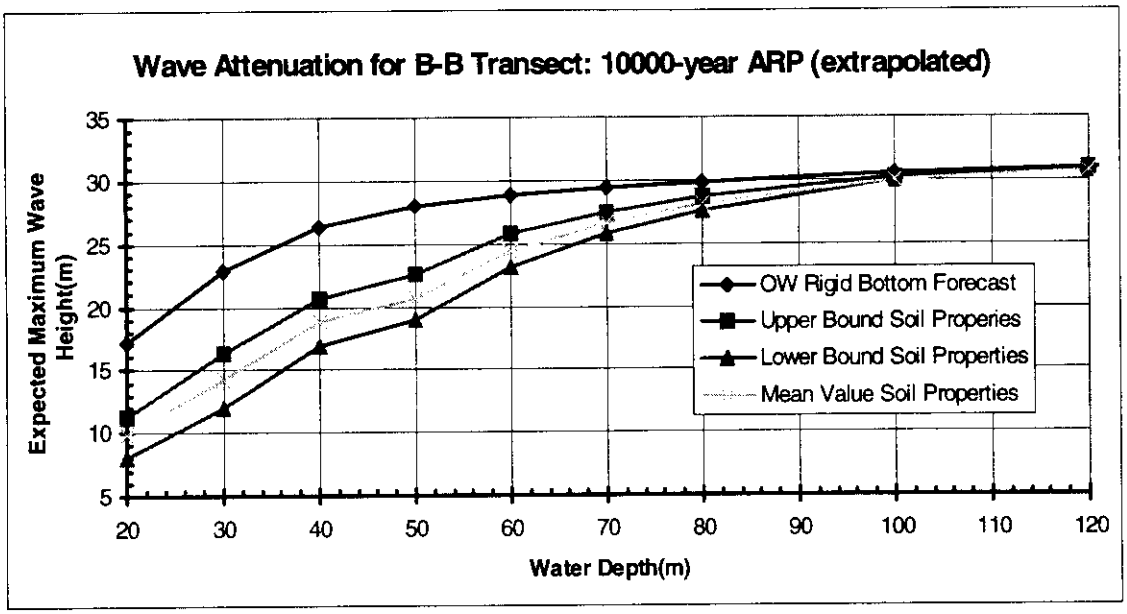

Fig 2.15a 10000-year ARP(extrapolated) expected maximum wave heights

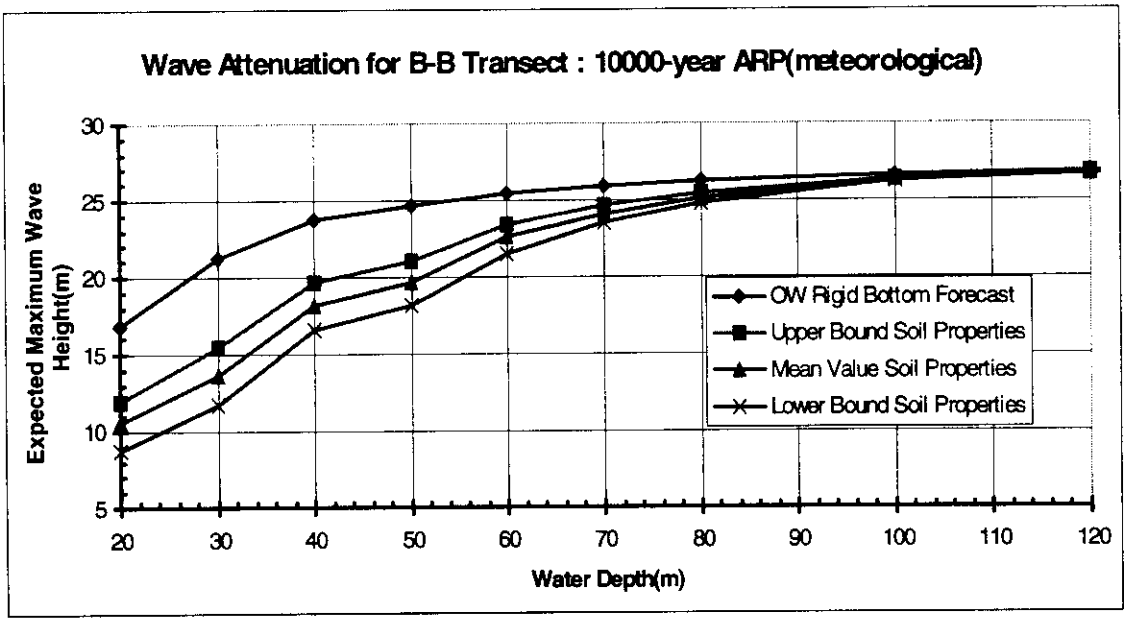

Fig 2.15b 10000-year ARP(meteorological) expected maximum wave heights

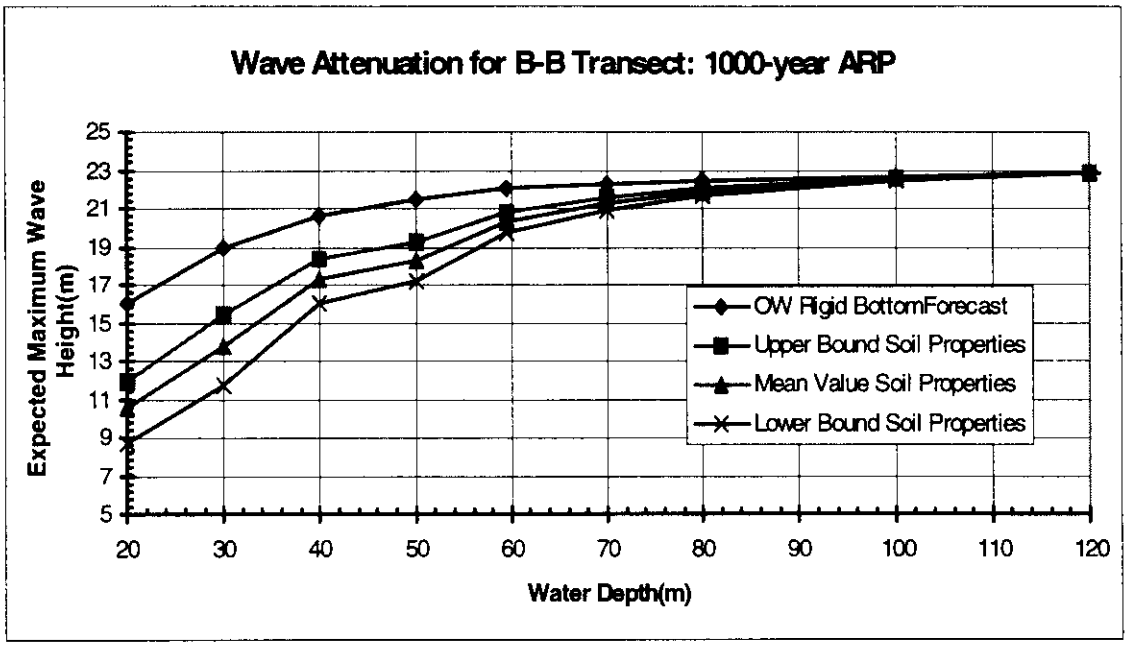

Fig 2.15c 1000-year ARP expected maximum wave heights

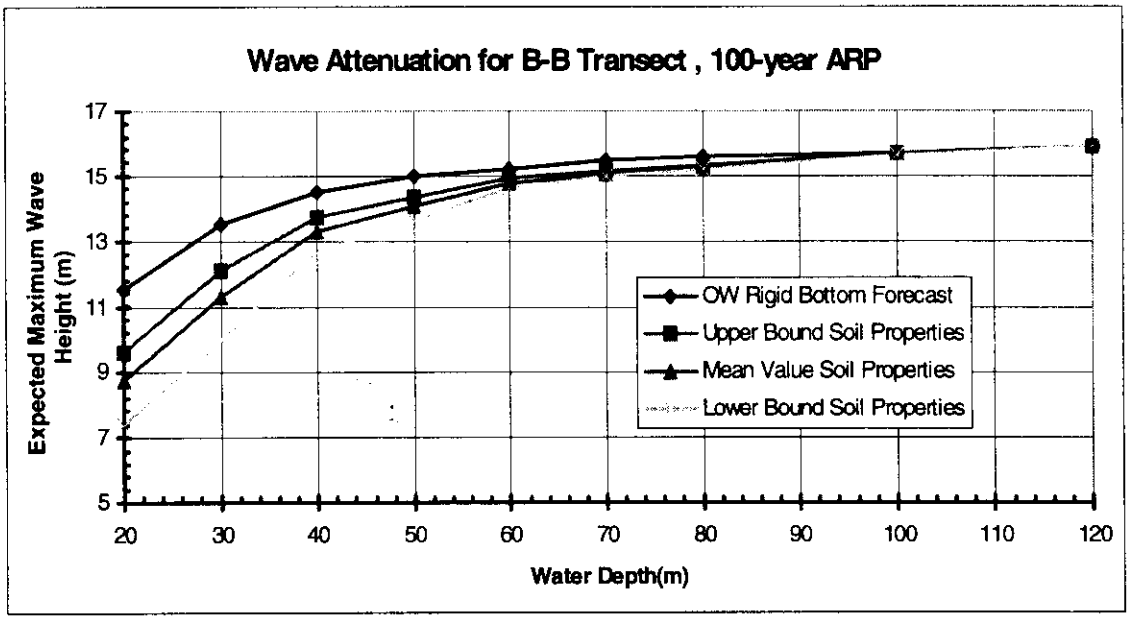

Fig 2.15d 100-year ARP expected maximum wave heights

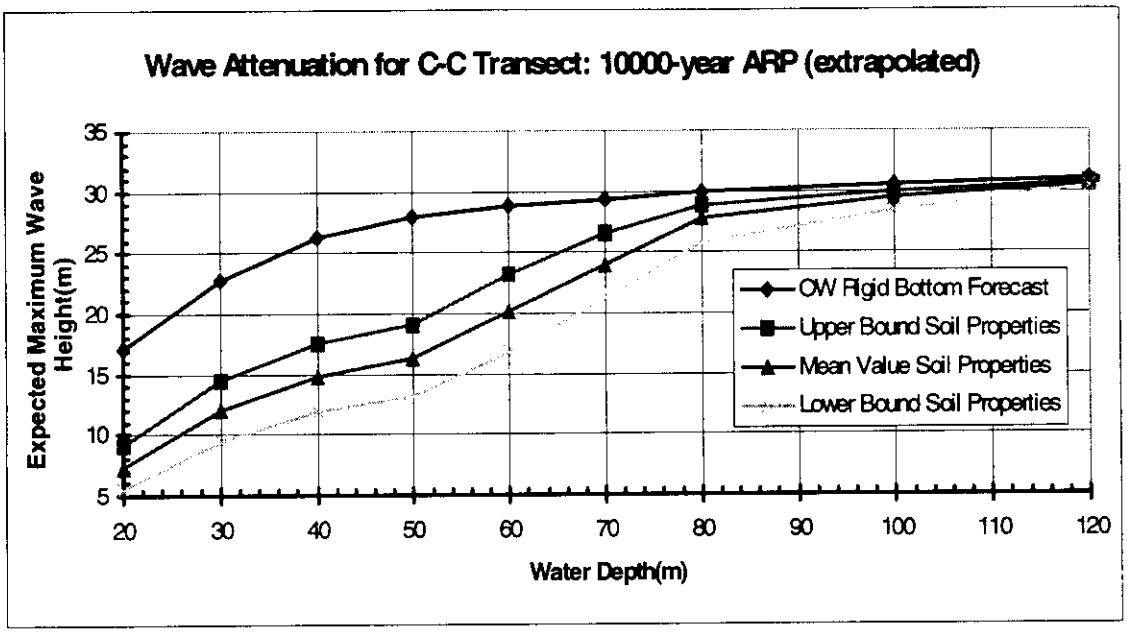

Fig 2.16a 10000-year ARP(extrapolated) expected maximum wave heights

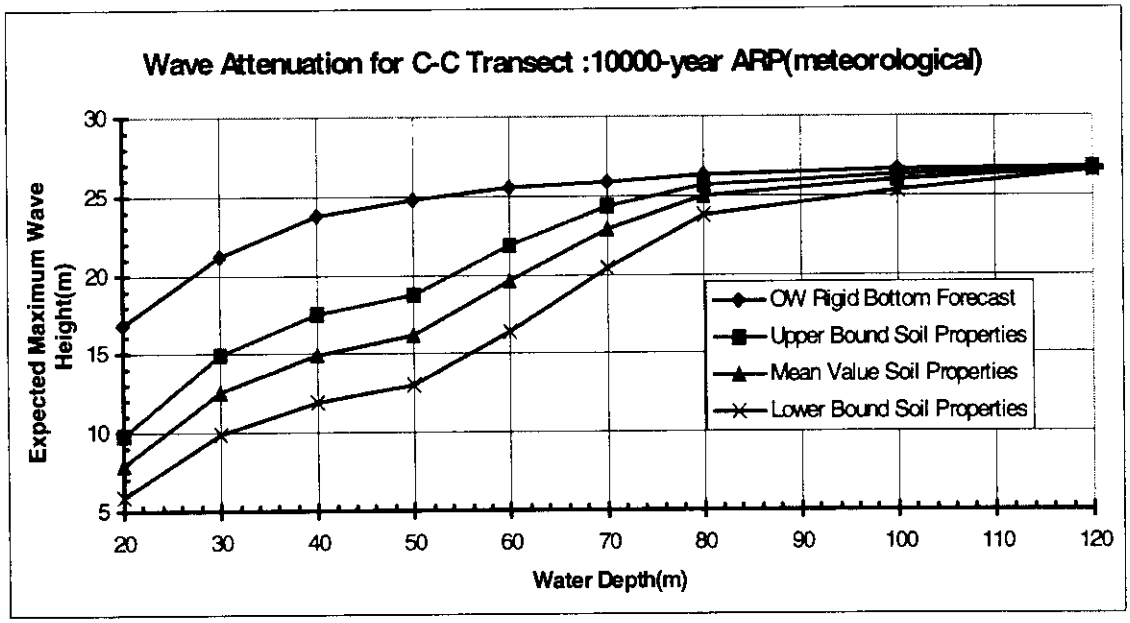

Fig 2.16b 10000-year ARP(meteorological) expected maximum wave heights

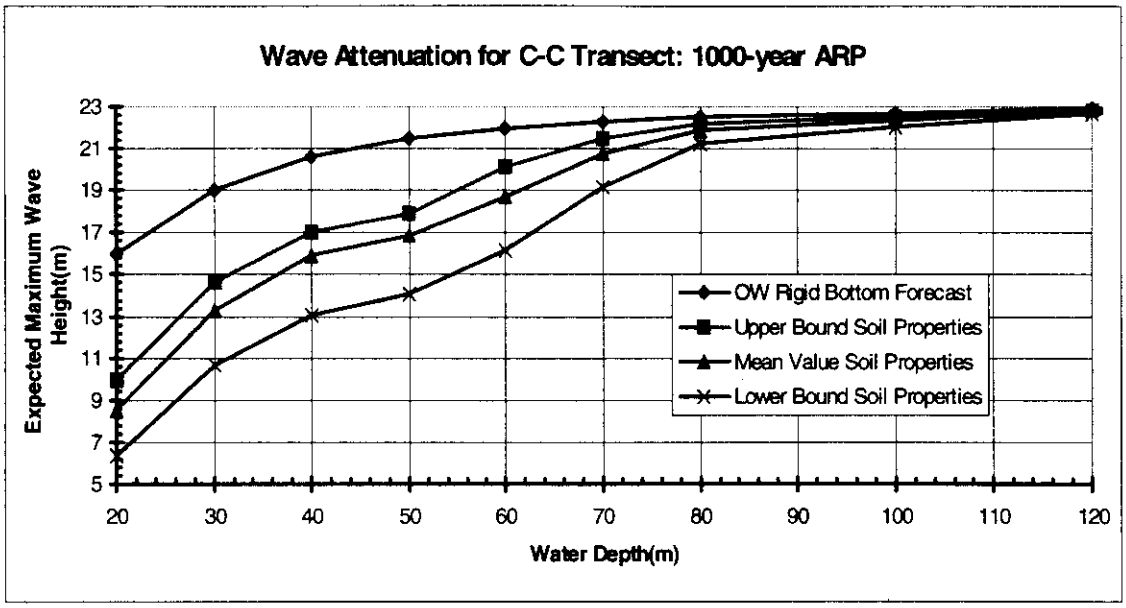

Fig 2.16c 1000-year ARP expected maximum wave heights

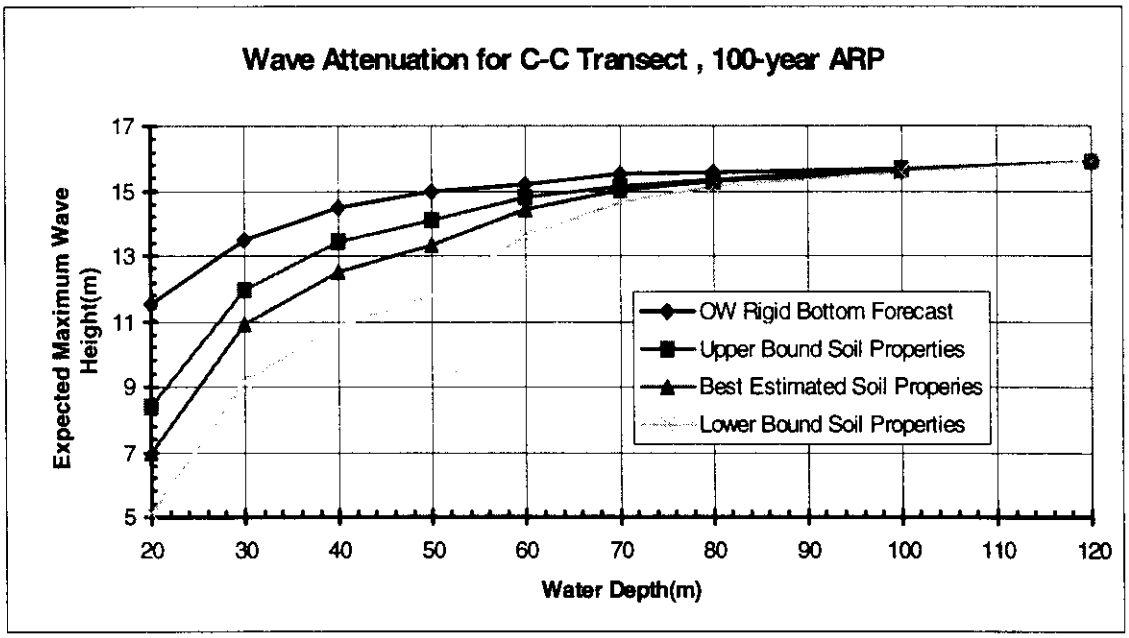

Fig 2.16d 100-year ARP expected maximum wave heights

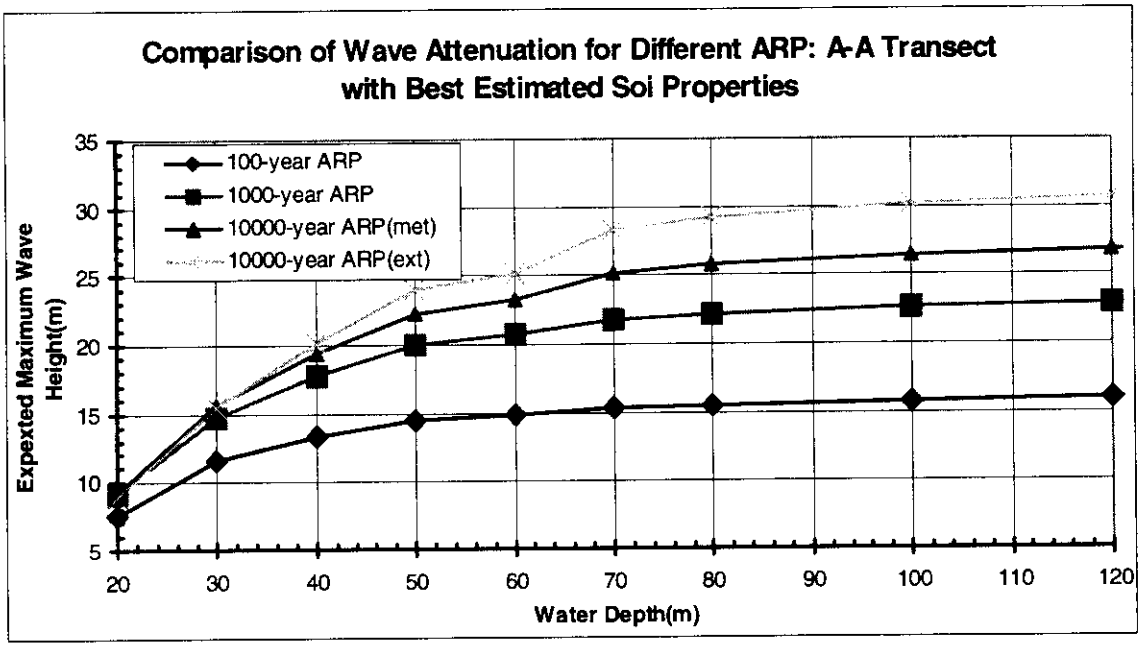

Fig 2.17a A-A wave transect

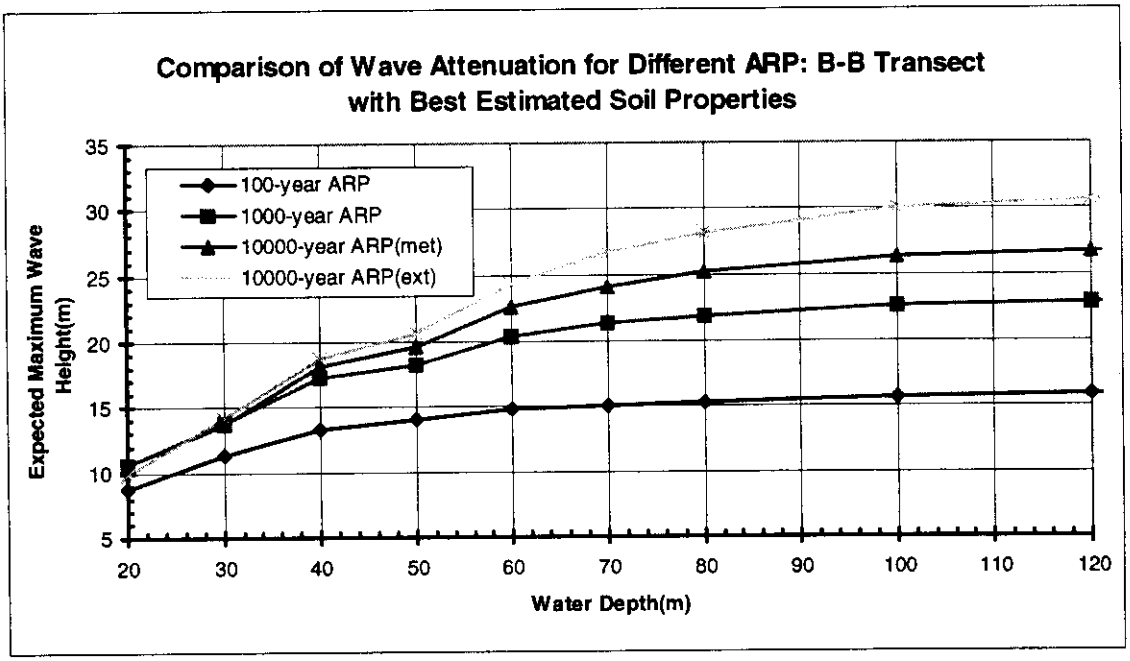

Fig 2.17b B-B wave transect

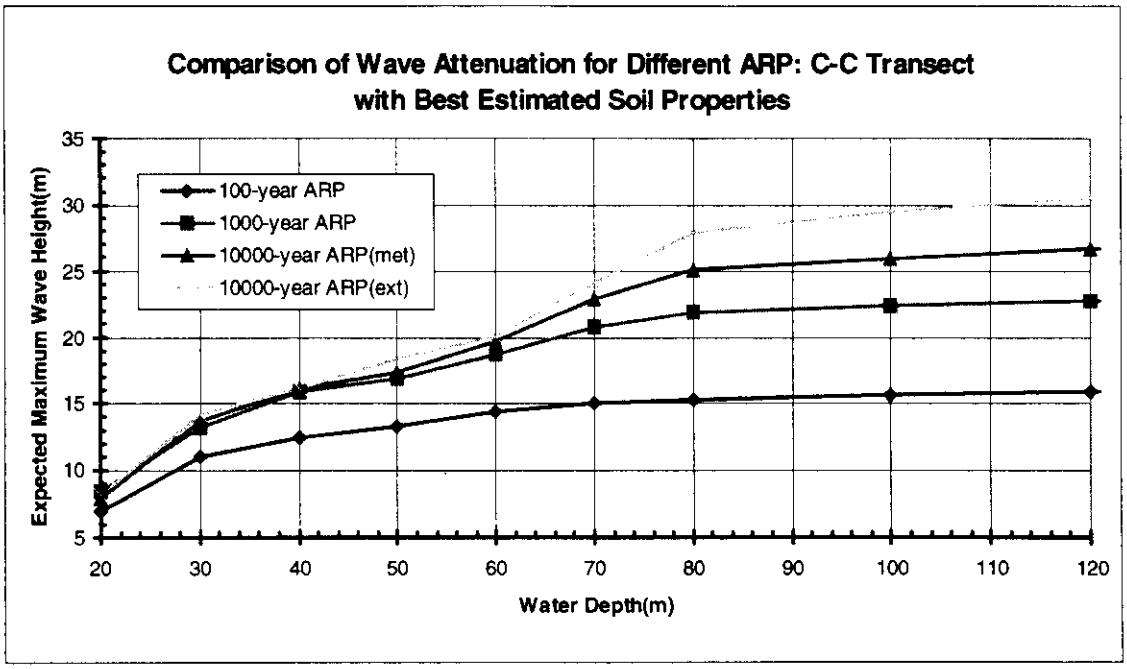

Fig. 2.17c C-C wave transect

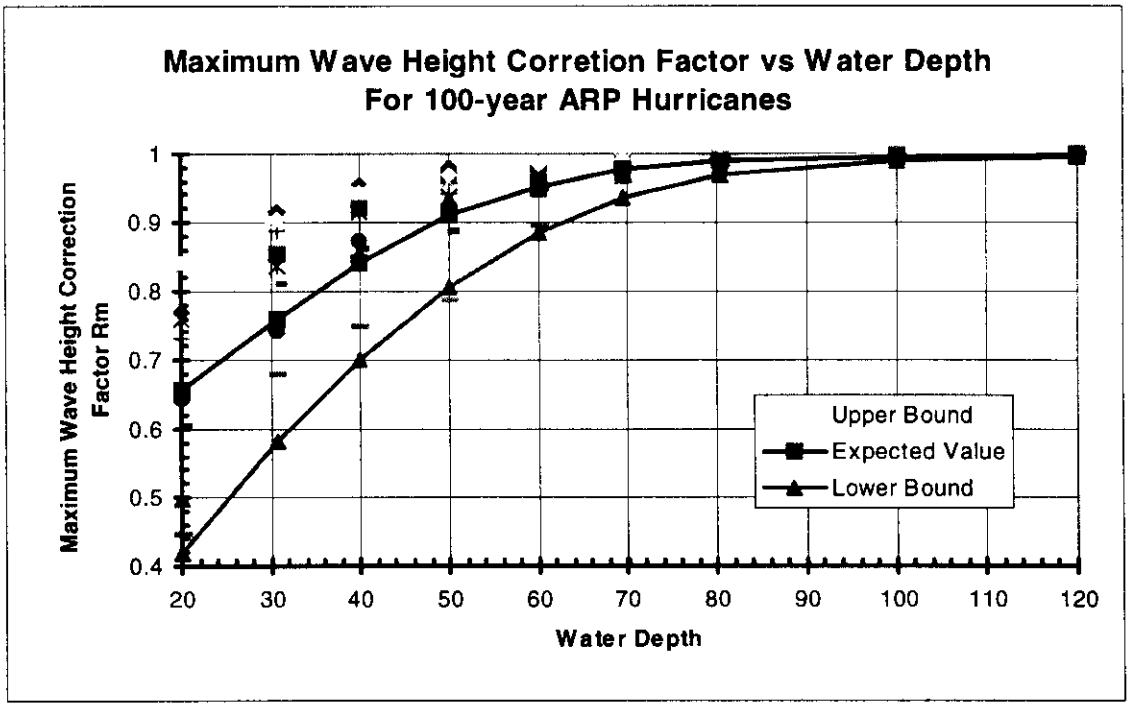

Fig 2.18a Envelope of correction factor R_m for 100-year ARP maximum wave heights

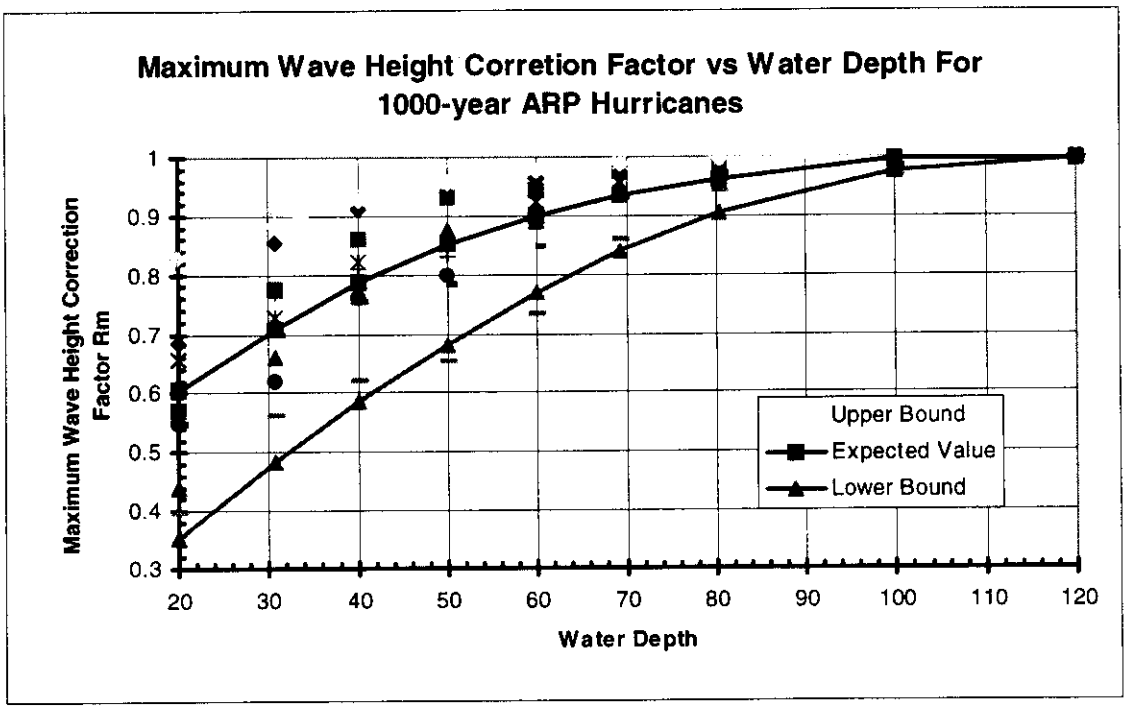

Fig 2.18b Envelope of correction factor R_m for 1000-year ARP maximum wave heights

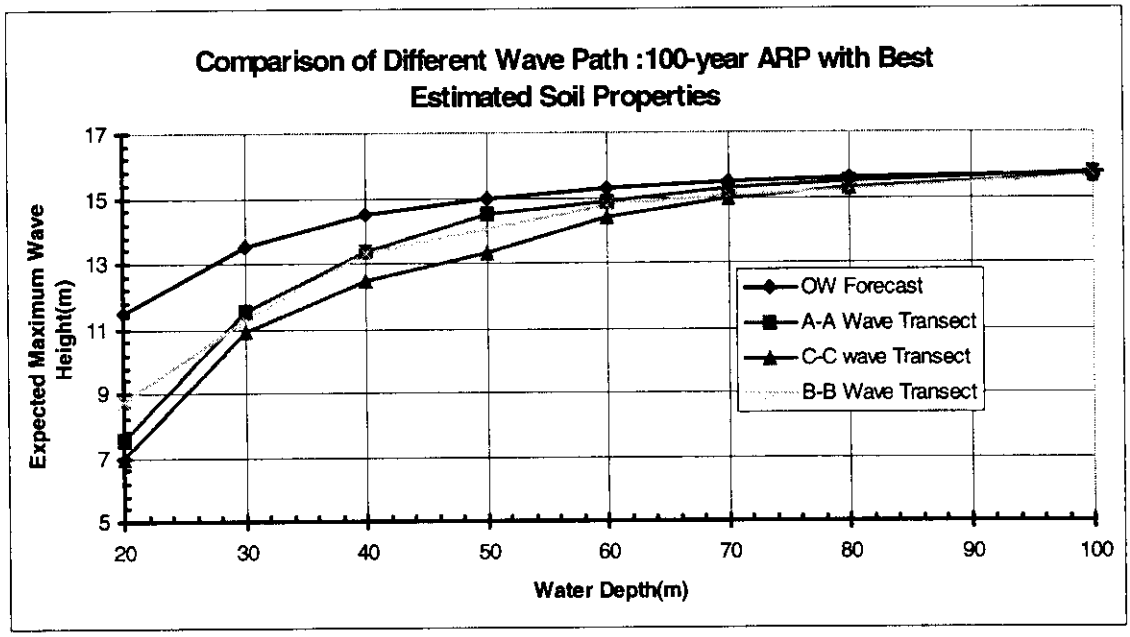

Fig. 2.19a 100-year ARP maximum wave heights with best estimated soil properties

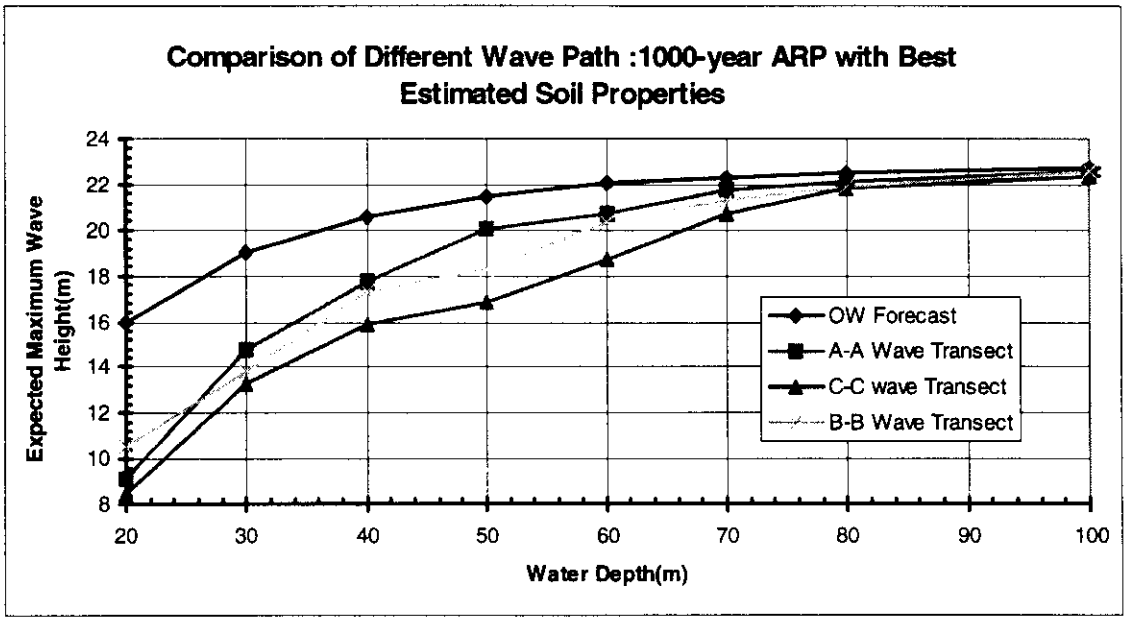

Fig. 2.19b 1000-year ARP maximum wave heights with best estimated soil properties

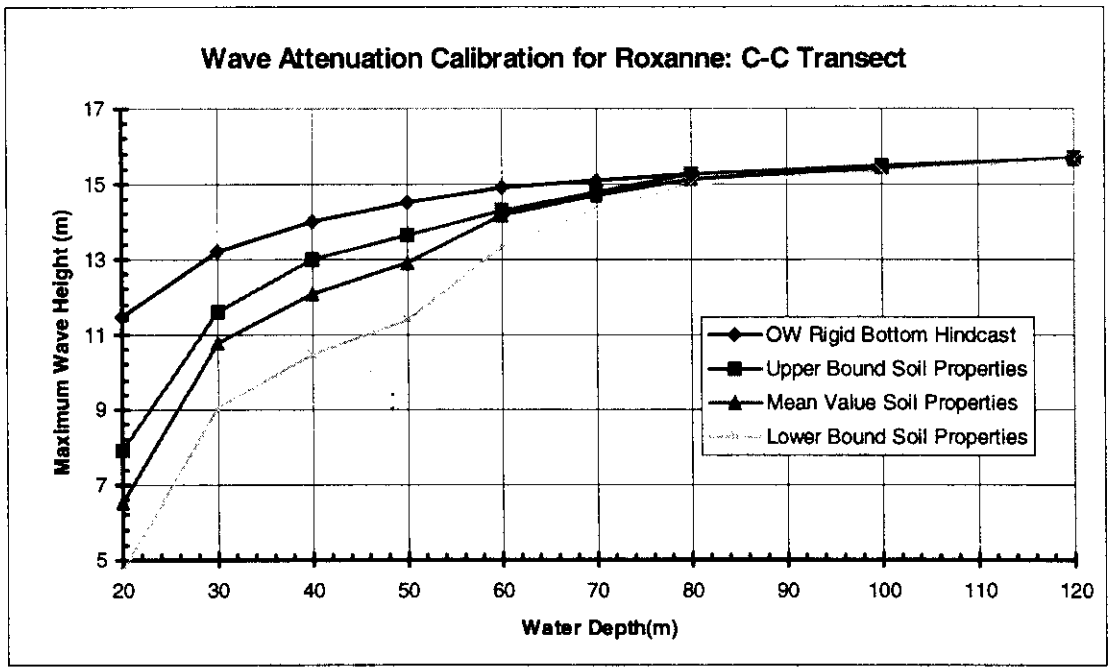

Fig. 2.20 Hurricane Roxanne Hindcast from Oceanweather and SWBI

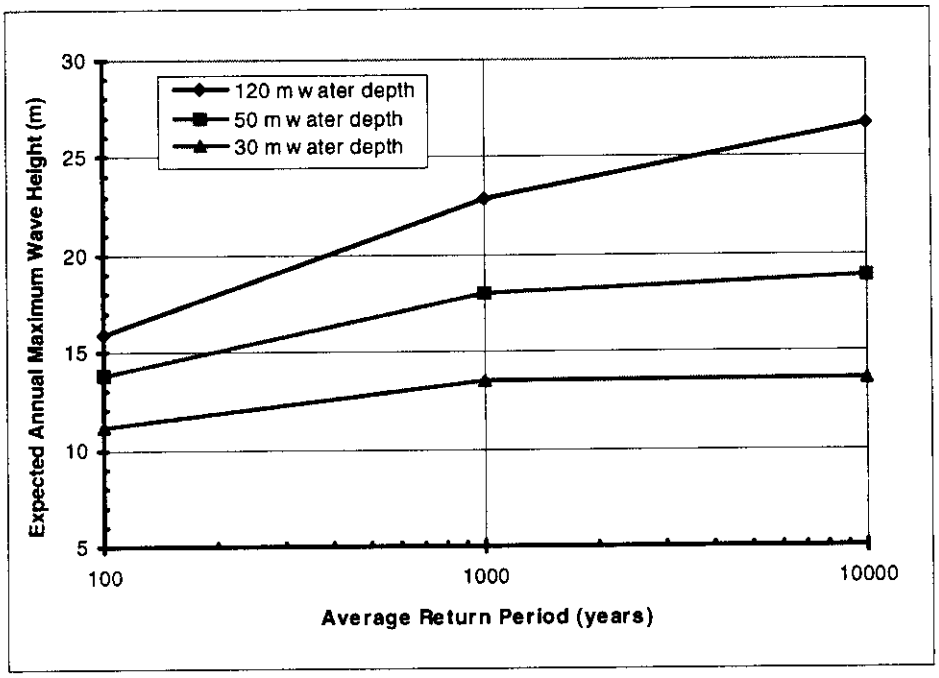

Fig. 2.21 Expected Annual Maximum Wave Heights for Different Return Periods and Water Depths

2.3.1.2 Discussion of the Results

Based on the foregoing analysis results, some interesting observation can be made and some useful conclusions can be drawn about the wave decay characteristics in the south region of the Bay of Campeche:

SWBI model predicts a large amount of wave attenuation when the wave propagates from deep water to shallow water in this region. Compared with Oceanweather's forecast, this analysis forecasts an attenuation percentage of 70-90% at the water depth of 50m and 40-80% at 20m. It is important to emphasize that these values are for the conservative wave propagating paths. More intensive attenuation can be expected to occur in the field. This has been confirmed by Roxanne calibration (Figure 2.22). Based on the results, the

predicted maximum wave height at the water depth of 50m along C-C transect is 11m. The wave height reported by weather station Ixtoc A is 9m. The variance may be due to following reasons: First, Ixtoc is not exactly on the C-C transect. Second, the actual wave attenuation path lead to this site during Roxanne may be different from the transects in the analysis. Third and the most important, the soil around the site, based on the boring log, has a great variability.

It is believed that the Roxanne path was different from C-C transect and should be much longer. Also, it is no surprise that soil properties vary by more than a factor of 2 over short distances. Therefore, from this point of view, Roxanne calibration did show a large potential of wave attenuation and a good agreement with the field data.

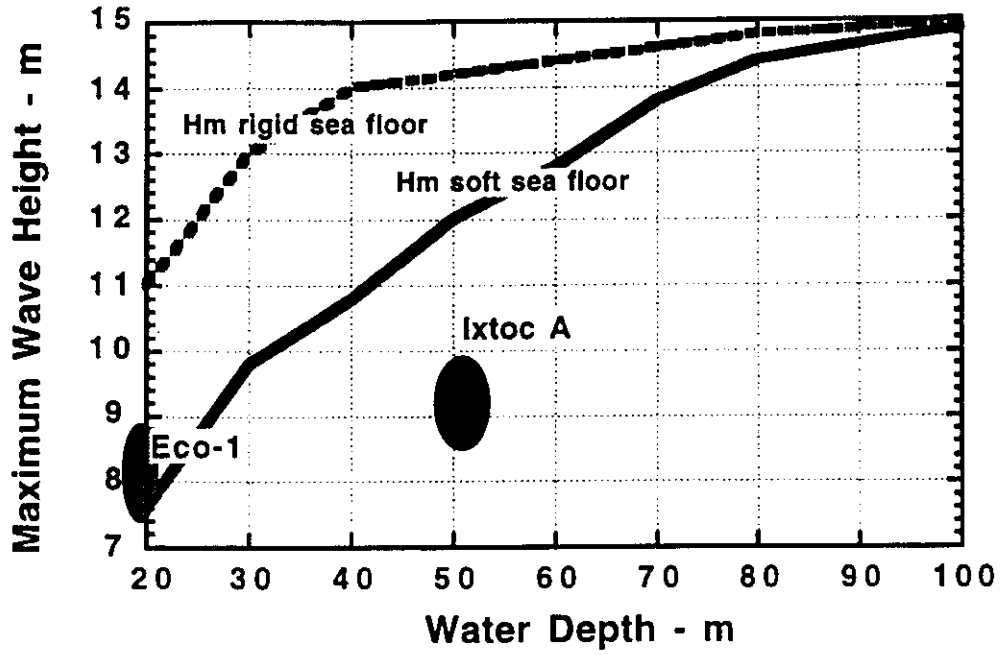

Figure 2.22 Hurricane Roxanne maximum wave height calibration

The comparison between different transects showed the influence of wave travel distance and sea floor bathymetry on wave attenuation. In the analysis, L_{10} , the distance over which wave loses 10 percent of its energy were computed by the SWBI program. For the same L_{10} , longer wave travel distance produces more attenuation. However, the influence of wave travel distance is not as significant as that of soil properties. Figure 2.17A summarizes the results of the longest path. Figure 2.17B summarizes the results of the shortest one. There is no significant difference between the wave decay patterns along them. The reason is that soft soil plays the major role in the wave attenuation. The soil conditions along the path of propagation of ocean waves are critical to the attenuation process. Wave heights at a site depend on the soil properties actually encountered along the propagation path. For an exposed site, wave direction becomes important because different directions of approach could present different soil profiles to the propagating waves.

The results in Fig 2.17 show some interesting trends for different return period wave heights. Hurricanes with different return periods, but traveling along the same transect, have the tendency to be attenuated so that the wave heights in the shallow water are almost the same. Wave attenuation caused by soft sea bottom imposes a "limit" on the wave height in shallow water. This means that the wave spectrum is "truncated". This confirms the conclusion that wave attenuation is very sensitive to deep water wave height and wave period (wave length). Longer waves interact with soil bottom more than shorter waves. Furthermore, this indicates that the variability of wave height in the shallow water is decreased dramatically due to the sea wave bottom interaction. For more intense

hurricanes, the wave attenuation starts earlier when it approaches to shallow water and the wave decays more quickly. The offshore soils absorb a large part of wave energy so that the near shore soils are protected from high strains. Figure 2.21 also presents similar interpretation. For water depth of 30m and 50m, the expected wave heights are almost the same for hurricanes with return periods of 1000 years and 10000years. The slopes in the graph from 10000-year to 1000-year are small.

Also in Figure 2.17, one can notice that at 20 meters water depth, 10000-year APR hurricane is attenuated more that 1000-year hurricane. This confirms the conclusion that longer wave with relatively lower height experience more attenuation than the shorter wave with higher height. The results also demonstrate that the soils in Bay of Campeche have very large potential to absorb the energy of incoming large ocean waves without failing themselves. This is illustrated in the maximum ratio of shear stress to shear strength, τ/Su, in the soil layers. The values were always less than 1.0, around 0.9, even for the extrapolated 10000-year return period hurricane.

For a selected wave transect, variability of wave height in shallow water is decreased. On the contrary, the rigid bottom wave height correction factor, R_m, has an increasing variability in shallow water as shown in Fig. 2.18. However, R_m involves large uncertainties of the wave attenuation in the whole region, including:

- the variability in wave direction,
- soil profiles along the wave propagating path,
- Cyclic degradation, and

- sea floor bathymetry, etc.

This results in large uncertainty of R_m in shallow water. Comparison of Figure 2.18A and Figure 2.18B turns out that R_m for 1000-year APR is a little smaller than 100-year APR. But the difference is not too large. It implies that the variability of R_m is small with respect to different hurricane intensity.

Examining the wave height decay curves, one can find some unusual changes in certain curves. Generally, this implies a change of soil profile at that station. Some of the changes are so abrupt that analysis program can not linearize them properly. To solve this problem, one can add more incremental intervals, or even interpolate an intermediate soil profile to smoothen the abrupt change. However, too small intervals may result in more computing time and sometimes difficulties of numerical converge during the nonlinear search. This problem is unavoidable for a continuum model in the analysis. For most cases, the influence of these kinks is small and overshadowed by other assumptions used in the analyses. However, these kinks do reflect the actual field soil behavior considering the fact that soil profiles may have great change over a very short distance.

In the parametric analysis, three versions of soil profiles gave a reasonable range of forecast wave height. As a sensitivity study, some extreme soil conditions were also used in the analysis, such as a Gmax/Su value as low as 30 and the top layers shear strength of 20-50pcf after the degradation due to cyclic wave loading. Although these are considered unlikely, the results did demonstrate the potential of very large amounts of wave

attenuation when deep water wave energy propagates in shallow water over soft sea bottom in this region. Actually, there is great uncertainty in the ratio of Gmax/Su. For a extreme case, Schapery and Dunlap once suggested this initial shear modulus ratio, Gmax/Su, to have a value of 32 at the site of Boring 1 in South Pass 57 in the Mississippi Delta(1979).

2.3.2 Wave Decay Analysis in the North Region

Unlike the situation in the south region, where there are a lot of boring logs from soil investigations, there is no such a database in the north region. This is another reason why we chose three representative soil properties in the study. Although unlikely, the soil properties are assumed to be of the same soil profiles as a reliability approach. By this approach, three cases can be derived: weak soil transects, strong soil transects and expected soil transects. This is intended to capture the mean, upper bound and lower bound of the sea floor soils' response to the propagating waves. Different combination of soil types along the wave transects from deep water to shallow water, such as strong-weak-weak, strong-expected-weak were also studied. This study analyzes about 30 cases with different wave, soil and bathymetric conditions.

2.3.2.1 Presentation of the Analysis Results

Around 100 runs of the SWBI program yielded a large amount of output data that are summarized in the following figures. The calculation results along S-S transect are summarized in Figure. 2.23a - Figure 2.23e, with different soil strength profiles, different G_{max}//Su values and different return period wave conditions. According to the results,

there is little soft sea floor wave attenuation along this transect in the water depth range of 60-200m. The soft sea floor effects become notable in shallow water with a depth less than 60m. Figure 2.24a - e summarizes the similar analysis results for N-N transect. Noted that the wave attenuation patterns with respect to the depth are different from those in the S-S transect. They are much smoother, without a drastic drop in the depth range of 40-60 meters.

There is evidence that the oceanographic characteristics in the deep water are not uniform in the north region. Besides the deep water wave heights and periods stated in Table 2.3, some new characteristics are also studied. The 100-year ARP hurricane has a maximum wave height of 19.0 meters and a wave period of 13.4 seconds. The 1000-year hurricane has a maximum wave height of 25.7 meters and a wave period of 15.5 seconds. For these cases, the wave height forecast for the expected soil properties are plotted in Figure 2.25 and Figure 2.26.

As to the combination of different soil properties along a wave transect, the S-S transect was taken as an analysis example because it has more intensive soft sea floor effect than the N-N transect. The results comparing these different combinations are summarized in Figure 2.27.

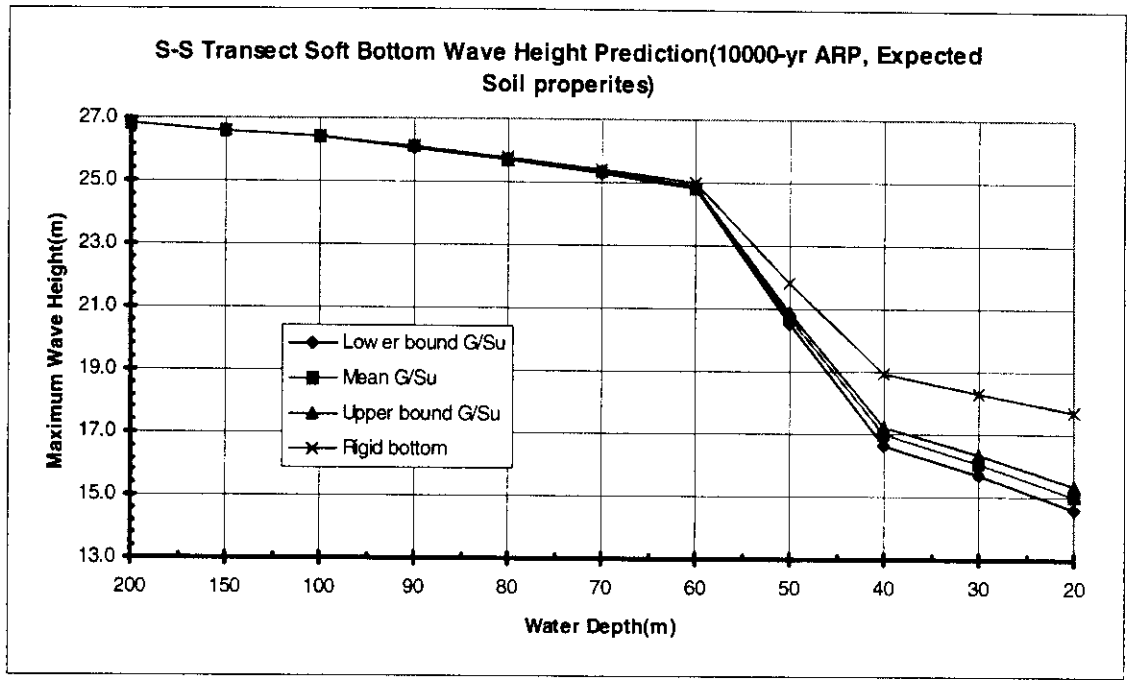

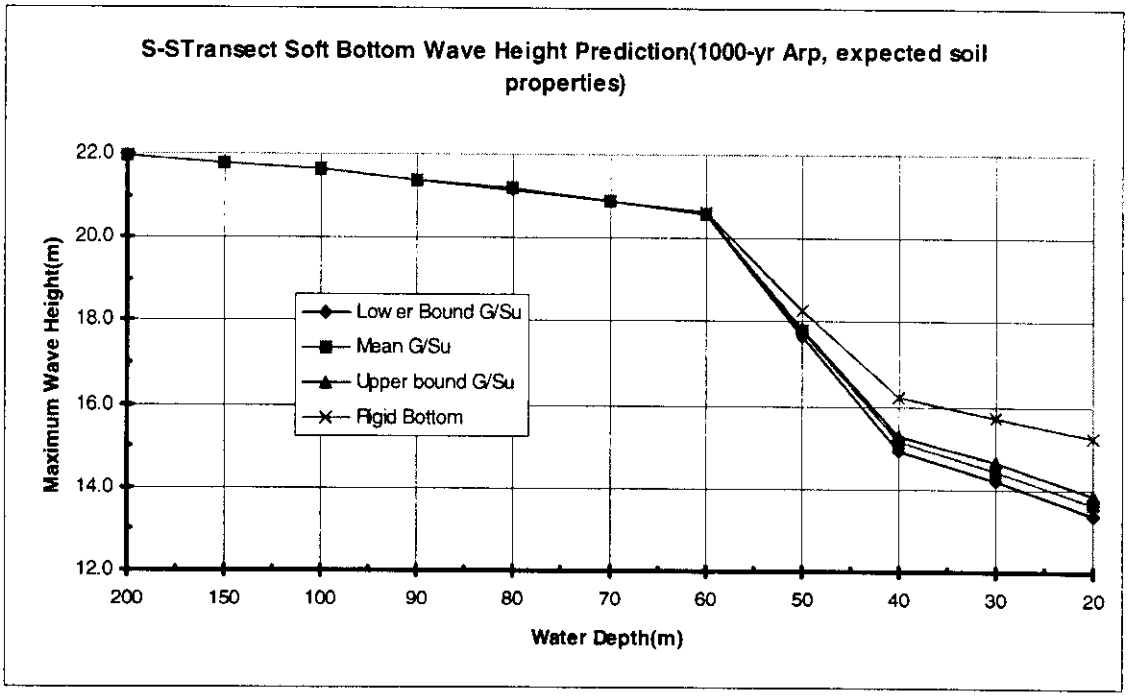

Fig 2.23a Wave height prediction at S-S transect with expected soils for the 1000 and 10000 years ARP hurricanes

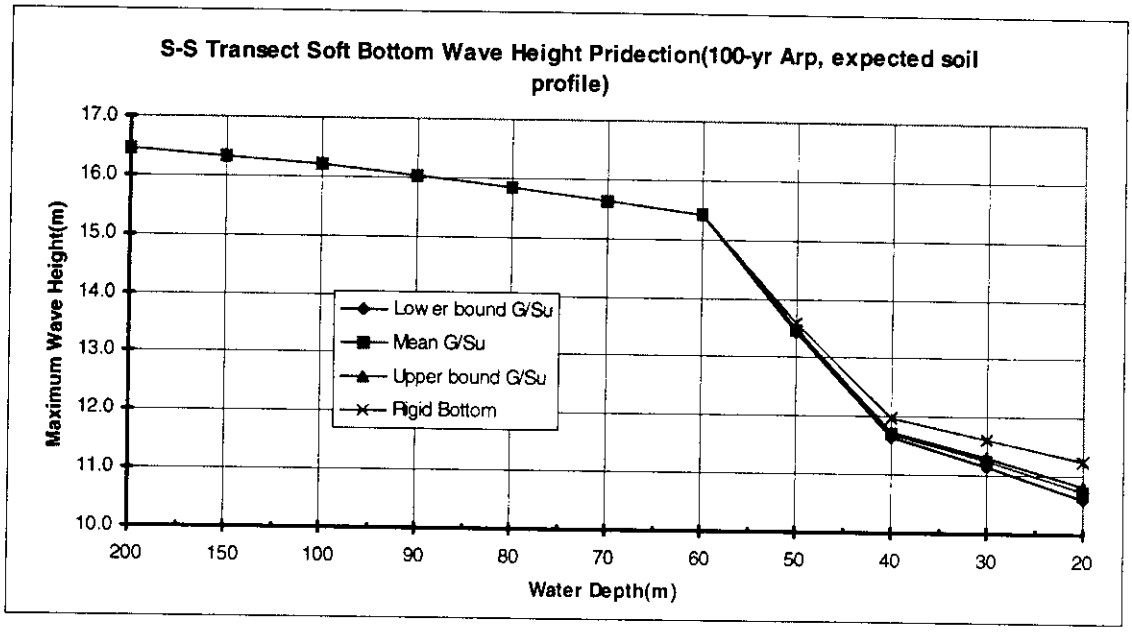

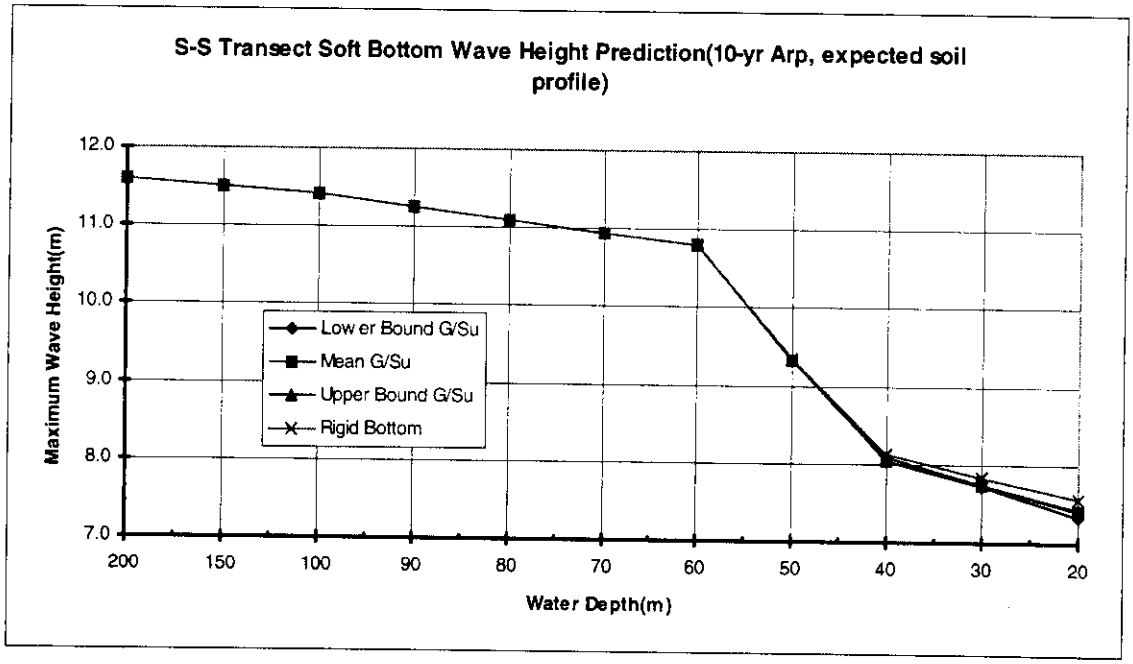

Fig. 2.23b Wave height prediction at S-S transect with expected soils for the 10 and 100 years ARP hurricanes

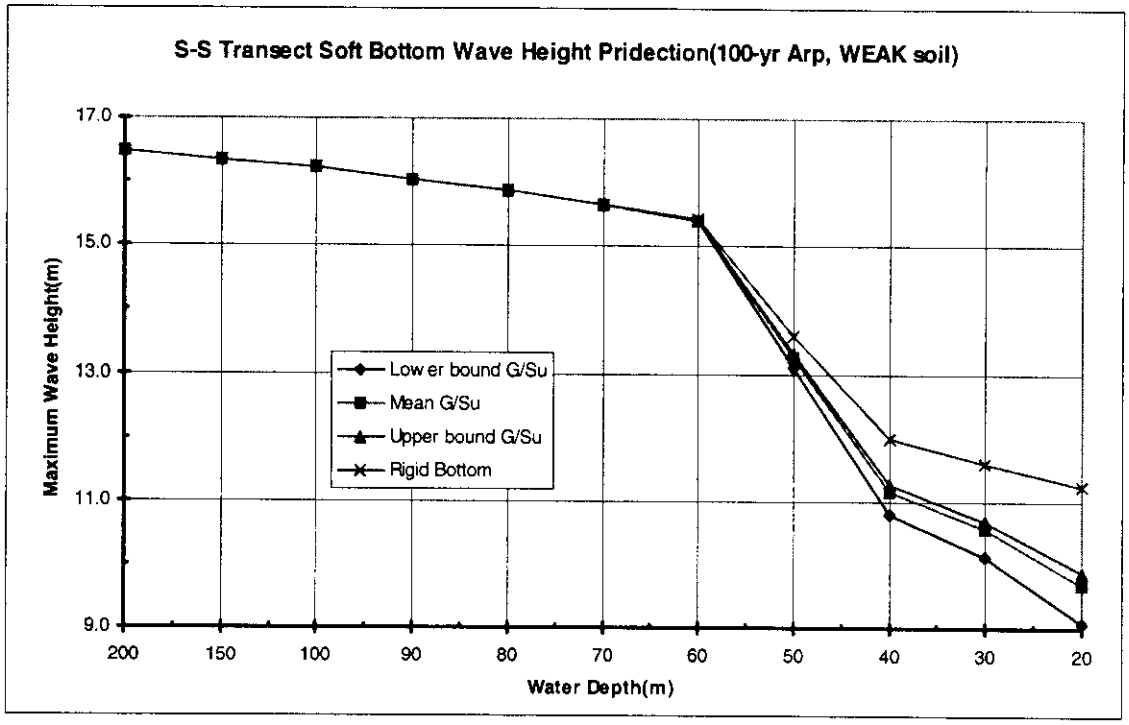

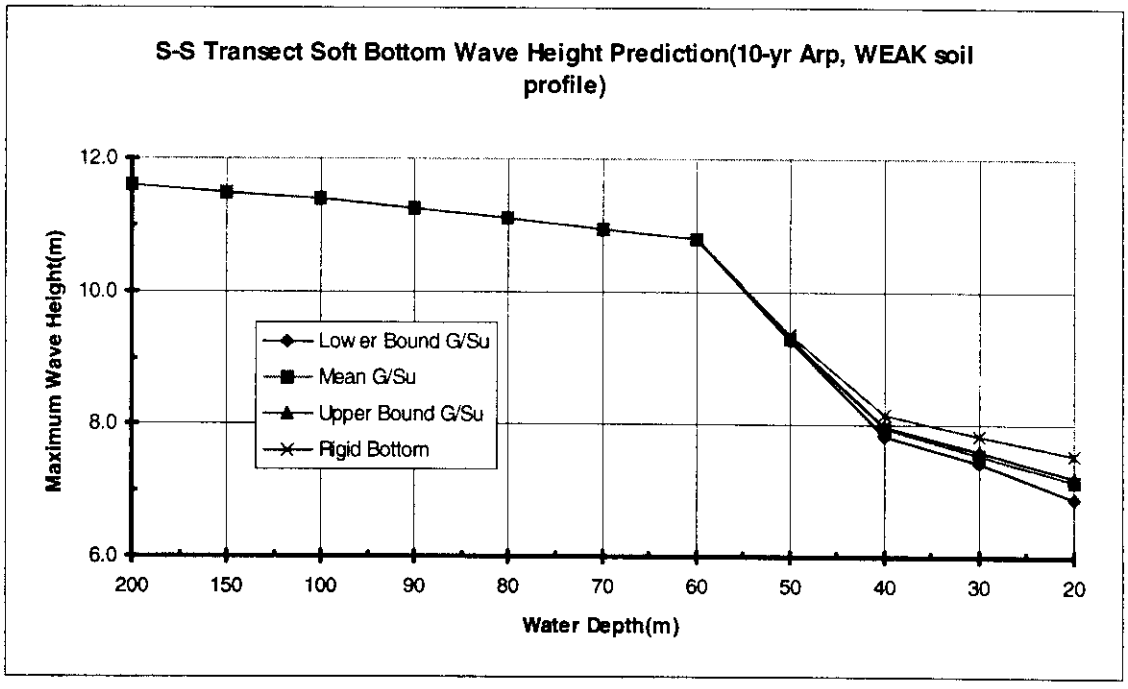

Fig. 2.23c Wave height prediction at S-S transect with weak soils for the 10 and 100 years ARP hurricanes

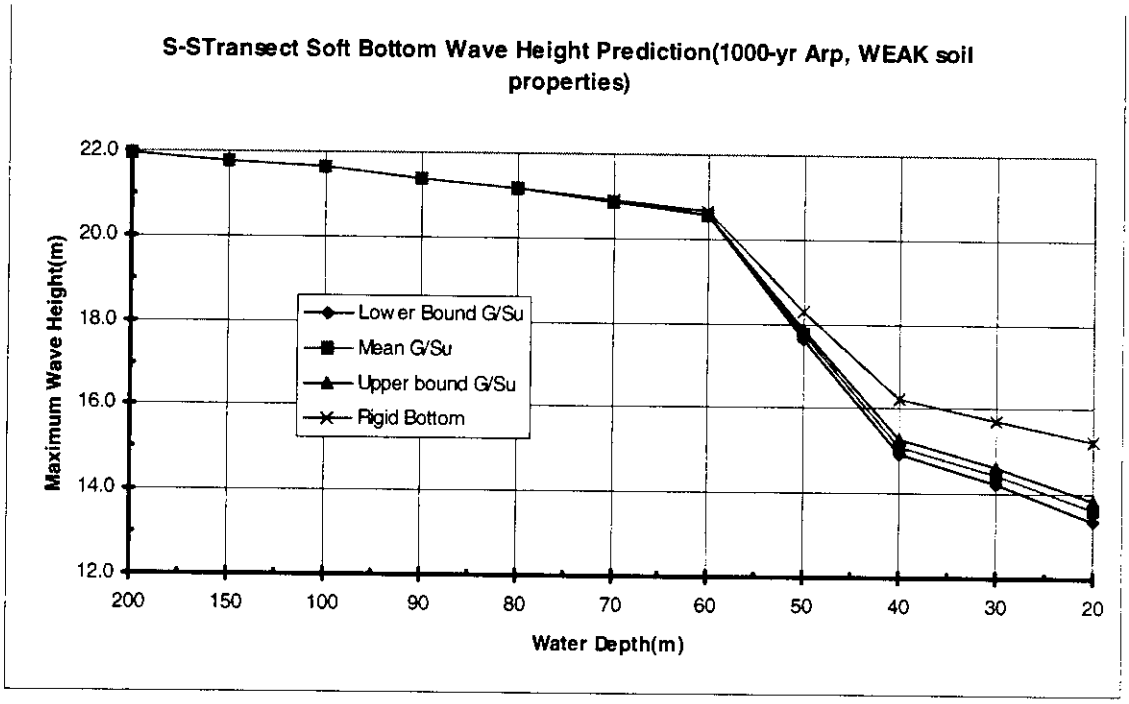

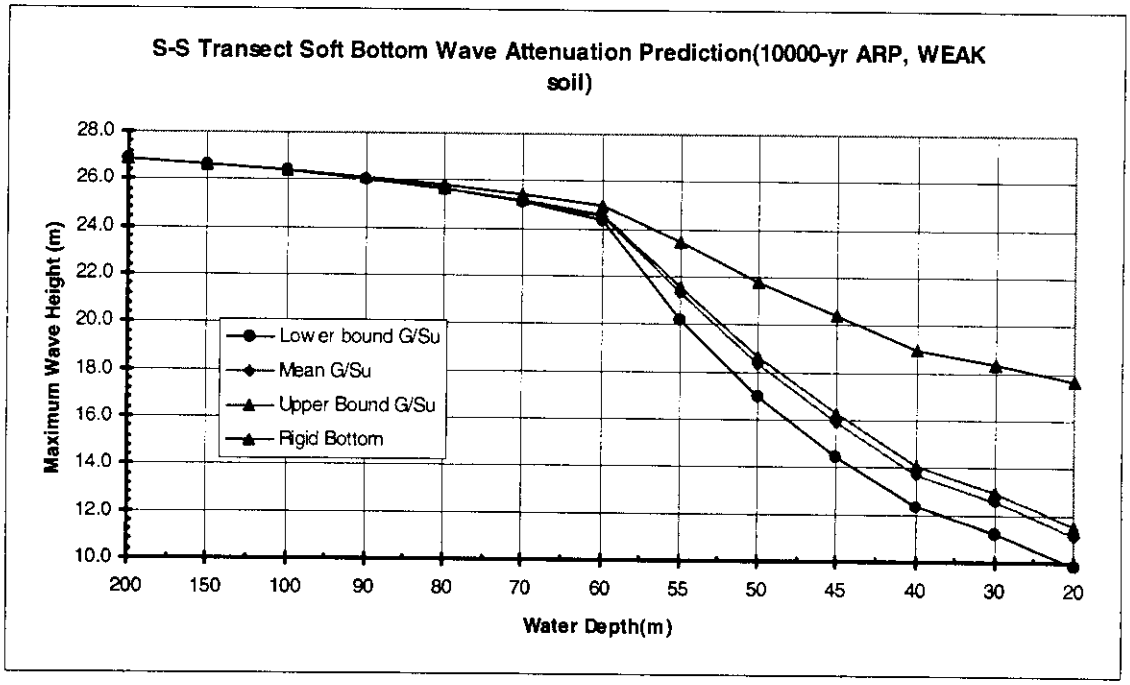

Fig. 2.23d Wave height prediction at S-S transect with weak soils for the 1000 and 10000 years ARP hurricanes

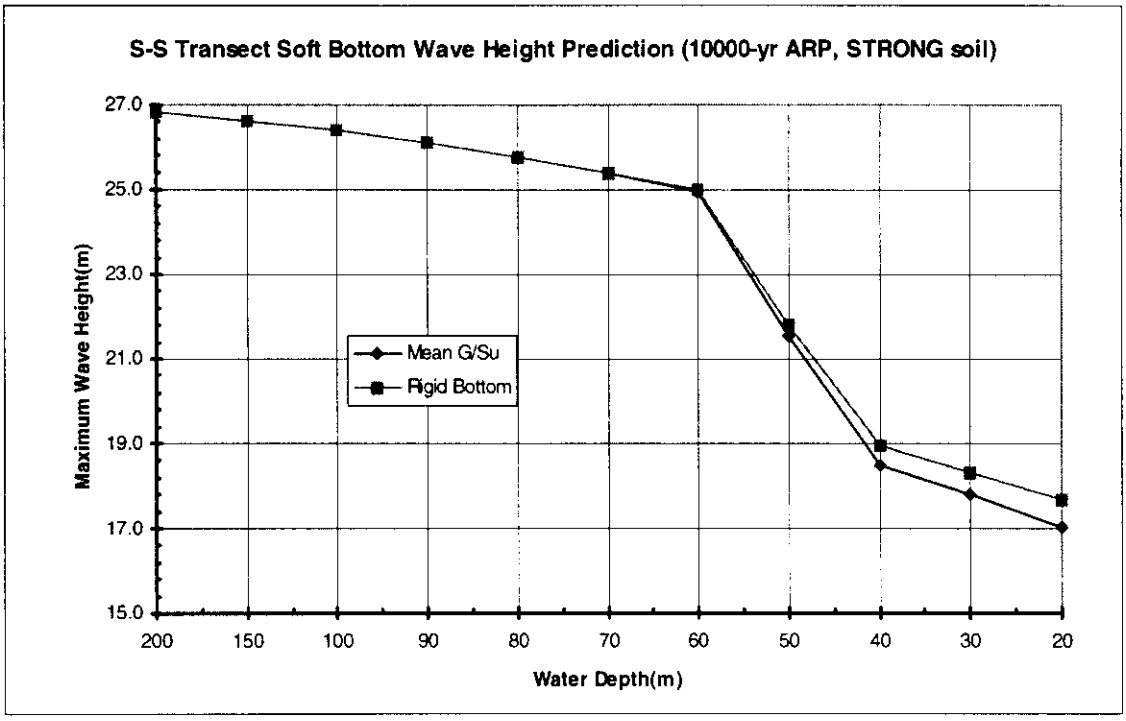

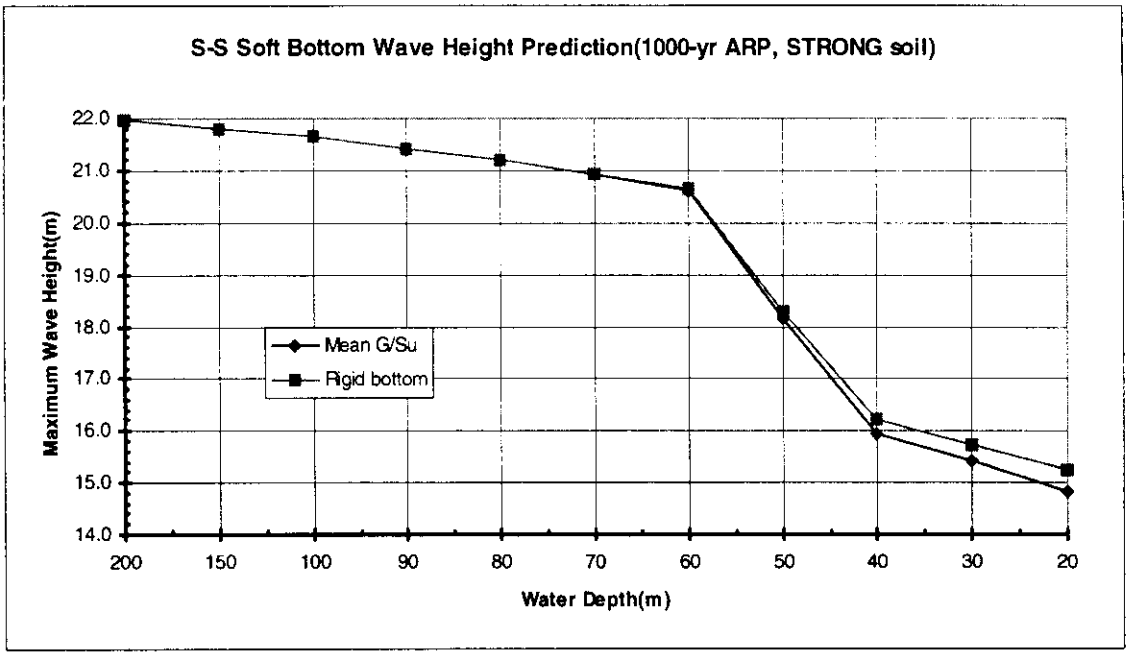

Fig. 2.23e Wave height prediction at S-S transect with strong soils for the 1000 and 10000 years ARP hurricanes

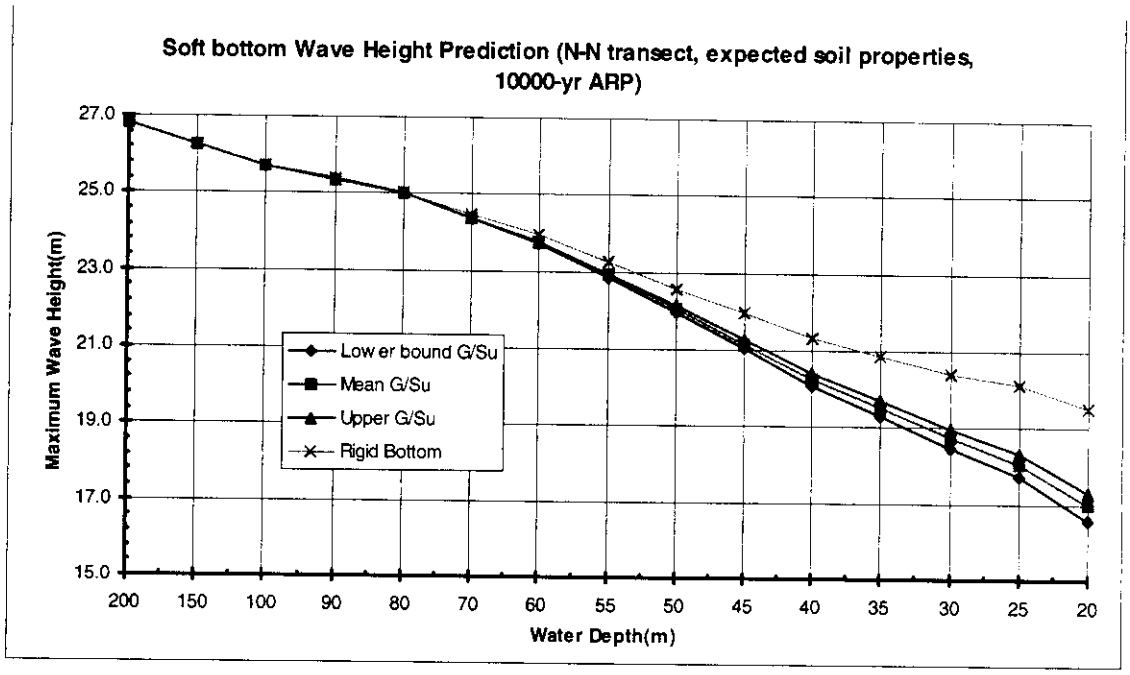

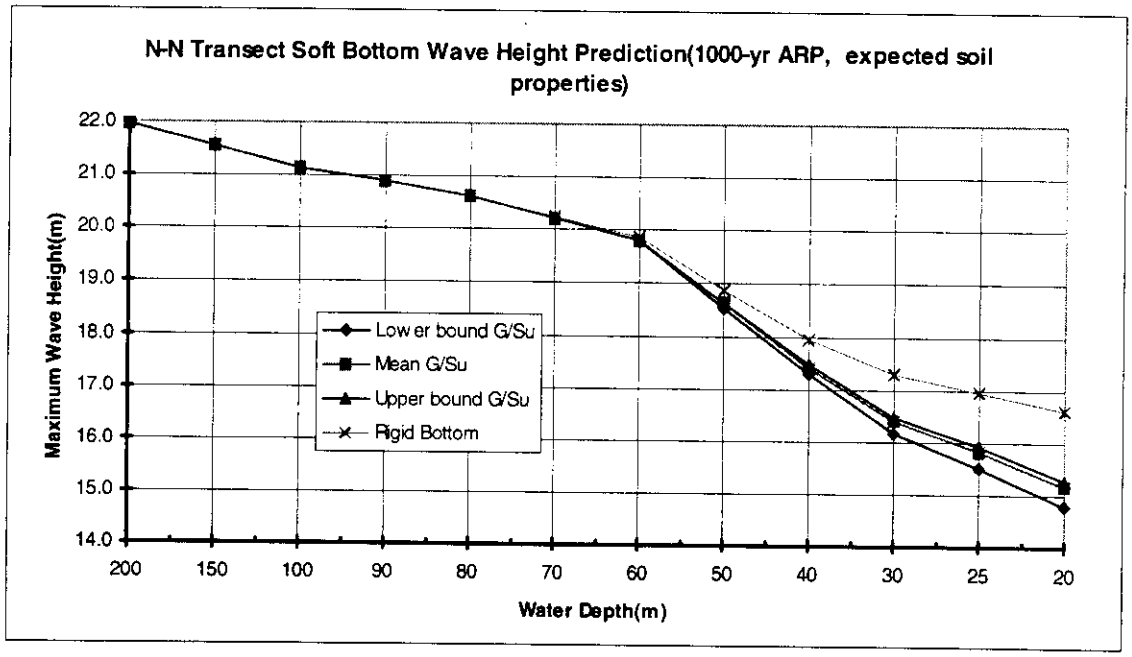

Fig. 2.24a Wave height prediction at N-N transect with expected soils for the 1000 and 10000 years ARP hurricanes

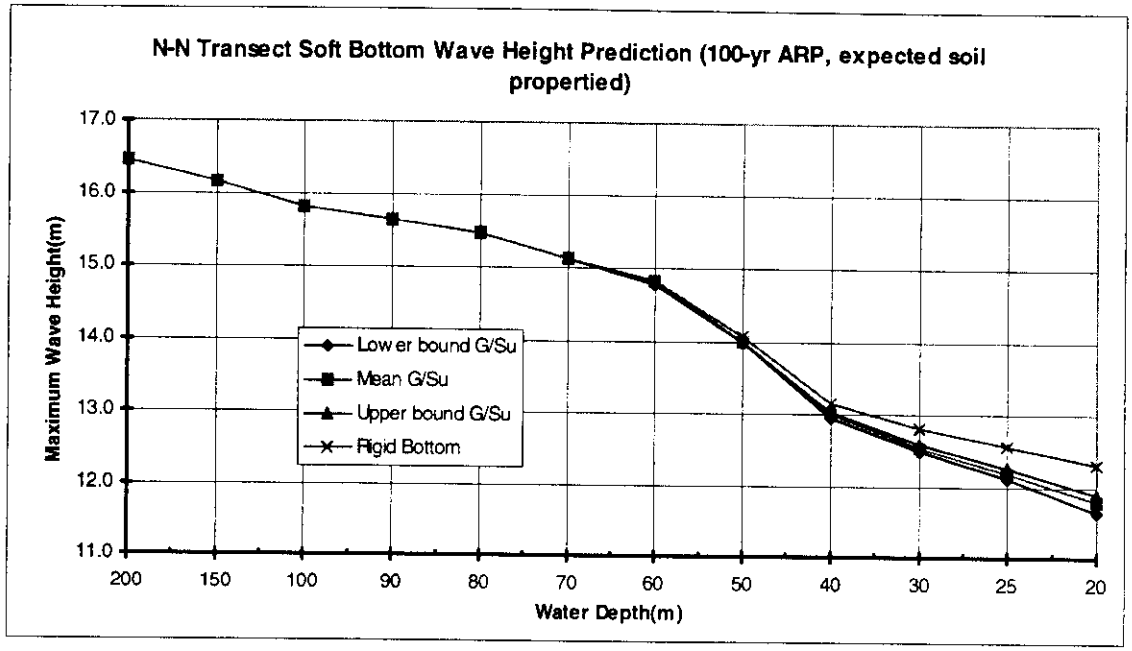

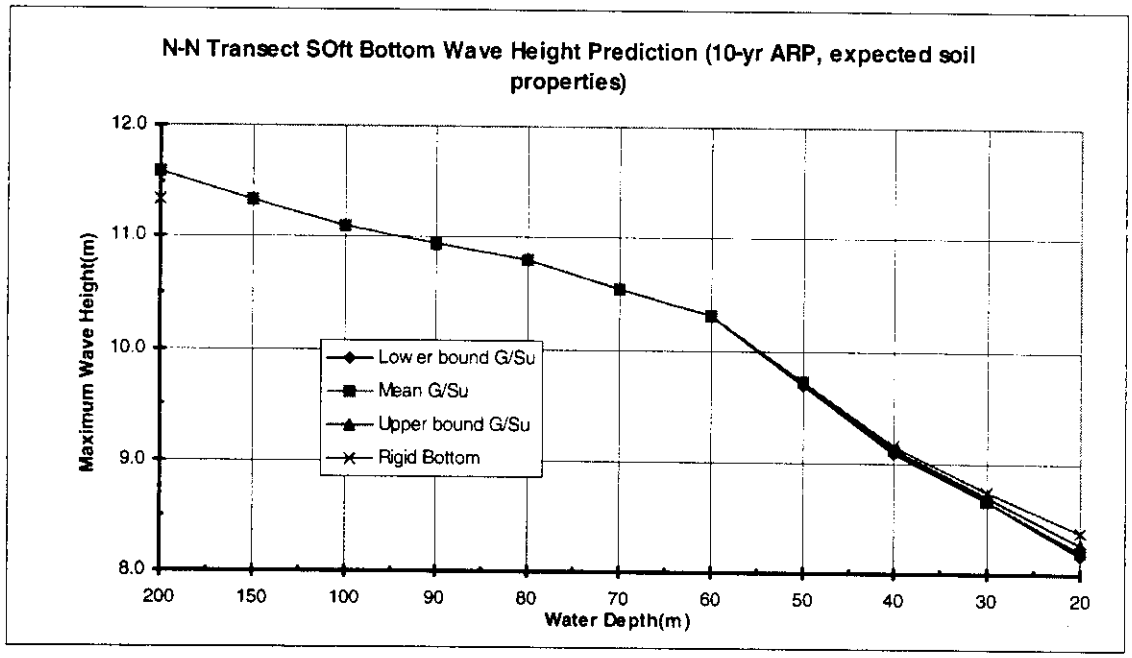

Fig. 2.24b Wave height prediction at N-N transect with expected soils for the 10 and 100 years ARP hurricanes

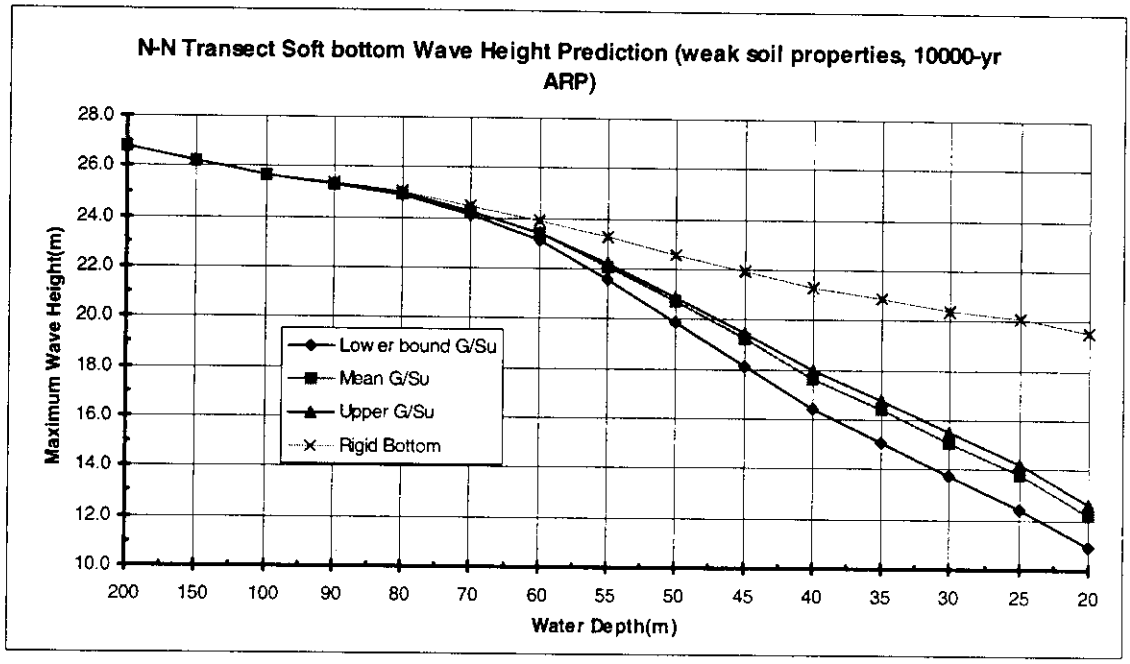

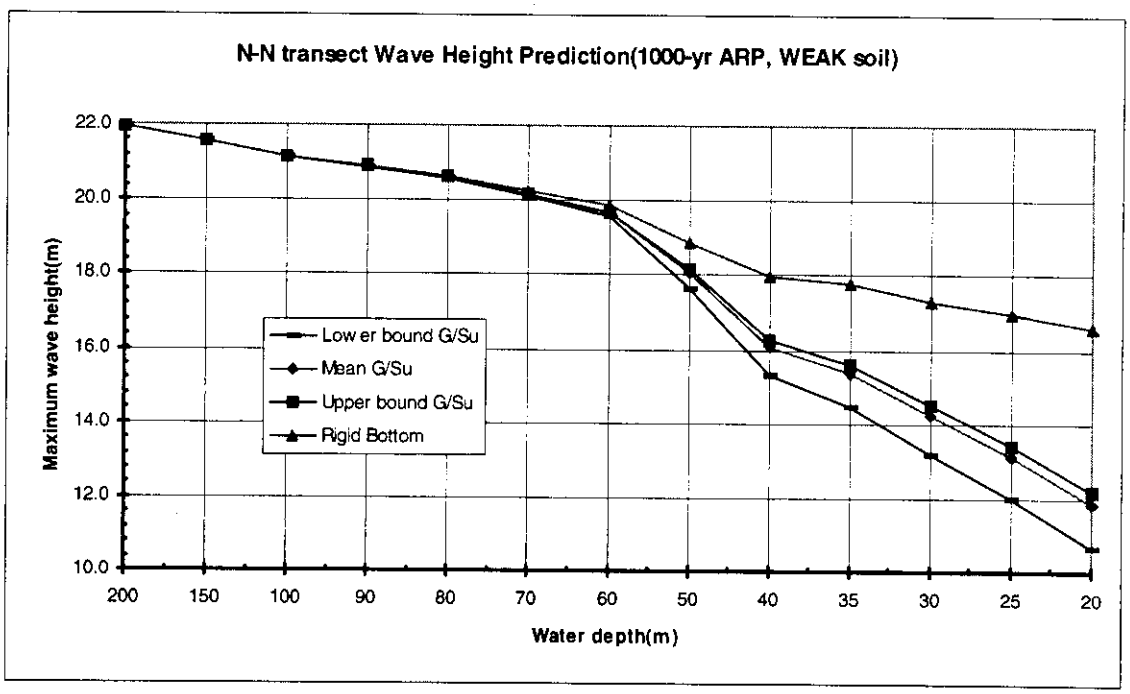

Fig. 2.24c Wave height prediction at N-N transect with weak soils for the 1000 and 10000 years ARP hurricanes

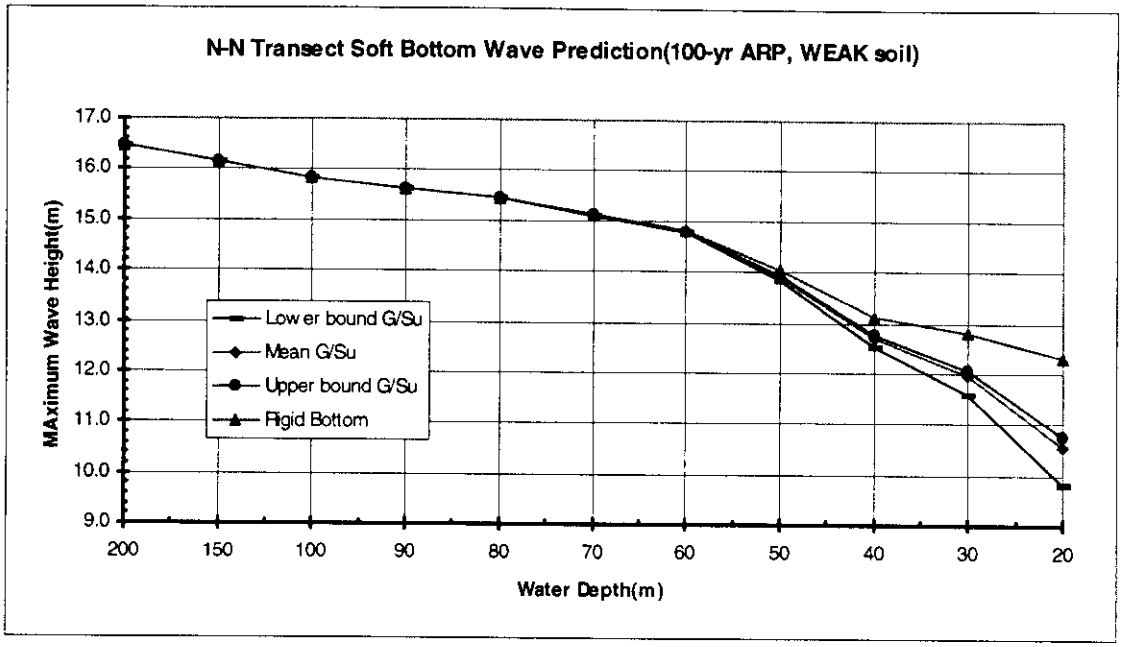

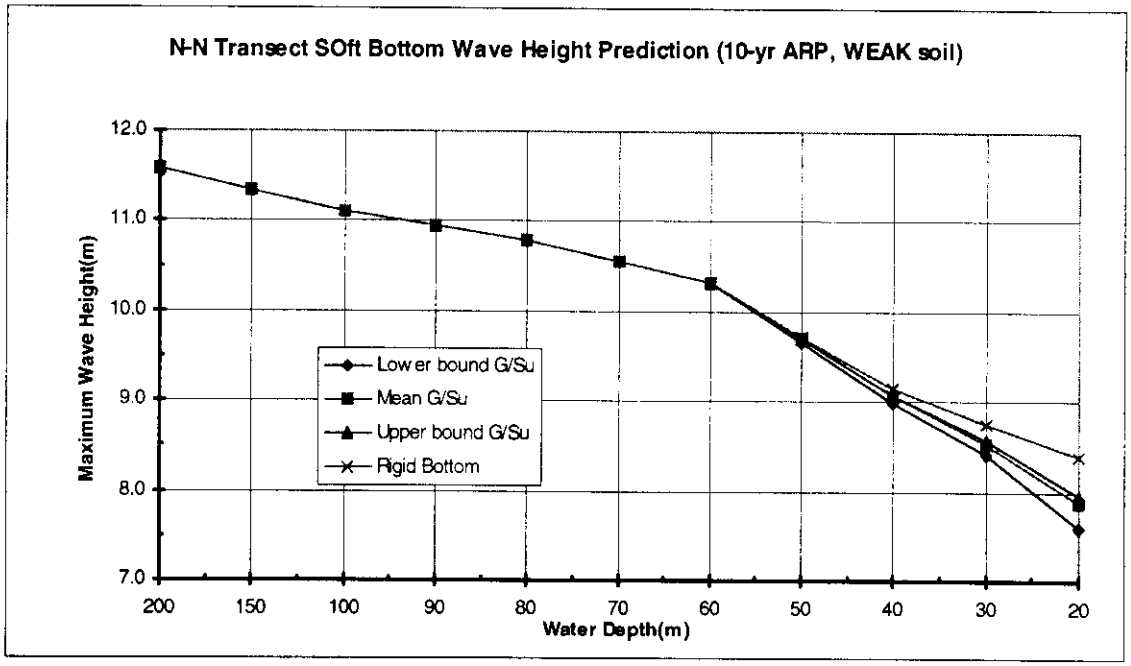

Fig 2.24d Wave height prediction at N-N transect with weak soils for the 10 and 100 years ARP hurricanes

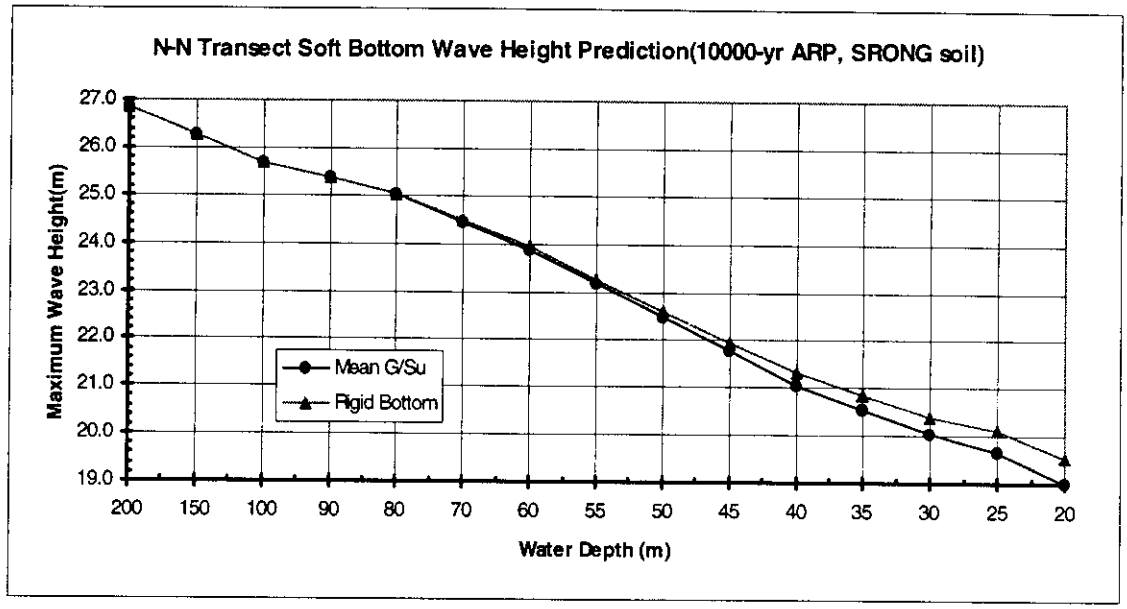

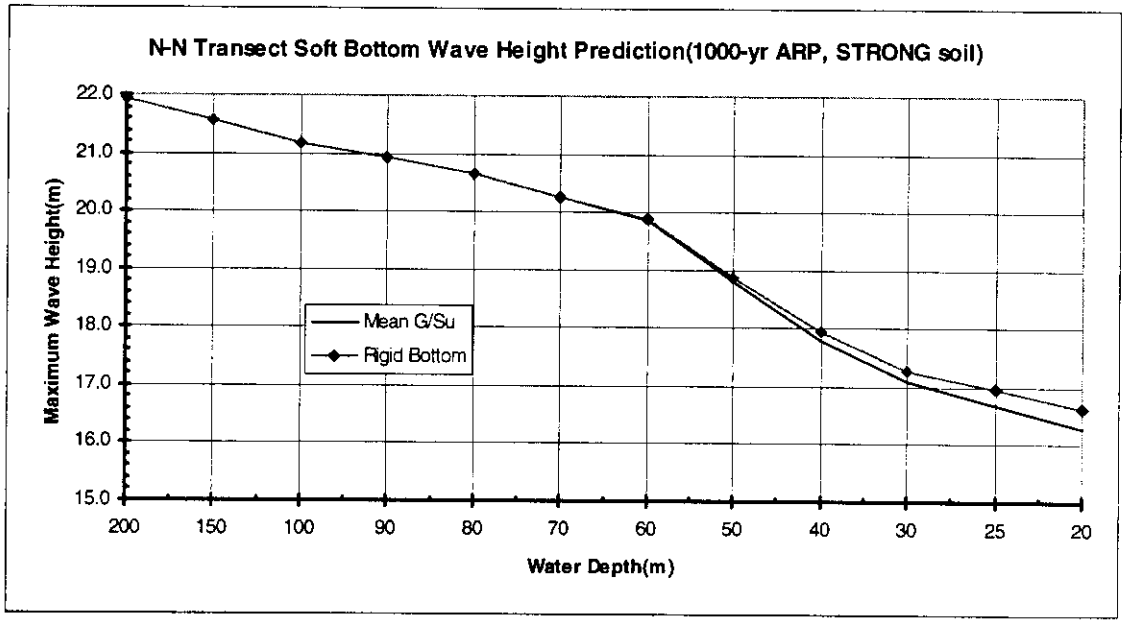

Fig. 2.24e Wave height prediction at N-N transect with strong soils for the 1000 and 10000 years ARP hurricanes

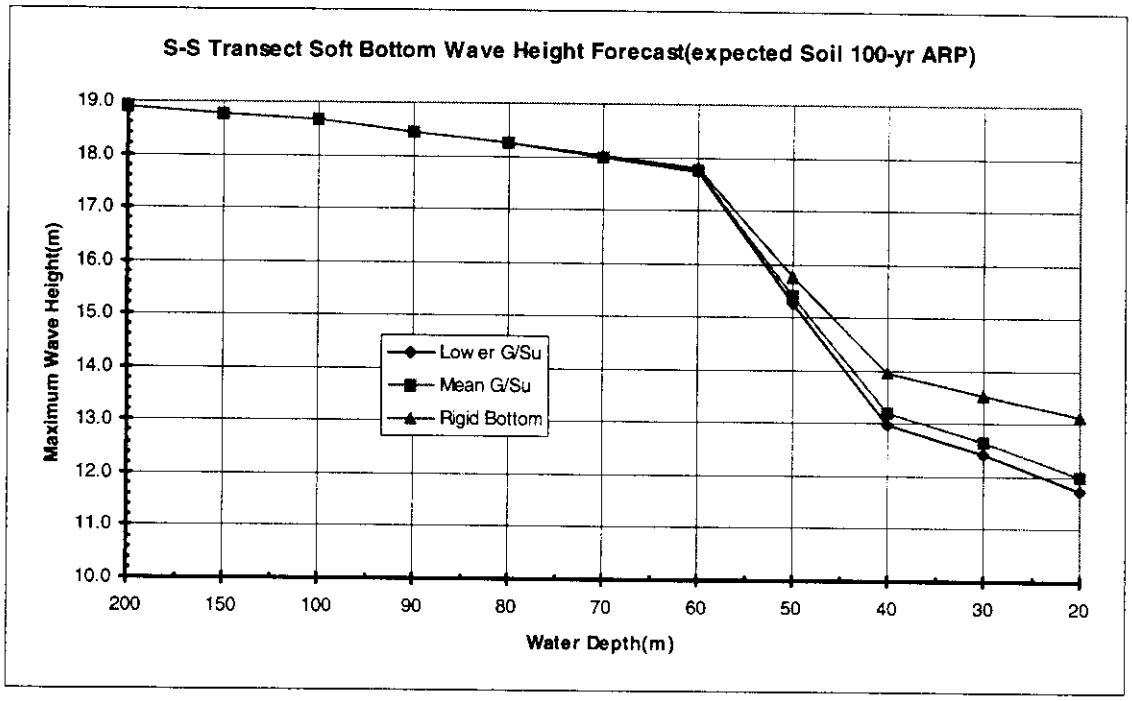

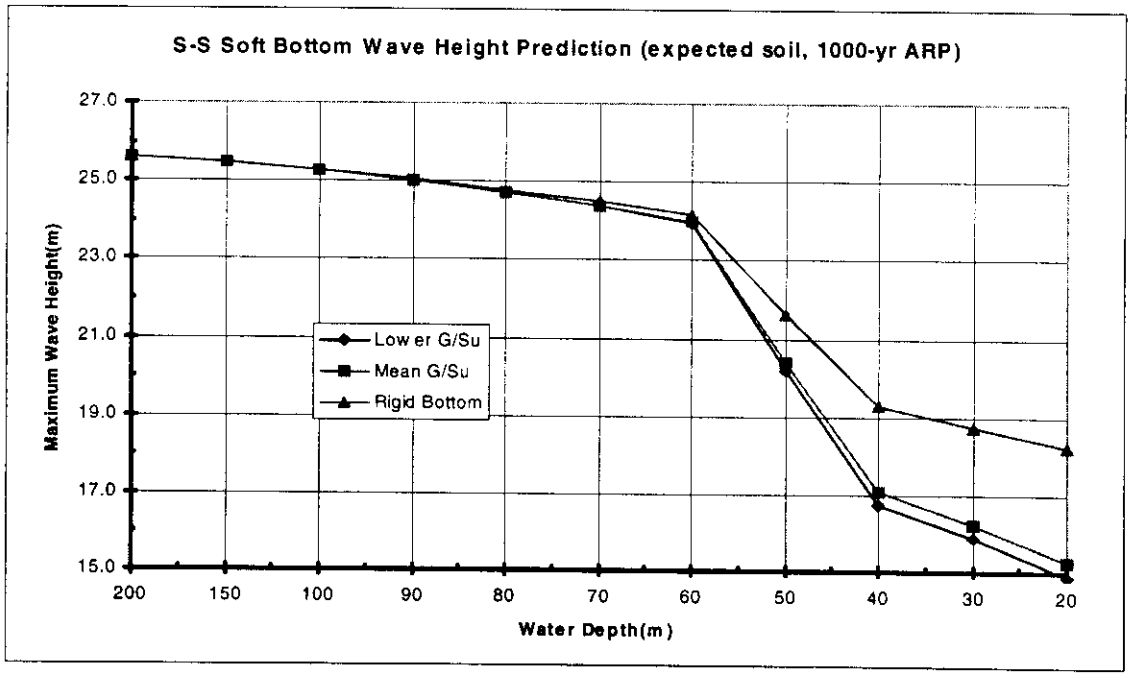

Fig. 2.25 Wave height predictions at S-S transect with expected soils for the 1000 and 100 years ARP hurricanes with new deep water characteristics

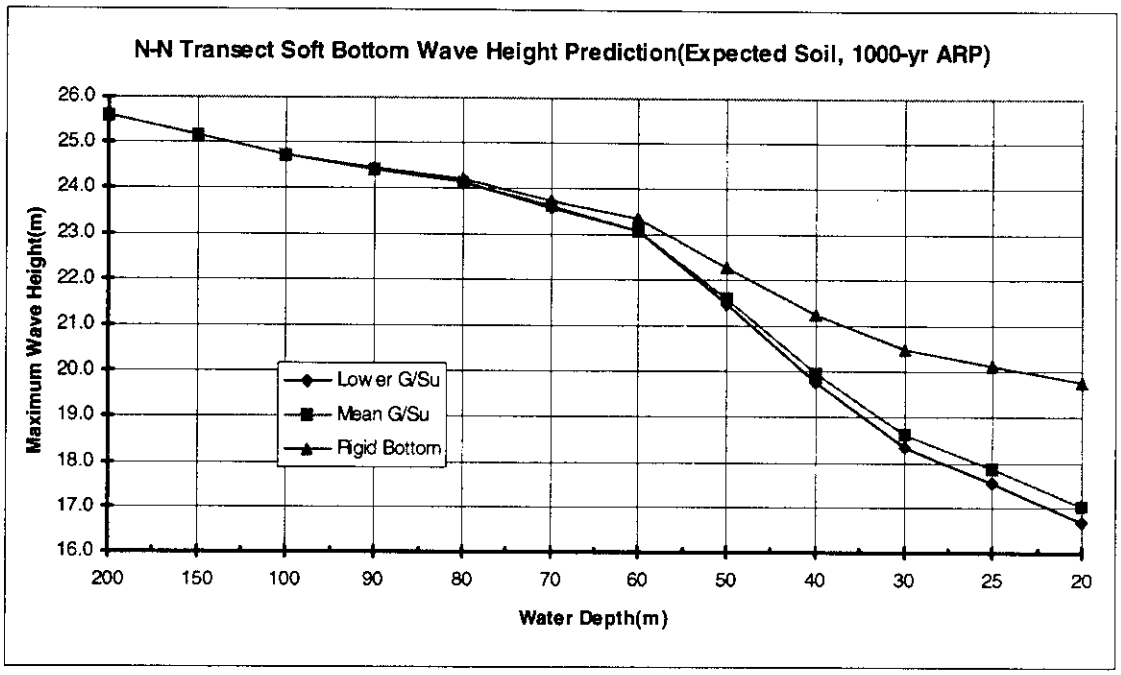

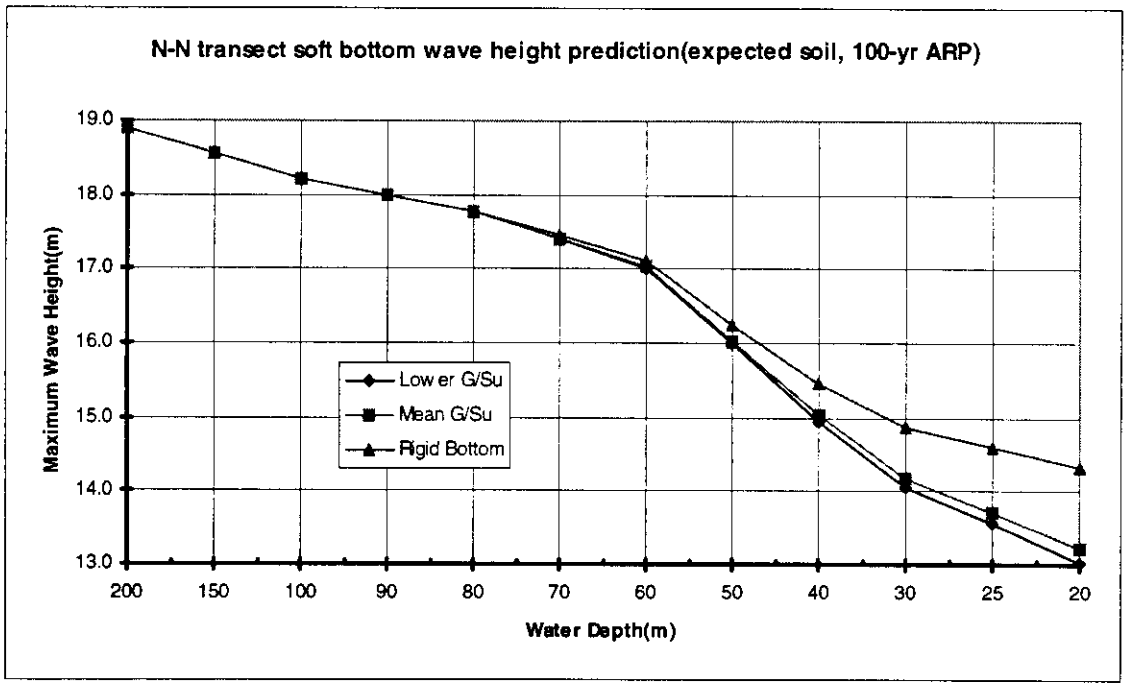

Fig. 2.26 Wave height predictions at N-N transect with expected soils for the 1000 and 100 years ARP hurricanes with new deep water characteristics

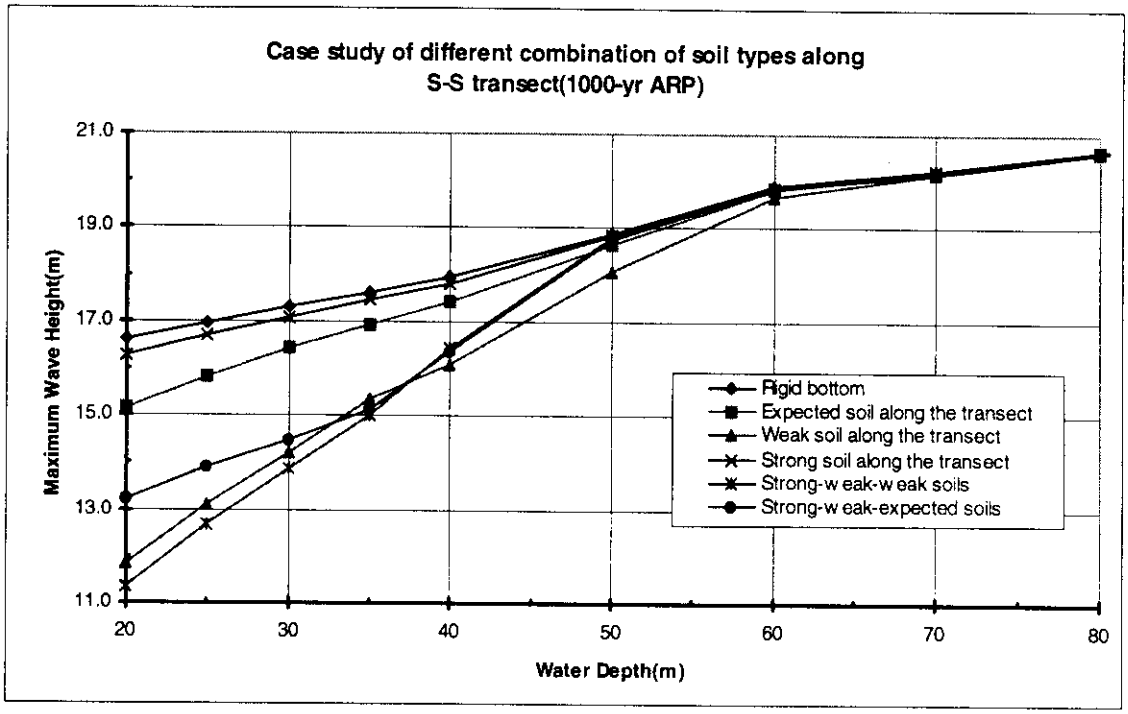

Figure 2.27 Wave height predictions at S-S transect with different combination of soil types for the 1000 years ARP hurricanes

2.3.2.2 Discussion of the Analysis Results

Based on the analysis results summarized above, there is some degree of soil sea floor wave attenuation in the north region. But it can be seen that the wave attenuation due to the sea wave bottom interaction is not as intensive as in the south region.

The SWBI model does not predict a large amount of wave attenuation due to soft sea floor when the wave propagates from deep water to shallow water for the expected and strong soil profiles. For the strong soil profile, there is almost no difference between the rigid bottom forecast and the soft bottom forecast. In this case, the soils are so strong that they are not highly strained by the wave pressures. This can be seen by comparing the results obtained by specifying different values of Gmax/Su. They are almost the same.

This is another difference from the wave attenuation in the south region, where the wave decay patterns are quite sensitive to the values of Gmax/Su. The Gmax/Su almost has no effects in the north region, given the expected or strong soil conditions. The reason for this is that the top layers of very soft soil are thin. The cyclic degradation of these layers have little impacts on the total wave attenuation, while the deeper layers of stiff clays have high resistance to wave induced shear stresses. The total attenuation coefficient is almost the same for different values of Gmax/Su. In all the cases for strong and expected soil profiles, the largest wave attenuation due to soft sea floor is 2 meters in wave height, which is relatively small compared with the total wave height. This small difference can be regarded as unimportant in the reliability model. The natural variation of other factors can easily overshadow this soft sea floor effect in the final reliability evaluation results.

There are also differences between the wave decay patterns at the N-N and S-S transects after the sea floor effect is taken into account. Considering the fact the soil profiles are the same in both transects, these difference can be credited to the bathymetric differences along the transects. This conclusion implies that the influence from other factors such as sea bottom friction, shoaling and wind are decisive in the North Region.

However, for the weak soil profile, which has similar Su values to that in the south region. The soil effect factor K_m has notable influence on the wave height, just the same as what happened in the south region. The Gmax/Su for this case also has great impacts on the K_m, thus significantly reducing the wave heights in the shallow water. The maximum magnitude of such reductions is 7 - 8 meters. These values are comparable to

the sea bottom wave interaction in the south region, though a little smaller. Considering that the wave transects in the north region are shorter than those in the Bay of Campeche, these results are quite reasonable. Given the presence of weak soil profiles, the soils again become the dominant factor in the shallow water wave decay pattern. Gmax/Su still plays a major role in this case.

The weak, strong and expected profiles do not represent a very large variability in S_u, but they result in quite different wave attenuation. This result indicates that there could be notable attenuation due to soil movement if one has an extreme case of the weak soil with relatively lower S_u in the north region. Although this is not a likely case according to the soil boring data in the north region, this parametric study shows that there is possibility of large wave attenuation in the north region. Meanwhile, it is emphasized that for the normal cases, the soils in the north region would not induce large amount of wave energy dissipation. The soft sea floor effect is not manifest here.

Examining the results for 10000-year ARP hurricanes in both the N-N transect and S-S transect, another exception for extreme case can be found. The attenuation due to the soft sea floor are notable. This implies that the soils in the North Region are not strong enough to resist the very intensive hurricanes. They will be forced to move by the wave pressure, coupling with the movement of the water and thus reducing the wave heights.

As a parametric study, a few more runs of SWBI program which combine the different soil profiles along a transect are also made. The logic for these runs is that the soil

properties do not keep unchanged through a whole wave transect. Usually there is a tendency that soil strength is stronger in the deep water and weaker in the shallow water. The soil strength and other properties may change dramatically in a short distance, just as what happened in the south region. The results in Figure 2.27 show that the lowest wave height can be predicted for the case of a combination of strong soil - weak soil - weak soil profiles along S-S transect. But the difference between the result from a weak-weak-weak transect is very small. This indicates that the weak-weak-weak transect does capture the lower bound of the wave attenuation due to the soft sea floor effect.

2.4 Summary and Conclusions of Wave Attenuation Analysis

The analyses of wave decay patterns in the Bay of Campeche has improved the understanding of the characteristics of sea bottom wave interaction in this area. Wave attenuation caused by sea bottom wave interaction is affected by wave height; wave period; shear resistance, shear modulus, and other properties of the soils; and sea floor bathymetry. Among them, soil properties are the most important.

Because of the coupling movement of water and soil, the wave attenuation can be related to the maximum stress level induced in the soil. The attenuation rate is very sensitive to the stress level in the soil. The maximum stress level includes the influence of wave height, wave period, and soil characteristics. The stresses induced by ocean waves vary throughout the soil mass, and the maximum shear stress in an element of soil varies in a nearly sinusoidal pattern along the wave length at a given depth.

The actual wave attenuation also depends on the time history of wave loading on the sea bottom as well as the soil's sensitivity to degradation of stiffness and strength with cyclic loading. Variation in the shear modulus, shear strength, and hysteretic damping characteristics of the soft soils over the path of wave propagation are quite important in the attenuation of waves, especially in water depth less than about 90 meters.

Based on the study of sea wave bottom interaction in the Bay of Campeche, the south region area does have very soft soils that are responsible for large amount of wave attenuation and mud movement during ocean storms. This interaction is not a negligible factor for the wave height forecast in shallow water. The rigid bottom wave height correction coefficients are developed for different water depths in this study. This correction factor summarizes the wave attenuation effects for the Bay of Campeche. This means that there is a significant correction of the extreme ocean wave loading conditions for the reliability analysis of the platforms in this region. This implication has been incorporated into the development of the design and re-qualification criteria of platforms in the Bay of Campeche.

In the north region, wave decay patterns are also affected by wave height; wave period; shear resistance, shear modulus, and other properties of the soils; and sea floor bathymetry. Unlike the situation in the south region, the major factors are sea floor bathymetry characteristics in the region. However, as an extreme case, if the soils are degraded to the extent that they exhibit the similar behavior as those in the south region, there is a possibility that the large amount of soft sea floor wave attenuation occurs. The

analysis results are helpful for the quantification of the uncertainties in the ocean environmental loading conditions in this region. The forecasted wave heights associated with the extreme loading cases in the reliability analysis are incorporated into the design and re-qualification criteria developed for the north region.

Chapter 3

Analyses of Pile Dynamic Response

3.1 General Background of the Analysis

In the field of Offshore Engineering, foundation design is an essential element for fixed platforms. General engineering guidelines for treatment of this problem are still under development and subject to updating. High quality experimental and analytical research needs are highlighted.

3.1.1 Review of the Current Research

Pile foundations are a classical research subject in the design and construction of offshore oil drilling platforms. Realistic modeling of pile foundations is crucial to the validity of the results of static and dynamic structural analyses of offshore platforms. Furthermore, the comprehension of both the static and dynamic response of a single pile to the external loading is the cornerstone for all the analyses in the field. The state-of-art design technique and theory concerning pile foundation is still under development, though there have been extensive research effort on this topic. In the past, foundation failures were often predicted to be the dominant failure mode of platforms. However rarely have the observed failure modes included failure of foundation elements. This fact indicates that the traditional methods of predicting the ultimate capacity of pile foundations are in general conservatively biased.

The state-of-practice design criteria for pile foundations are generally founded on a static or pseudo-static approach. To keep the analysis tractable in interpreting of complicated pile-soil interaction phenomenon, this kind of method has several simplifying assumptions:

- The capacities of offshore piles can be calculated using methods based primarily upon tests of relatively short onshore piles that were loaded slowly to failure, i.e. the validity of the method are usually correlated to the static loading test;
- Pile capacity reductions due to the degradation of soil resistance by cyclically applied loading do not need to be considered explicitly; and
- Pile capacity increase that can occur in clay soils during rapid loading also does not need to be considered explicitly.

Static pile-capacity methods have been used to determine the pile foundation configuration for the pile foundations of the more than 10,000 offshore platforms that are now located on the world's continental shelves. These foundations have had a remarkable record of reliability. The American Petroleum Institute (API) has developed guidelines for evaluation of the capacity of the pile foundations (API RP2A, 20th edition 1993). These guidelines address operating and environmental loading; determination of static capacity; influences on capacity, stiffness; applications of discrete element and continuum analytical models; use of in situ and laboratory soil test and prototype pile-load tests in soil characterizations; evaluation of load, resistance, and deformation characterizations at serviceability and ultimate limit states; and interpretations and

applications of results. These guidelines represent the culmination of a 20-year development effort of worldwide research regarding pile foundation performance.

However, as stated in the principal assumption of the static-capacity calculation method, two important factors, which affects the in-situ performance of pile foundations are not addressed: the loss of strength and stiffness of the pile-soil system due to cyclic loading, which is obvious in the wave loading during a storm; and the increase of strength and stiffness due to the high loading rate effects, which is typical in earthquakes and storms. Bea (1984) summarized trends that have been observed of piles tested for these two effects. Load rate effects can result in effective increases in pile strength and stiffness on the order of 20% to 80% for loading rates consistent with wave action. Assuming the trend continues without degradation, the expected increases for earthquake loading rates would be much higher, shall be to the order of 2-3. Cyclic loading tends to result in progressive deterioration of pile foundation strength and stiffness. Hysteresis curves generated for piles will tend to exhibit pinching and softening for repeated cycles. Tests have shown that the soil support for the pile in the top stratums will suffer a drastic reduction due to cyclic loading from wave force. How to reflect these two effects in the prediction of the real in-situ pile foundation response is still under investigation. To be conservative, current state-of-the-practice in offshore engineering tends to recognize cyclic degradation in determining response. This is achieved by implicitly incorporating these effects into the static capacity analysis, or by including such negative effects in the safety index in pile foundation design. Meanwhile, the beneficial loading rate effects are

not taken into account. It is obvious that further research is needed in this area to better define the interaction between these two phenomena.

Assessing the structural integrity of an offshore platform requires balance between considerations of strength and economy. In the case of foundations, this requirement translates into the need of better understanding of their performance and more realistic modeling of their behavior so that the foundation are not designed with unnecessary reserve capacity. This need has led to focus on the study of dynamic response of pile foundations. This analysis incorporates the two major factors not addressed by static method. It also involves other important factors affecting the real dynamic response of the pile foundations. This effort has resulted in numerous valuable information in guiding the design and construction.

Bea (1984) published a keynote paper on the dynamic response of the pile foundation. This paper provides a comprehensive treatment of the basic approaches to this problem. The main concerns in the prediction of the pile foundation behaviors are as follows:

- Dynamic response depends primarily on external loading patterns and the inherent structure properties;
- Environmental loadings are dynamic. Loadings on platforms are developed from the motionless ocean and earth crust. It is crucial that they are well understood;

- Nonlinearity is a key concern in the analysis: in presence of soil, which are highly nonlinear, the pile foundation exhibits complicated coupling action between the soil and the steel piles;
- High strain rates increase strength and stiffness;
- Cyclic strains decrease strength and stiffness;
- Cyclic loading leads to accumulated displacements; and
- Damping developed from pile foundation is important.

3.1.2 Uncertainties in the Pile Response Prediction

The analyses in this report are founded on a reliability approach. This approach overcomes the drawback of the usual approaches that do not permit a quantitative and systematic treatment of the unavoidable uncertainties in a complicated design and construction process. One key step in the reliability analysis procedure is the identification of the uncertainties involved, their characteristics, and the bias introduced in the various calculation methods used in the analysis. The statistics of such factors shall be figured out so that the contribution of these factors to the total structure reliability can be obtained.

In practice, designers of offshore platforms and pile foundations deal with numerous uncertainties, including imperfect knowledge of the frontier such as: the loads to which the superstructure is subjected; the behavior of the superstructure under those loads; and how the founding soils respond when those loads are transmitted to them via the foundation piles.

In the frontiers mentioned above, Tang (1988, 1990), Bea (1983), Folse (1989), Ruiz (1984, 1986), Yegian and Hadley (1979), Olson (1984), Kullhawy (1984), Briaud and Tucker (1986) have identified various factors affecting offshore pile capacity prediction. These studies suggested estimation of the calculation bias the uncertainty statistics properties associated with these factors. The conclusions concerning the major component of uncertainties involved in the prediction of pile capacity can be summarized as follows:

- Soil properties uncertainties,
- Load parameters uncertainties, and
- Prediction model error.

Uncertainties in the soil properties are a major contribution to the overall system uncertainties. There are several very important soil parameters needed to define the p-y and t-z curves for pile foundation analysis, such as undrained shear strength, unit weight, friction angle, and shear modulus. As an inherent character of soil mechanics, these parameters subject to large variation due to natural inhomogeneous properties of in-situ soils, and distribution during lab or in-situ test, not to mention the system variation derived from various test methods. The major uncertainty sources in soil parameters are listed as follows:

- Non-standard sampling or test methods. Their effects are not completely avoidable on the determination of the soil properties, even though very high quality test are performed.
- Spatial variation of soil properties. This variation is due to the randomness associated with the natural deposition process, which is the inherent variability with the macro geological structure. Consequently, soil properties do vary along the length of a pile and across the site.
- Insufficient number of soil samples. This leads to error in the interpretation of the soil properties based on widely scattered locations in field, thus affect the averaged soil properties input to the analytical prediction model.
- Systematic error of soil properties. Sometimes, despite the availability of a large amount of measured data, the estimation of the soil properties could still be subject to significant error. The reason is simply that all the measurements made could have been consistently too high or too low due to common sample disturbance, calibration error of instrument, or other factors.

Load uncertainties can also be very large. An offshore platform can be subjected to environmental load induced by waves, wind and possibly earthquakes, which all have large inherent probability of variation. For example, the annual maximum wave height fluctuates considerably between years. This inherent variability is further magnified by the uncertain dynamic transfer function relating the wave characteristics to the induced loading at the pile head. The main loadings transmitted onto a pile head take the form of axial load, lateral load and possibly bending and torsion moments. However, the structure

behavior at connection between jackets and piles is extremely difficult to predict. The forms and values of actual loading and boundary restraint on the pile have a large range of variation. Moreover, the patterns of cyclic degradation and high loading rate effects in the dynamic analysis are subject to insufficient understanding, thus involve large uncertainties in the pile capacity prediction.

Each pile capacity prediction method has some simplifying assumptions. This uncertainty is a systematic error that varies among different prediction methods. Experiments and field tests indicate that even if the soil parameters in the input to prediction model could be accurately determined and if the applied loads are carefully controlled, discrepancies would still develop between the predicted and measure pile responses. Besides this, the numerical and discretization procedure in the current prediction models to solve the beam-column equation could also impose additional uncertainties. Furthermore, most present prediction models are correlated to the load test results to verify their validity. Thus the discrepancy between in situ pile capacity during operation and that measured in load test program imposes another uncertainties on the pile foundation analysis. The pile capacity measured at a load test does not necessarily have the same capacity of a similar pile during a storm.

For instance, load tests are generally performed within 100 days of pile installation, whereas the maximum load applied to a pile during a structure's lifetime may occur years after installation. For most normally consolidated clay where soil strength around a pile generally increases with time after pile installation, the capacity measured during load

tests could significantly underestimate the actual pile capacity due to this re-consolidation effect. Generally the capacity measured during the load tests with relatively slower loading rate underestimate the actual pile capacity. Other factors can also be identified that would cause a discrepancy between the load test capacity and the actual capacity during operation, such as soil re-consolidation, pile compressibility, jacking error during load test, etc., thus increase the uncertainties in the prediction model.

This study focuses the research effort on identifying the uncertainties in the prediction models by the means of comparing predicted capacities obtained from several methods.

3.2 Analysis models

The prevailing analytical models in use at present time is the discrete Winkler foundation model of beam-column based on non-linear soil support. Numerous researchers have studied the pile-soil capacity problems using this model (Matlock, 1978; Kagawa, 1986; PMB, 1988; Bea, 1992; Wang, 1996; Lok and Pestana 1997). This model is superior to the finite element model since its prediction fits the measured pile behaviors better. The Winkler foundation model is illustrated in Fig. 3.1. This report also takes the discrete element method as basic approach. There are three prediction models in this study: the SPASM lateral response prediction model, the more versatile analytical model developed by DRAIN3D structure analysis software package, and the platform capacity assessment tool ULSLEA/TOPCAT. The purpose of these models is to investigate the ultimate behavior of the pile-soil system.

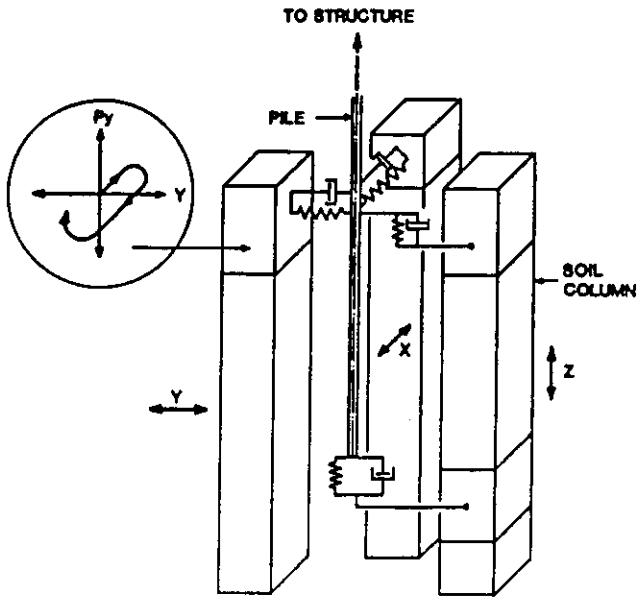

Figure 3.1 Winkler pile foundation model

3.2.1 SPASM model

SPASM is general beam-column analysis computer program, developed by H. Matlock and S. H. C. Foo(1978). It enables the study of the lateral response of soil-pile systems under various loading histories. In the SPASM program, the single pile member is represented by a discrete-element mechanical model and is restricted to linearly elastic behavior. Simplified superstructure effects can be simulated by increased stiffness along the pile member and by coupled rotational restraints at appropriate joints.

The typical Winkler discrete element model of near field soil is used in the SPASM model. The soil-pile coupling at each node along the embedded length of the pile is represented by a multi-element assemblage of friction blocks, springs, and dashpots that

facilitate the examination of hysteretic soil-pile interaction. These elasto-plastic sub-elements represent the nonlinear-inelastic behavior of the lateral soil support. The combination of the actions of these sub-elements is intended to simulate the characteristic reaction-deflection behavior of the soil support, which is expressed as p-y curves at different depths. The nonlinear-inelastic soil support model allows either degradation or hardening of resistance as a function of deflection and of the number of reversals of deflection in the range beyond an initially elastic condition. Furthermore, the formation of gaps is allowed to properly represent the expected soil-pile interplay in the upper layers of the soil.

To simplify the analysis procedure, there are some principal assumptions and idealizations in the model. The pile is made up of an assemblage of rigid discrete elements (bar). The pile elasticity, external loading and restraints are concentrated at the nodal points (pile station) between two elements. The shear forces and axial thrusts are transferred across the rigid bar. The axial deformations of the pile are neglected. The behavior of the pile is in the range of elasticity. The soil response is simulated by a series of closely spaced springs, friction blocks and dashpots. The adjacent springs, friction blocks and dashpots are unaffected by each other under deformation.

The numerical solution method applied in the program is of an implicit type (Crank-Nicolson, 1947). With this method of formulation, compatibility of displacement is enforced along the beam-column member at each time step. This numerical method

yields desired computation accuracy, stability and reliability in the dynamic analysis. The dynamic beam-column model of the combined pile-soil system is illustrated in Fig. 3.2.

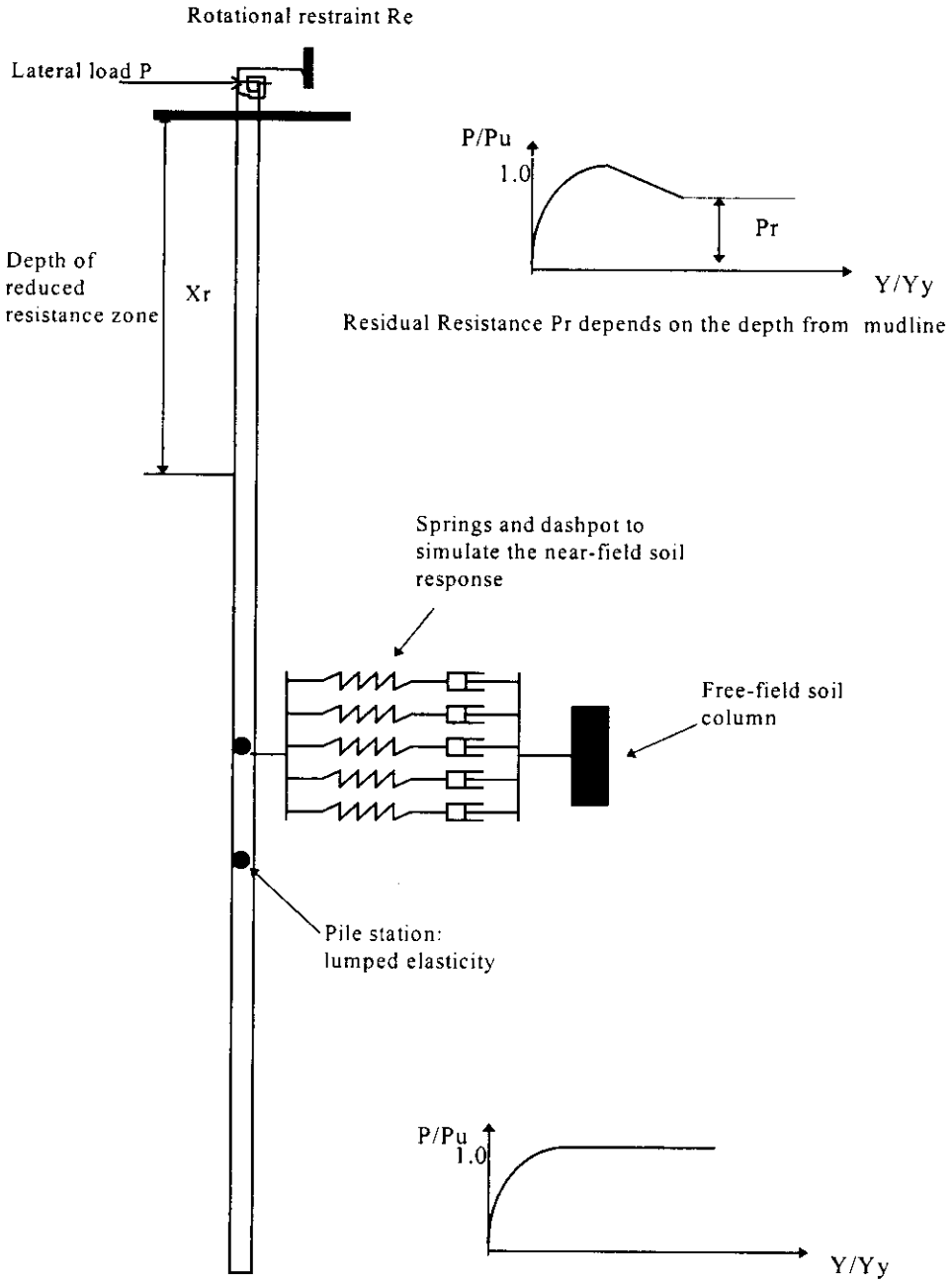

Figure 3.2 SPASM model of pile-soil interaction

One thing shall be noted is that this model assumes an elastic pile in soils. The validity of the model is doubtable after the first yielding occurs in the pile. To keep a clear total picture of the pile response, this study assumes the steel pile exhibits an elastic-perfectly-plastic behavior. The second-order strain hardening phenomenon is neglected. This means the stiffness of the pile will reduce to zero after yielding take places. So there will be a significant loss in the stiffness of the steel beam-column based on non-linear soil supports.

If the lateral load on pile element in the SPASM model keeps increasing after yielding, this analytical model will miss to capture the real deformation of the pile. However, theory and experiments have proved an ultimate collapse mechanism of such a beam-column. The pile will collapse after formation of two plastic hinges at certain locations along the pile length. For a beam with annular cross section and rotational fixed end, empirical and theoretical formulae have demonstrated the ultimate bending moment for such section is around 1.3 times the first yielding bending moment. Loading to this level will form the first plastic hinge in the beam. And it will usually take 1.4~1.5 times this loading to form the second plastic hinges. Based on this argument, an analysis by SPASM is performed to estimate the ultimate capacity of a laterally loaded single pile. It shall be emphasized that this analysis can only roughly capture the ultimate behavior of the pile with respect to the magnitude of loading at the pile head. Neither can it predict the real displacement of the pile head, nor can it indicate the final collapse patterns of the pile. The results from this study by SPASM are taken as a reference to the more powerful prediction model by DRAIN3D. They are also correlated to the ultimate capacity

prediction obtained by ULSLEA/TOPCAT. The detailed results are documented in the following sections.

3.2.2 DRAIN3D model

To evaluate the ultimate capacity of the pile foundation, an analytical model that is capable of handling both non-linear steel pile and non-linear-hysteretic soil supports is needed. In this study, such a model is developed using the structure analysis software package DRAIN3D.

DRAIN3D (Dynamic Response Analysis of Inelastic 3-Dimensional Structures) computer program is a member of the family developed from DRAIN-2D at the University of California at Berkeley. The most recent version DRAIN3DX was developed in 1994. It is a powerful structure analysis tool for general use. The software package consists of a "base" program which manages the data and controls the analysis procedure, plus a set of subroutines for each element type which control the element details. Information is transferred between the base program and the elements through an interface that is the same for all the element types.

To perform an analysis of a structure, the structure is decomposed into an assemblage of 3-dimensional nonlinear elements connected at nodes. Nodes are identified by number, and need not be numbered sequentially. Each node has six degrees of freedom (translation and rotation). The elements are divided into groups. All elements in a group are of the same type. An element is identified by its group number and element number.

The structure mass is lumped at the nodes, and the mass matrix is diagonal. A viscous damping matrix that is proportional to the element stiffness and nodal masses can be specified. The form of this matrix is:

$$C = \Sigma \alpha M + \Sigma \beta K_{\beta} \qquad 3.1$$

where M is the mass matrix, and K is stiffness matrix.

In effect, mass dependent damping introduces translational and/or rotational dampers at each node, with damping coefficients α. Different values of α can be specified for each node of desired. Stiffness dependent damping introduces dampers in parallel with the elements. Different values of β can be specified for each element group. The damping matrix, K_{β}, for any element, however, remains constant. In the current version of many elements, K_{β}, is set equal to the initial element stiffness, K_0. If desired the α and β values can be globally scaled between analyses.

The program uses an event-to-event strategy to solve the nonlinear problem, where each event corresponds to a significant change in stiffness. When an event occurs, the structure stiffness matrix is modified and an analysis is performed for the next step. It also permits a detailed energy balance calculation. This calculation accounts for the external work on the nodes, static elastic-plastic work on the elements, kinetic energy, and viscous damping work. If there is a significant energy unbalance, the analysis results are likely to be inaccurate. This scheme is simpler and more stable. But it requires more calculating

time. To reduce the execution time, provision is made for event overshoot tolerances to be specified, so that the structure stiffness is not modified at each exact event but at a somewhat larger load.

Although the pile foundation response problem is principally a 2-dimensional problem, DRAIN3D is chosen over DRAIN2DX because the recent 3D version contains more versatile elements which are needed to simulate the unique stress-strain curve and cyclic degradation characteristics of the soil support. The elements contained in the recent DRAIN3D version element library are as follows:

- Element type 1: inelastic truss bar;
- Element type 4: simple connection element;
- Element type 5: friction bearing element;
- Element type 8: fiber hinge beam-column element;
- Element type 9: compression/tension link element;
- Element type 15: fiber beam-column element;
- Element type 17: elastic beam-column element;

The elements used in this report are element type 1, 4, 15. Type 1 element is a simple inelastic bar. It's nonlinear force-displacement curve can specified by defining the material properties of the bar. It can transmit axial load only. So it is an ideal element to simulate the axially loaded steel pile. It is also used to represent the artificial rigid bar at

each node by define a large stiffness coefficient. The purpose of such a rigid bar is explained in the following sections.

Type 4 is a simple inelastic element for modeling structure connections with rotational and/or translational flexibility. It is used to form the elastic-perfectly-plastic spring group parallel or vertical to the pile axis direction to simulate the total t-z(or q-z) curves and p-y curves respectively. It is also used to specify the rotational restraint at pile head. The mechanism of this element is quite simple thus doesn't cost much calculation time. However, this element has no capability to simulate the displacement softening of the soil. Thus it is not suitable to use for the case of cyclic lateral loading and the axial loading analysis. A simple illustration of the mechanism of this element is given in Figure 3.3.

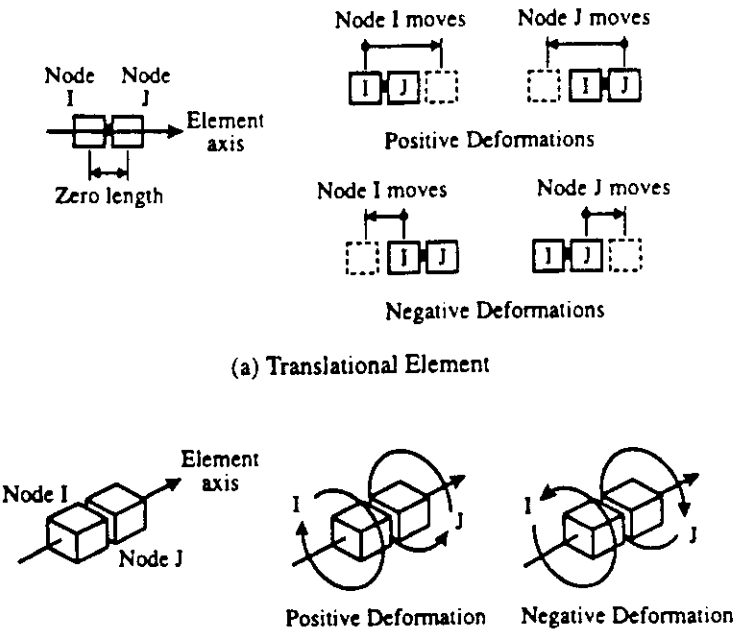

Figure 3.3 Illustration of the connection element used in Drain3D model

Type 15 is the most useful element, but also the most complicated one. The element of this type is further divided into a set of subelements. There are a lot of choices to define various subelements to simulate different element behavior. A typical subelement configuration is illustrated in Fig 3.4. The deformable part of the element is divided into segments. The behavior is monitored at the center cross section ("slice") in each segment. The cross section properties are assumed to be constant within each segment, but can vary from segment to segment. Each cross section is either elastic or is divided into a number of fibers. The fibers can have non-linear stress-strain relationships for various types of material. The typical stress-strain curve can be used in the element is shown in Fig. 3.5. Note that it has the ability to handle the displacement softening of the material. It also has degradation feature in strength and stiffness of the connection hinge in the element. By specifying the inelastic unloading pattern, the hysteretic damping is involved automatically. By determining the value of the viscous damping coefficient β, a dashpot parallel to the element is added implicitly to the element. This feature can represent the radiation damping of the soil. This element is used widely in the DRAIN3D pile foundation model to simulate the complicated supporting behavior derived from the near-field soils.

Proper use of these elements can form a structure frame that can numerically simulate the combined pile-soil system response to lateral and axial loading. The layout of such a structure frame is different for these loading cases. The detailed descriptions of these frames are documented in the following sections.

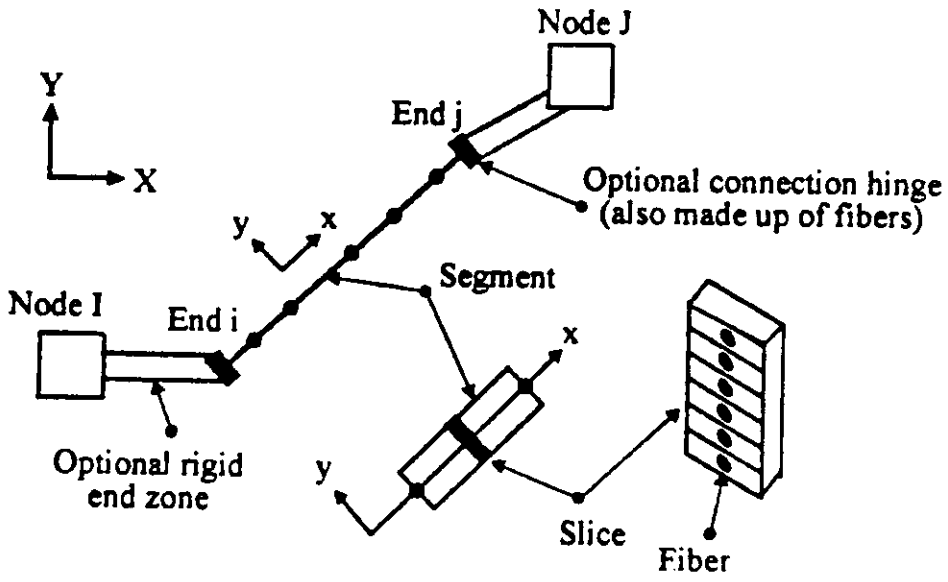

Figure 3.4 Element type 15 in Drain3D model: nonlinear beam with distributed plasticity

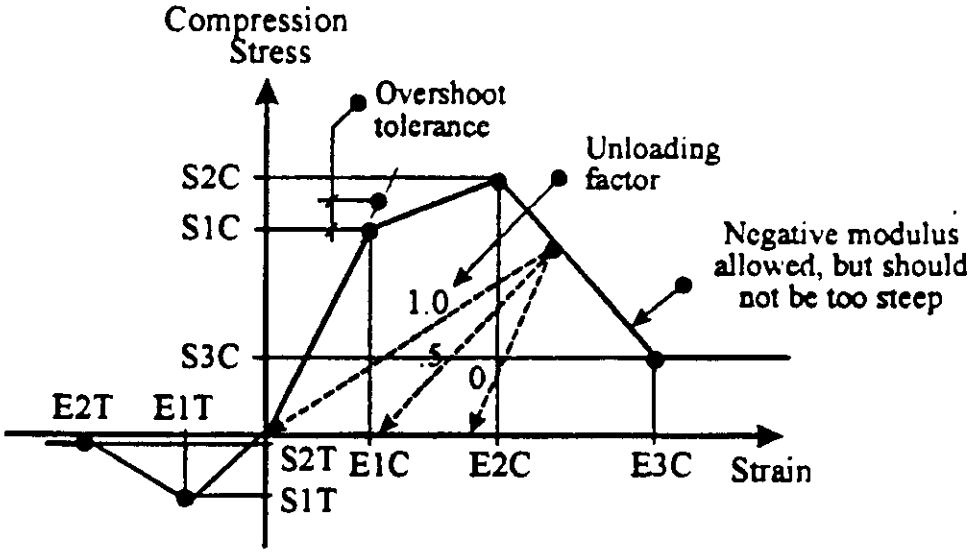

Figure 3.5 Typical "concrete" material stress-strain properties for the soil beams in Drain3D pile foundation model

3.2.3 ULSLEA/TOPCAT MODEL

The ULSLEA/TOPCAT program is a simplified screening method for platform assessments and re-qualifications. It has subroutines calculating the static lateral and axial capacities of the pile foundation. The previous version of ULSLEA/TOPCAT (V. 3.0) assumes that the foundation soil of either exclusively cohesive (with variable soil shear strength) or exclusively cohesionless. The new version ULSLEA/TOPCAT modifies the current pile capacity strength formulation to allow for the ultimate lateral and axial strengths of a pile imbedded in separate layers of cohesive and cohesionless material to be estimated.

In ULSLEA/TOPCAT model, a pile is assumed to reach its lateral capacity when plastic hinges form at the mudline and at some depth where the moment on the pile reaches the fully plastic bending moment. By considering the soil at each incremental length along the pile to absorb load up to the soil's maximum bearing capacity, the point of zero shear in the pile can be estimated; this is also the point of fully plastic bending moment in the pile. Therefore, the depth at which the maximum moment occurs determines the length of the pile with which the collapse mechanism is formed. This mechanism is shown in Figure 3.6.

The pile ultimate lateral load and the point of zero shear L_d may be related by integrating the incremental soil resistance S_u over the presumed L_d :

$$P_{u,l} = \int_0^{L_d} S_u(z)dz \qquad 3.2$$

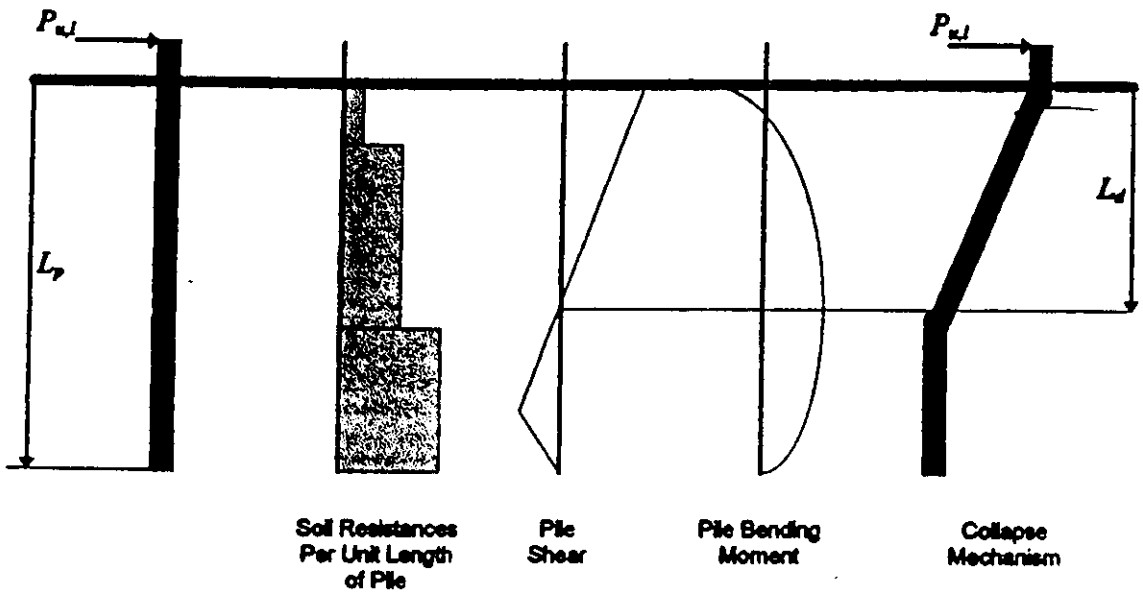

Figure 3.6 ULSLEA/TOPCAT collapse mechanism for analysis of laterally loaded piles

Using virtual work, another equation relating the point of zero shear and the pile ultimate lateral load can be developed:

$$P_{u,l} = \frac{2M_p}{L_d} + \frac{1}{L_d}\int_0^{L_d} S_u(z) z dz \qquad 3.3$$

Equating the two relations by dropping L_d allows $P_{u,l}$ to be related to the plastic moment capacity of the pile M_p and the cumulative soil resistance.

The formulae used in previous ULSLEA version (V. 3.0) was documented by Mortazavi (1996). Following is a brief summarization for the case of linear increasing strength with depth, which is an estimation of the soil characteristics in the Bay of Campeche.

For this case, the ultimate lateral capacity of the pile, $P_{u,l}$, can be estimated from the following equation:

$$P_{u,l}(C+\xi) - 2M_{u,l} - (A+\eta\xi)\frac{C^2}{2} - \left(\frac{\eta}{2}\right)\frac{C^3}{3} = 0 \qquad 3.4$$

where,

$$C = \frac{1}{\eta}\left[(-A+\eta\xi) + \sqrt{(A+\eta\xi)^2 + 2\eta P_{u,l}}\right]$$

$$\eta = \frac{B-A}{L_p}$$

$$\xi = 15D + X$$

$A = 9S_{u1}D$ and $B = 9S_{u2}D$

S_{u1} and S_{u2} denote the undrained shear strength at mudline and at the pile tip respectively

As to the axial pile capacity formulae in ULSLEA/TOPCAT, a pile is assumed to reach its vertical capacity when all vertical resisting mechanisms (shaft friction and end bearing) have yielded. The axial resistance of a pile is based on the combined effects of a shear yield force acting on the lateral surface of the pile and a normal yield force acting over the entire based end of the pile (Figure 3.7). Thus the ultimate axial capacity Q_u, can be expressed as:

$$Q_u = Q_p + Q_s = qA_p + f_{av}A_{sh} \quad 3.5$$

Q_p denotes the ultimate end bearing; Q_s is the ultimate shaft capacity; q is the normal end yield force per unit of pile-end area acting on the area of pile tip A_p; and f_{av} denotes the ultimate average shear yield force per unit of lateral surface area of the pile acting on embedded area of pile shaft A_{sh}. It is assumed that the pile is rigid and that shaft friction and end bearing forces are activated simultaneously. It is further assumed that the spacing of the piles is sufficiently large so that there is no interaction between the piles.

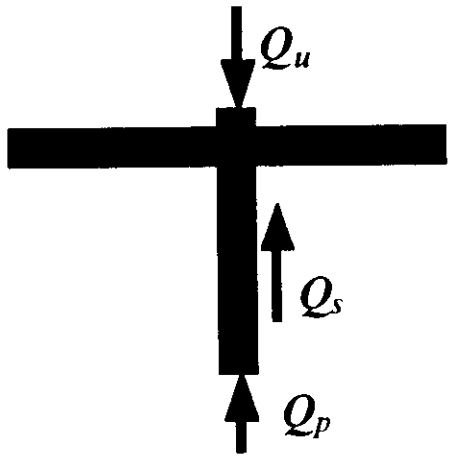

Figure 3.7 ULSLEA/TOPCAT analytical model for pile axial capacity

After considering the weight of the pile and the soil plug (for open-end piles), the ultimate compressive loading capacity of the pile, Q_c, can be calculated as:

$$Q = \frac{q\pi D}{4} + (f_{av}\pi D - W)L \quad 3.6$$

$$W_p = \gamma_{st} A_{st} + \gamma_s A_s = \frac{1}{4}\left[\gamma_{st}\pi(D_o^2 - D_i^2) + \gamma_s \pi D_i^2\right] \quad 3.7$$

where,

A_{st} = cross-sectional area of the steel pile

A_s = cross-sectional area of the soil plug

D_0 = outside diameter of the pile

D_i = inside diameter of the pile

f_v = yield stress

γ_{st} = submerged specific weight of steel

γ_s = submerged specific weight of soil

L_p = pile embedded length

W_p = weight of pile and soil plug per unit length

The end bearing capacity can be fully activated only when the shaft frictional capacity of the internal soil plug exceeds the full end bearing (Focht and Kraft, 1986). This condition can be formulated as:

$$\frac{q\pi D_i^2}{4} \leq \left(f_{av} D_o + W_p\right) L_p \quad 3.8$$

For cohesive soils with an undrained shear strength, S_u, the ultimate bearing capacity is taken as the bearing of a pile in clay:

$$q = 9S_u \quad 3.9$$

The ultimate shaft friction is taken as:

$$f_{av} = kS_{ua} \quad 3.10$$

where k is the side resistance factor and a function of the average undrained shear strength S_{uav} as given in Table 3.1.

Table 3.1 Side resistance factor formulated in ULSLEA 3.0

Undrained shear strength $S_{u,av}$(ksf)	Side Resistance Factor K
< 0.5	1
0.5 - 1.5	1-0.5
>1.5	0.5

The above approach is similar to that suggested in the API RP-2A guideline except the side resistance factor. The API guideline has a effective overburden pressure approach. For Pile piles in cohesive soils just as the soils in the Bay of Campeche, the shaft friction f, in lb/ft^2(kPa) at any point along the pile may be calculated by the equation,

$$f = \alpha c \qquad 3.11$$

where:

α = a dimensionless factor

c = undrained shear strength of the soil at the point in question

The factor, α, can be computed by the equations

$$\alpha = 0.5\ \psi^{-0.5} \psi \leq 1.0 \qquad 3.12$$

$$\alpha = 0.5\ \psi^{-0.25}\ \psi > 1.0$$

with the constraint that, $\alpha \leq 1.0$,

where:

$\psi = c/P_0'$ for the point in question

P_0' = effective overburden pressure at the point in question lb/ft² (kPa)

For comparison with this approach, the ultimate axial capacity calculation follows the API guideline is also performed and summarized in the following sections.

3.3 Lateral Pile Response

Three analysis models are used in this report: SPASM, DRAIN3D, and ULSLEA/TOPCAT. This section describes the typical lateral pile response obtained from these models in the Bay of Campeche.

3.3.1 Pile Parameters, Load Patterns and Soil Properties

3.3.1.1 Pile Configurations

The piles in this study are all driven piles. The pile configurations are typical for a platform of moderate size in the Bay of Campeche, with a water depth of around 150 feet (45m). The pile has a diameter of 48 inches, with a penetration of 200 feet (61m). In SPASM and Drain3D models, the increment between two successive pile stations is set to be 4 feet to adequately reflect the layered nature of the soil support. Thus the pile are divided into 50 uniform segments. The starting pile station number has a value of zero and is assigned to be the pile head at the mudline. The bar numbering starts from 1 and is located above the pile station with the same number. The pile stiffness is uniform along the length, 1.8E+12 lb.in². The pile weight is 3.0 E+3lb/station. Thus the density of the pile used in the computer program is 7.764lb.sec²/in/station. The wall thickness of the

pile is 1.5 in. Two cases of rotational restraints are assumed at the pile head to approximately simulate the effects of the platform jacket: grouted pile head (with a rotational restraint R_e =3E+10lb.in/rad) and non-grouted pile head (R_e =5.25 E+9lb.in/rad). For the purpose of systematic parametric study, two extreme cases were also studied: rotationally fixed head; and free pile head.

3.3.1.2 Different Loading Patterns

The pile-soil systems respond to different loading patterns in different ways. Quick loading increases the strength and stiffness of the support soil, thus increases the resistance to the lateral loading by the soil. On the contrary, cyclic loading decreases soil strength and stiffness and causes degradation. In practice, the design of platform pile foundation usually takes a static approach as recommended in API. To demonstrate the effects of these different loading histories, three cases of loading are studied: quasi-static; quick loading; and cyclic loading. This study took a time history approach. The loading magnitude in these analyses is linearly increased with respect to time.

As the typical storm wave period in the Bay of Campeche (100-year ARP hurricane) is about 12 seconds. One-forth of the period is 3 seconds, in which the wave loading increases from its lowest value to peak value. So the quasi-static analysis has a loading duration of 3.6 seconds, and it takes 3 seconds to bring the pile to yielding point. The extra 0.6 second is added to guarantee the numerical consistency and stability at the end of each calculated time history. This loading pattern is regarded as quasi-static loading.

Study of this loading pattern gives an estimation of the resistance capacity of the pile-soil system to the idealized static or quasi-static lateral loading.

Similarly, for the quick loading, the loading duration to produce yielding of the pile is taken to be 0.10 second, which is close to the loading rate of a typical earthquake. In the actual model, an extra 0.01second is added to the loading history for the same reason of numerical stability described above. The load increases monotonically until yielding occurs. This case of quick loading studies the sensitivity of the soils in the Bay of Campeche to the loading rate effects.

As to the cyclic loading, the soil shear strength is time dependent in this case. The degradation procedure suggested by Matlock is applied in the analysis. The lateral load amplitude is increased cycle by cycle. As stated before, the period of one cycle is taken to be 12 seconds to simulate the wave loads. Meanwhile the shear strength is degraded cycle by cycle, too. Study of the soil properties in the Bay of Campeche has shown that the number of cycles needed to get 50% degradation, N_{50} , is equal to 4, and has a range of 4-6. It means that 15 cycles will cause almost full degradation of the soil resistance to the lateral loading. So the cyclic loading duration to bring the pile to the point of yielding is chosen to be 180 seconds, etc., 15 cycles. Similar as other loading patterns, ¾ cycle of loading is added at the end of the loading history to guarantee numerical stability. The detailed soil degradation process will be discussed in section about the nonlinear and hysteretic soil model.

3.3.1.3 Generalized Soil Properties

Soil Proiles

The properties of the soil in the Bay of Campeche are interpreted and summarized into the input data for the analysis models. These data include: generalized soil profile; p-y curves for static, dynamic and cyclic loading; degradation process due to cyclic loading; and gapping effect.

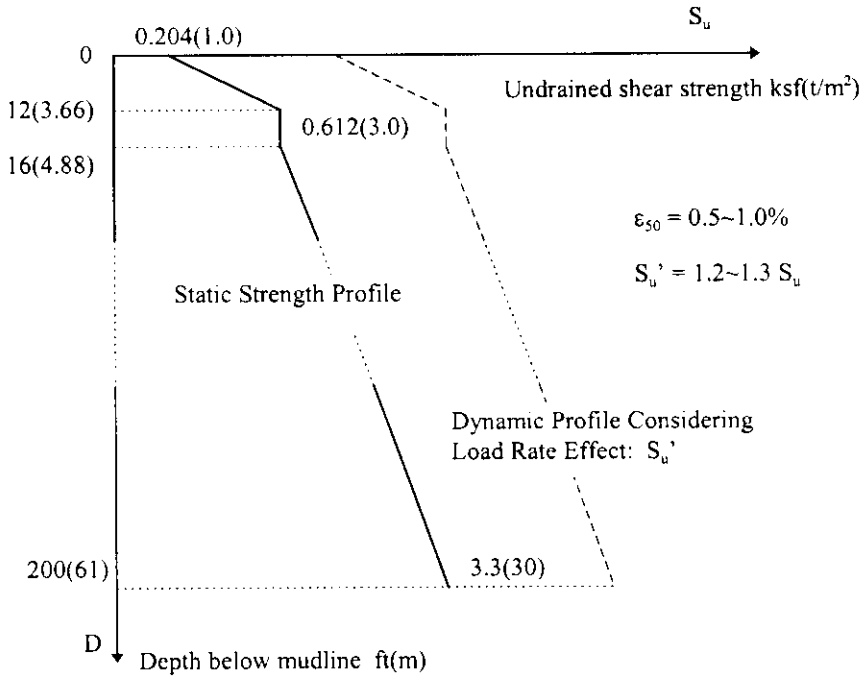

Figure 3.8 Generalized soil profile in the Bay of Campeche

Based on the soil investigation information provided by PEMEX, this study used a generalized soil profile that reflects the typical soil characteristics in the Bay of Campeche. The soil profile is illustrated Figure 3.8. It shall be noted that the solid line in the graph is the profile for static and quasi-static loading. The dash line is the profile for

quick loading. The soil strength and stiffness is increased due to rate effect of loading. The increasing ratio is 1.2~1.3 based on the in-situ test and laboratory data. A sensitivity study has confirmed this argument. Another parameter, ε_{50} , which is used in the construction of p-y curve, is also extracted from the soil investigation data. The value is in the range of 0.5 to 1%. Sensitivity study about this parameter is also conducted.

Construction of P-Y Curves

In the practice of design, both static and cyclic p-y curves are utilized, depending on the loading patterns. The static curve is the resistance-deflection path on the initial loading. The cyclic curves, modified on the basis of the static backbone p-y curves, are intended to represent a lower bound of resistance for the purpose of equivalent static analysis. They represent the lower bound of the lateral resistance mobilized by the near-field soils. The cyclic p-y curves can not be taken as the actual dynamic loading path. To get the exact dynamic response of the pile under cyclic loading, a time-history approach is taken to simulate this process. The complicated soil degradation and gapping effects in the top soil layers are counted in this process. Presumably, this process, with a large amount of cycles can lead to reasonable agreement with the conventional lower-bound cyclic p-y curves. This has been confirmed by the study conducted.

To construct p-y curves, the shape of the static backbone p-y curve recommended by Matlock is used in this study. The lateral loading P and lateral deflection Y are both normalized by proper critical values. The non-dimensional relationship between them is given by:

$$p / p_u = 0.5(y / y_c)^{1/3} \quad (3.13)$$

$$y_c = 2.5\,\varepsilon_{50}\,D \quad (3.14)$$

Where, p_u is the ultimate static lateral resistance capacity at the depth of concern. D is the pile diameter. ε_{50} is the strain which occurs at one-half the maximum stress on laboratory undrained compression tests of undisturbed soil samples.

Based on API guideline, the ultimate static lateral soil resistance capacity can be determined:

$$P_u = 3 \cdot C + \gamma \cdot x + J \cdot \frac{C \cdot x}{D} \qquad x < X_r \quad (3.15)$$

$$P_u = 9 \cdot C \qquad x > X_r \quad (3.16)$$

Where, C is the undrained shear strength of soil at depth x; γ is the effective unit weight of soil; J is a dimensionless empirical constant; D is the pile diameter. X_r is the depth of the reduced resistance zone.

In this study, the soil shear strength varies with respect to depth below mudline. So, the depth of reduced resistance zone was taken as x value at the intersection of Equation 3.15 and 3.16. Using this method, the X_r of the soil turns out to be around 35.5ft. For the actual SPASM or Drain3D discrete model, the reduced resistance zone depth is taken to be 36ft, i.e., at the 9^{th} pile station. Above the 9^{th} station, the ultimate lateral soil resistance for each layer of soil is calculated using Equation 3.15. Equation 3.16 is used to calculate the ultimate lateral soil resistance below the 9^{th} station.

The non-dimensional static backbone p-y curve is actually the same for all soil layers. The exponential curve is approximated by five straight line segments. The curve shape is controlled by the following pairs of coordinates.

Table 3.2 Control points of P-y curve

P/P_u	0.0	0.42	0.5	0.70	1.0	1.0
y/y_u	0.0	0.6	1.0	2.744	8.0	50.0

Two multipliers, one for loading and the other for deflection, are applied to scale the backbone curve to reflect the real soil support characteristics at each soil layers. These scaled p-y curves are input to the analysis models.

The p-y curve for quick loading is derived from the static backbone curve. The rate effect is reflected in a coefficient K_r. Let S_u' be the soil shear strength under quick loading. Then, $S_u' = K_r \times S_u$. The value of K_r is obtained from the soil investigation data. As stated before, this value has a range from 1.2~1.3. Based on this new soil strength profile, the same construction procedure as described above is taken to generate the p-y curves used in the quick loading analysis.

As to the cyclic loading, this study didn't use the cyclic p-y curves derived from static curves. A time history approach is taken instead. Using the static p-y curve for the initial loading cycle, the soil support capacity is degraded cycle by cycle.

Internally, the analysis models in this report simulate the P-Y curve with a group of individual mechanical sub-elements whose combined actions are expected to correspond exactly to the input P-Y curve at any given pile station. These sub-elements are assumed to be elastic-perfectly-plastic springs. As shown in Figure 3.2, four or five parallel springs are placed at each pile station. This process is illustrated in Figure 3.9. It is demonstrated that the total soil resistance at any deflection is equal to the sum of all the sub-elements' forces.

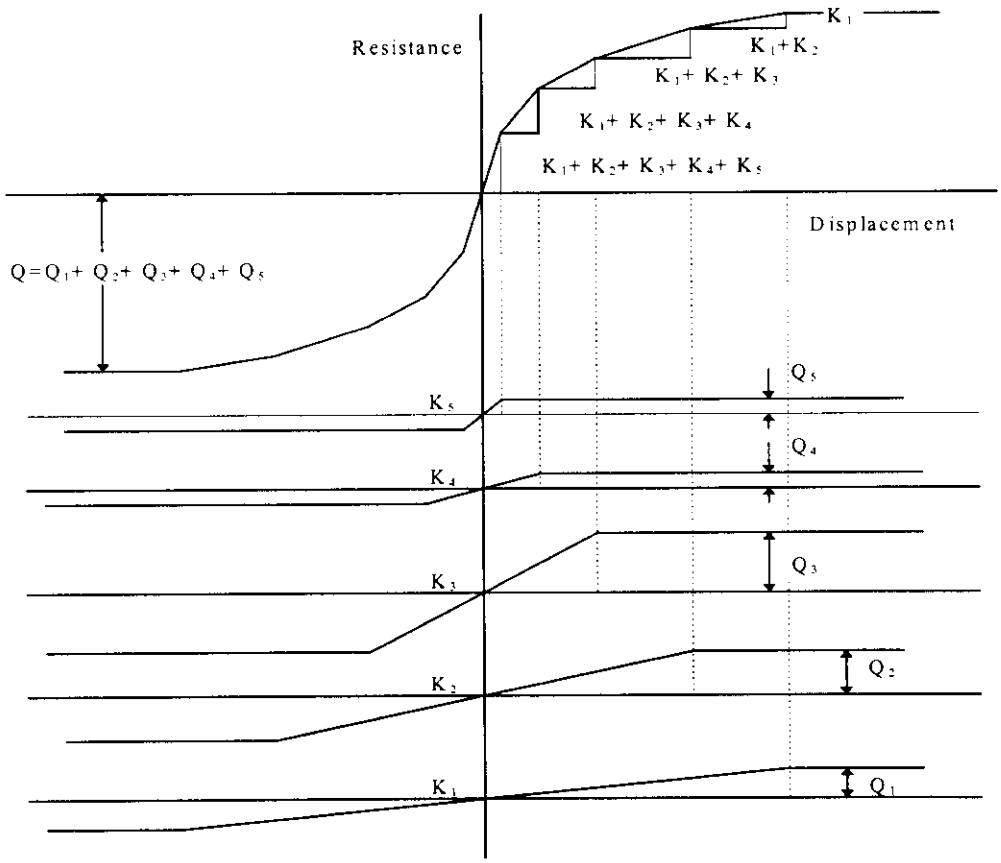

Fig. 3.9 Parallel elastic-perfectly-plastic spring model to simulate the p-y curves

Degrading Soil Model

The ultimate resistance capacity of many materials decreases somewhat after a full reversal of yielding in both directions. This is true for soils. There will be a softening process of soil strength upon each reversal of loading direction. In this analysis, the softening procedure operates on each P-Y spring sub-element separately. The degradation factor, λ, is applied to the ultimate plastic resistance of each sub-element only upon the occurrence of a full reversal of direction of slip.

In addition to the initial ultimate resistance Q_u and the factor λ, a residual lower-bound resistance, Q_{min}, is specified for each sub-element, which is asymptotically approached as degradation proceeds cycle by cycle. For the soils in the Bay of Campeche studied in this report, Q_{min} =75% Q_u. The degradation factor λ is 20%~16%. For the sake of conservativeness, λ is chosen to be 20%. A parametric study of λ is taken as base case.

The degradation formula of the soil resistance is given by Matlock. Whenever the reduction in strength is applied, the existing ultimate resistance Q_1 is degraded to a new ultimate resistance Q_2 according to the following relation:

$$Q_2 = (1-\lambda)(Q_1 - Q_{min}) + Q_{min} \qquad 3.17$$

A graphical representation of this process as applied to single sub-element is shown in Figure 3.10. The graph shows the degradation occur in the first cycle.

It should be noted that the soils in the top layers experience much more degradation. The residual minimum resistance of soils in the reduced resistance zone depends on the depth

below the mudline. For the soils in the Bay of Campeche, the residual minimum resistance P_r is 0 at mudline and 75% P_u at the depth of X_r. P_r in the reduced resistance zone is given by:

$$\frac{P}{P_u} = 0.75 \frac{X}{X_r}$$

$$\frac{P_r}{P_u} = 0.75 \qquad 3.18$$

The same relationship is applied to the ultimate lower-bound resistance of the spring sub-elements, Q_{min}.

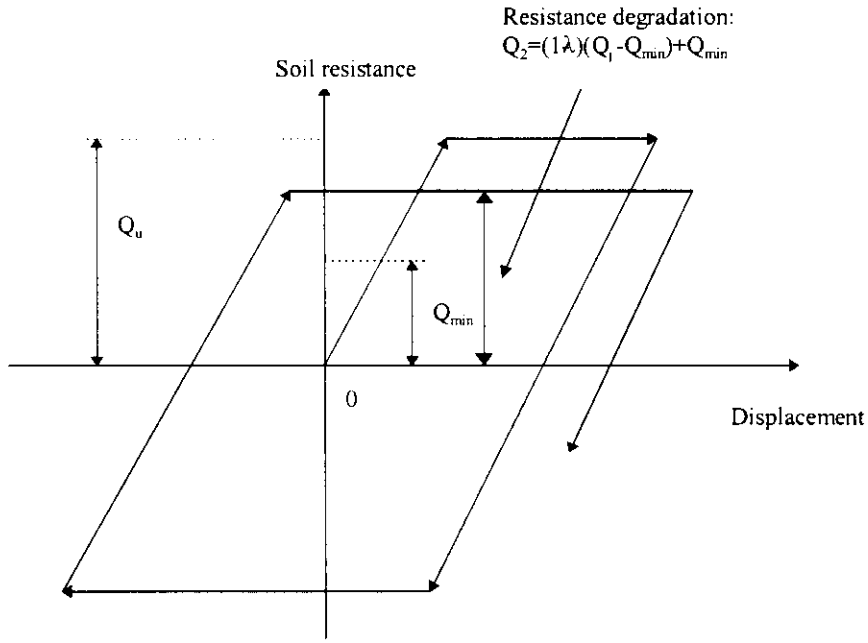

Figure 3.10 Soil Degradation Model Demonstration

Simulation of Gap Zone

After a number of cycles of loading, a molding-away zone, in which there is no or little soil resistance to the lateral loading, will develop in the top layers of soils. To simulate

the presence of this gap zone between the pile and the soil, which generally occurs near the mudline, the spring sub-element representing the soil resistance are specified as gap elements. This kind of element will be attached to the pile in one direction, while will be detached from the pile as the pile moves in the other direction. Only when the pile returns to the point where it left this element previously, will the element be activated again. To represent the presence of drag resistance on the pile in the gap zone, only a portion of the sub-elements may be assigned as gap elements while the rest of the sub-elements will remain attached to the pile. To represent fully confined plane strain resistance below X_r, all sub-elements of those p-y curves are specified as non-gap elements. On the other hand, to represent a fully opened gap with no resistance at the mudline, all sub-elements of this p-y curve are assigned as gap elements. In the reduced resistance zone, the portion of the gap elements is assumed to be linearly decreased with respect to depth below mudline.

3.3.1.4 Some Considerations

In this study, there are some simplification and consideration that is needed to be clarified:

Internal and External Damping

The internal damping and external damping in the pile-soil system are intentionally neglected. The argument is based on the fact that the damping is not a main influence factor in the pile lateral response to dynamic loading in the range of frequencies of interest (Chan 1972, Matlock 1979, Bea 1984). A parametric study also proved that small

damping (damping ratio of 1%~3%) has little influence on the results yielded by SPASM. So they are neglected to keep the whole picture clear for the dynamic analysis.

Shear Stress in Piles

As to the shear stress in the pile cross section, it is also neglected in the calculation of the yielding state of the pile. The maximum shear stress occurs at station 1, where the bending moment is not maximum. The shear stress has an order of 10^3 lb/in^2 , relatively small compared with normal stress caused by bending moment. So shear stress is not considered in this analysis.

P-Δ effect

The P-Δ effect is neglected in this study. There are several reasons for this. First, P-Δ effect is of the second order compared with the beam-column bending behavior, i.e., P-M effect. It's influence is relatively small. A parametric study of the SPASM model has proven this. Second, Motlock's P-Y response model is developed on the basis of a series of systematic experiments. These experiments have not counted in the effect of the superstructure of platform. This model mainly deals with a single pile response. The bias and uncertainty involved in the pile ultimate lateral capacity can be easily get by comparing the analytical results with the experimental results. So, for the sake of comparison and consistency, the P-Δ effect is not considered in this study.

3.3.2 Configurations of the pile-soil models

3.3.2.1 SPASM Model

Based on the information in the above section, the SPASM analysis model is easy to build. The configuration of this model is illustrated in Figure 3.2. The p-y curve for each stratum of the soil is simulated by the combined action of the elastic-perfectly-plastic springs at each pile node. As explained before, the pile in SPASM model is loaded to the state that the bending moment at certain pile nodes reach 1.5 times the ultimate bending moment across the pile section. The load values are taken as estimation of the ultimate capacity the pile-soil system can develop. The analysis results are compared with DRAIN3D and ULSLEA/TOPCAT in the following sections.

3.3.2.2 DRAIN3D Model

As DRAIN3D is a general analysis program mainly dealing with the non-linear structure problems of buildings, it's set up is not as convenient as the specific soil mechanics programs such as SPASM. The pile-soil system is translated into an equivalent "solid" structure frame just the same as the steel-concrete structures in building. The equivalent structure in this study is a truss frame, which is an assembly of beams, columns, bars and nonlinear connections. The configuration of such a truss frame is shown in Figure 3.11.

In the truss frame shown in Figure 3.11, the only "real" component is the vertical column that represents the steel pile. This pile consists of 50 type 15 elements. As the failure of the pile-soil system is not owed to the failure of soil supports, but the formation of plastic hinge in the pile, the cross section is divided into 8 non-linear fibers, which can simulate

the plastic behavior of the pile segment after yielding take places. The features of these fibers are carefully determined so that the geometry properties of the cross section, such as cross area, section modulus, principal axis, do not change.

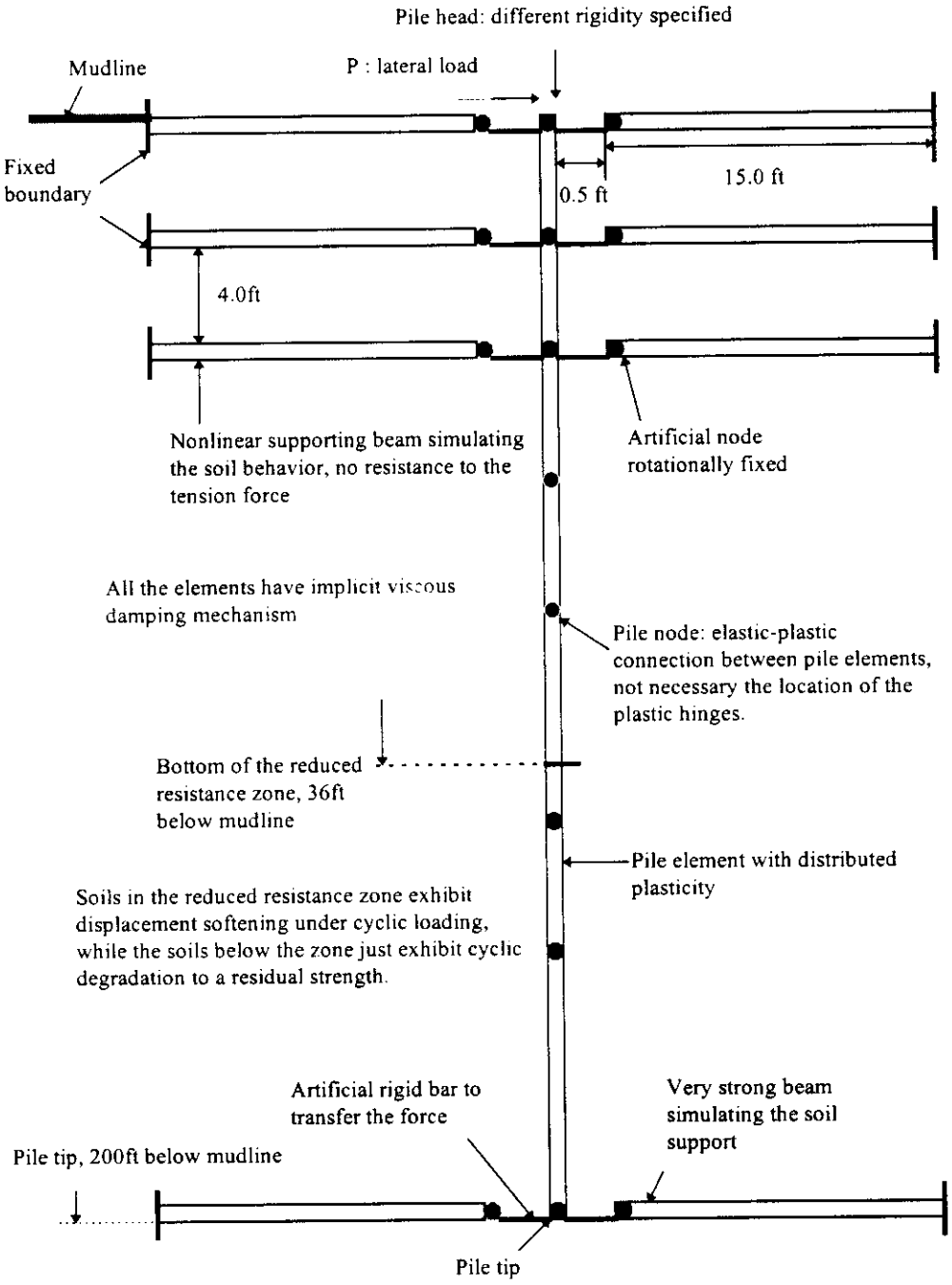

Figure 3.11 Configuration of equivalent truss frame in Drain3D simulating the p-y response of the pile-soil system

The supporting beams in the truss frame are added to each pile node to simulate the non-linear-hysteretic soil resistance. They are artificially "faked" elements. Their responses to loading are carefully evaluated to guarantee that the force-displacement relationship at each pile node is consistent with the specified p-y curve in that soil layer. The material of these beams are of typical "concrete" type in DRAIN3D element library, which are at least trilinear in compression and can simulate the displacement softening phenomenon. That means the modulus of such an element may become negative if strain is larger than certain value. This softening may induce a problem of numerical stability in calculation that shall be solved by certain means. The stress-strain curve of this kind of "concrete" material was plotted in Figure 3.5. Note that the shape of the curve is just the same as the shape of a t-z curve with softening after the peak stress, or the cyclic p-y curve. As the t-z curve and p-y curve reflect the force-displacement relationship, care shall be taken to transfer the stress-strain curve of the element material into force-displacement curve. Since the supporting beams are under compression, the following formula is used to relate the stress-strain curve to force-displacement curve:

$$\Delta = \frac{P}{AE} L \qquad 3.19$$

Where, Δ is the displacement, L is the element length, P is the axial force on the element, E is the stiffness, A is the cross section area. E can be easily determined according to the coordinates in the p-y curves. L should be large enough so that the strain can be calculated directly, assuming the total deformation of the element is small. The possible maximum deformation in the near-field soil is 15 times y_c, i.e., 1.5 feet. So the beams

simulating the p-y springs are set to be 15 feet long so that the total strain is at most 10%. In this range of strain, Equation 3.19 is regarded valid.

In Figure 3.5, the stress-strain curve are not two-way symmetrical, meaning that the typical "concrete" material in DRAIN3D does not exhibit the same response to compression as to tension. So the supporting beams in the truss frame are specified to have no resistance to tension. Meanwhile, as shown in Fig 3.11, two such beams, one on each side, are attached to each pile node. The combined response of the two beams can simulate the two-way symmetric soil p-y springs.

During the build-up of the DRAIN3D model, one unexpected problem developed. The calculation algorithm of DRAIN3D is so detailed and delicate that it can reflect the complicated distribution of forces and moments among the elements connected at each node. This is desirable in a real structure analysis, but not desirable in the simulation of the soil resistance. The earlier DRAIN3D models in this study have no rigid bar (Figure 3.12) at each node. Analyses by these models always can not be loaded to the ultimate state. They stopped before the formation of the second plastic hinge in the pile. A careful examination of the input and output turned out that the beams simulating the soil resistance were unstable at those stop points. The beams buckled under compression just as what may happen in a real building structure. Obviously, this is not true for soil resistance. The near-field soils never buckle. Their response to external load follows the special p-y curves. The simulation of the soil resistance by plastic beams fails at the stop points. Several attempts were tried to solve the problem: such as change the beams'

length, increasing the cross section area. The purpose is to stabilize the beams by increasing the Euler stress. But all these efforts yielded no positive results. Finally, the buckling was traced to the distributed bending moment from the node to the beams. When the pile bends under lateral loading. Bending moments are created at each pile node. In the calculation algorithm in DRAIN3D, a small portion of this moment is distributed to the beams. This means that the beams are under combined action of axial compression and bend moment. According to the structural mechanics, we know the disturbance of small external bending moment can greatly reduce the Euler stress thus lead to much earlier buckling of the compression beam. This conclusion is supported by the fact that the instability always takes place in the first segment of the beams, which is connected to the pile node. The deformation in this segment is much larger than the rest ones. To get rid of the unnecessary small bending moment, short rigid bars are added to connect the pile node to the soil supporting beams. The connection nodes between these rigid bars and beams are specified to have only one degree of freedom. The connections are rotationally fixed so that only the axial force can be transferred to the supporting beams. The function of these rigid bars and the restrained connection nodes can filter the undesirable disturbance of the small bending moments. The illustration in Fig 3.12 gives details of the configuration of the elements, their subelements, connections and rigid bars at each node.

In Fig 3.12, the material for the supporting beams at each pile node are set to have their special stress-strain relationship to simulate the characteristics of p-y response of the layered soils. The radiation damping of the soil is implicitly simulated by the viscous

damping in each element. The rotational restraint at pile head can be obtained by adding a type 4 rotation simple connection at pile head. The external loading at pile head can be either displacement-controlled or load-controlled. Load control pattern is used to calculate the elastic response of the pile. After the pile is loaded to the point of the first yielding. The load pattern is changed to displacement control to capture the ultimate response of the pile. This is because that there are a lot of elements, both pile segments and soil supporting beams, yield during this loading process. When the second plastic hinge is being formed in the pile, a small increase in the loading may cause a very large displacement. This is another reason why the displacement control pattern is applied in the ultimate state analysis.

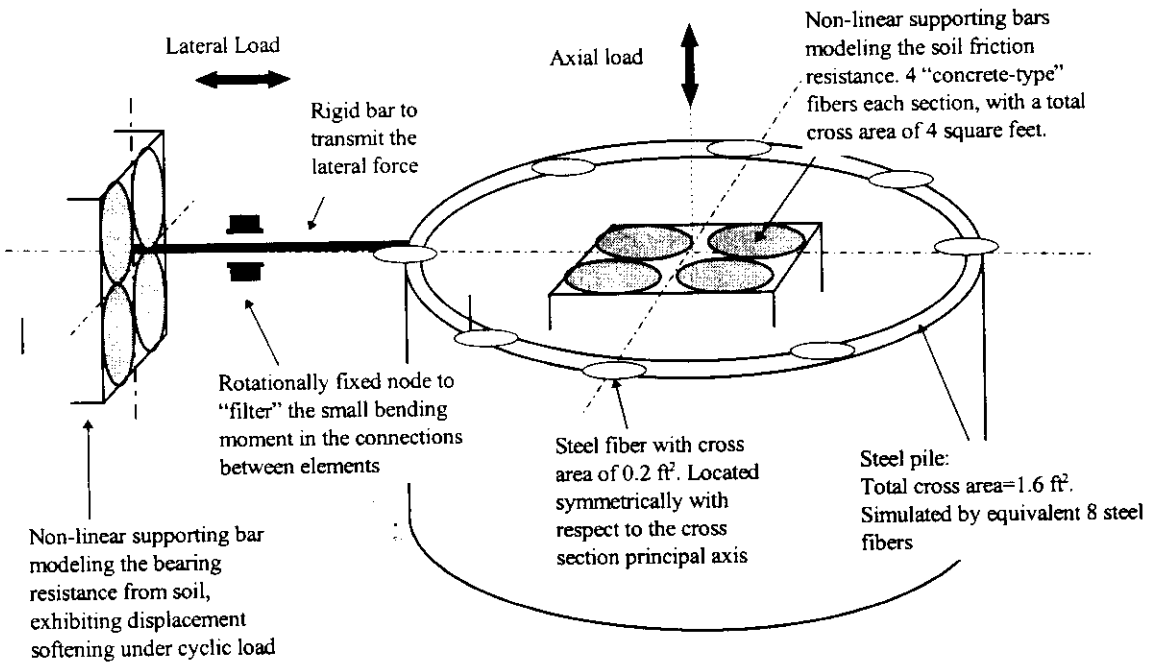

Fig. 3.12 Details of the configuration of elements and sub-elements at pile node

3.3.3 Lateral Response of a Pile to the Static Loading

The present approach used in the design of pile foundation has a pseudo-static style. The static response of the pile-soil system is the basis for more realistic in-field response. Analyzing and understanding the static response of such piles is a principal problem in analyzing and understanding their dynamic response. This is because that the static response is a critical element in realistic loadings that can be characterized as being static on those that are dynamic. Also, if one does not properly understand the response of a system to its static loadings, it is unlikely that one can properly understand the response of the system to its dynamic loading. The two philosophical and analytical frameworks are complementary and necessary to each other.

3.3.3.1 First Yielding Capacities

There are usually three failure modes in lateral pile design. The first is excessive displacement at the pile head, which may affect the production equipment thus cause the loss of serviceability of the platform system. The second is initial yielding of steel pile, which causes permanent deformation in file. The third is the final collapse of the steel pile resulting from formation of plastic hinges.

The results of static loading analysis of the first yielding capacities are shown in Table 3.3. The first yielding capacities are calculated by Drain3D and SPASM. It can be seen that there is a great agreement between the results from two models.

3.3.3.2 Ultimate Capacities

The ultimate capacity is the focus of this study. The static lateral ultimate capacities for the four different cases of pile head rigidities are predicted by three computer programs: SPASM, Drain3D and ULSLEA/TOPCAT. The Drain3D model is the most detailed model and is regarded as the "exact" prediction method. ULSLEA is the simplified estimation of the static ultimate capacity. Amazingly, the prediction by this very simple model has very good agreement with the complicated Drain3D model. The results are shown in Table 3.3 and 3.4. The detailed force-pile head displacement is shown in Fig. 3.13.

3.3.4 Lateral Response of a Pile to the Dynamic Loading

Two dynamic load patterns are studied for the lateral response of a pile. The SPASM model has a time-history approach for both fast loading. The model directly incorporated the load rate effect in the modified p-y curves based on the static backbone p-y curves. The same approach is taken in the Drain3D model for the case of fast loading. For the cyclic loading, SPASM still has a time-history approach. The cyclic loading effects are reflected by the cycle-by-cycle degradation mechanism suggested by Matlock. The Drain3D model uses a different approach. The cyclic p-y curves modified from the static backbone curves are used in the model. It is intended to capture the residue ultimate capacity when the final equilibrium state of soil characteristics is reached after a large number of load cycles.

3.3.4.1 Fast Loading

The results from SPASM and Drain3D are summarized in Table 3.3 and 3.4. The Fast loading analysis by SPASM gives some overestimated ultimate capacities compared with those by Drain3D. This is due to the estimation method by SPASM is based on the static response of the pile. It is questionable whether this method works well for dynamic problem. The calculation results have proved this doubt. Using an overestimated pile stiffness in the plastic range results in an overestimated ultimate capacity for the dynamic loading. The pile head displacement is much underestimated thus the pile can survive much longer than it should be.

The Drain3D model gives more reasonable prediction. The time-history record of the fast loading to the final pile collapse is shown in Fig 3.14. The agreement between them and the results from SPASM before initial yielding is significant. After the first yielding, the SPASM model is no longer valid in predicting the ultimate response. The ultimate response calculated by Drain3D is more realistic. In Fig 3.14, a normalized loading factor P/P_u is plotted vs. pile head displacement for all cases of pile head rigidities. When P/P_u reach the value of 0.95, the second plastic hinge is in the procedure of formation. Keep increasing loading on the pile head, the pile head displacement will increase dramatically. This is the obvious indication that the collapse of the pile takes place. It can be seen that the fixed and restrained pile head cases have almost the same ultimate capacities.

The case of free pile head has a much lower capacity because the failure mechanism is quite different from other cases. For free pile head, the pile-soil system will collapse

shortly after the formation of the first plastic hinge, when all the supporting beams in the top soil layers fail. The ultimate pile head displacements are in the range of 1.1-1.3 feet. The variation is very small, not like what is expected before the calculation. From Fig. 3.14, another thing shall be noted. For large pile head rigidity, such as the cases of fixed and grouted pile heads, the initial yielding occurs earlier in the loading history than the small rigidity cases such as shimmed and free pile head. This means the later cases have smaller residue strength after initial yielding. For the practice of pile design, these conclusions are meaningful. If you design a pile with large pile rigidity (grouted pile head), the boundary restraints of the pile is so stiff that the first yielding is easy to take place in the pile. The pile tends to suffer permanent deformations at relatively lower loading. But it has a large portion of reserve strength. It has enough robustness to resist additional loading. On the contrary, the pile with small pile head rigidity is more flexible. It is not easy to yield thus can avoid permanent deformation at high loading. However, it has small reserve strength. The ultimate strength is just a little higher than the initial yielding strength. For this kind of pile, it is very dangerous if yielding take place in the pile. The pile has no robustness.

3.3.4.2 Cyclic Loading

As to the cyclic loading, the ultimate capacities obtained by SPASM and Drain3D are listed in Fig. 3.15. Comparing the time-history record of the SPASM and Drain3D in the elastic range, one can find that they are comparable. Although the two models have different approaches, there is a good match between them in the prediction of initial yielding capacities and pile head displacements. The application of the cyclic p-y curve

can reflect the final fully degraded soil characteristics. In the plastic range, only the prediction of Drain3D is considered as valid. The SPASM results are overestimated.

In Fig. 3.14, it can be seen again that the cyclic ultimate capacities of the pile are almost the same except the free pile head. Compared with the fast loading results, the ultimate capacities are much lower. This is because the support from the soils is much lower than the former case. The pile takes a much larger portion of the loading thus develops plastic hinges much earlier at lower external loading. But the ultimate pile head displacements are still in the range of 1.1-1.3 feet. This is an implication that there is a maximum lateral pile head displacement for the pile-soil system under study. This may be an important conclusion for the pile foundation performance in the Bay of Campeche.

3.3.4.3 Correlation with ULSLEA /TOPCAT

As to the static ultimate capacity, there are several kinds of calculation methods in this study. Drain3D is the complicated method that simulates all the details of the ultimate lateral pile response. ULSLEA/TOPCAT is a simplified approach, which does not address the detailed process of the response. It only considers the ultimate state of the pile-soil system. By introducing the virtual work principle, the complicated fully plastic problem is simplified to only two balance equations, one for force, the other for bending moments. The two equations are very easy to solve. Although ULSLEA/TOPCAT gives no information about the pile head displacement, it gives quite good estimation of the static ultimate capacity of the pile and the location of the second plastic hinges. The comparisons of the results from different methods are listed in Table 3.3, 3.4 and 3.5.

By correlating the ULSLEA/TOPCAT results to those from the complicated models, one amazing fact turns out that the predicted capacity values are quite close. This is an implication that the simplified model such as ULSLEA/TOPCAT can assess the pile capacity as well as the advanced, complicated model such as Drain3D. A more surprising phenomenon can be observed by correlating the ULSLEA/TOPCAT and Drain3d results. The ultimate pile capacity and pile head displacement are not sensitive to the pile head rigidity if the pile head restrain is large enough. The difference between the fixed, grouted and shimmed pile head does not cause much difference in the final ultimate state of the pile soil system. Of course, the free pile head behavior predicted by Drain3D is quite different from the restrained pile head. Is seems the ultimate capacity will become sensitive to the pile head rigidity if the rotational restrain from the jacket drops to a very low value. However, the piles in field never have free pile heads. They are at least shimmed. The rotational restrain is usually in the insensitive range. This implies that the ULSLEA/TOPCAT can give a very good estimation of the pile lateral ultimate capacity no matter what kind of pile head rigidity presents. In the offshore engineering practice, the difficulty in estimating the stiffness at the connection between the pile head and the superstructure has been cognized for a long time. Considering the fact that there is a large amount of uncertainty in determining the pile head rigidity in field, the above conclusion has great practical value. Again, the ULSLEA/TOPCAT model demonstrates its advantage of simplicity and correctness.

Table 3.3 Lateral capacities calculated by SPASM

Lateral capacities of a single pile (CALCULATED BY SPASM)						
	First Yielding Capacity (kips)			Ultimate Capacity(kips)		
Head Rigidity	Quasi-static	Quick	Cyclic	Quasi-static	Quick	Cyclic
Fixed Head	479.3	550.0	453.1	812.5	968.2	778.1
Free head	383.3	460.1	359.0	626.7	870.9	598.5
Grouted	525.2	618.3	495.8	866.7	1072.7	831.1
Non-grouted	630.0	740.2	598.5	1045.8	1400	1002

Table 3.4 Lateral capacities calculated by Drain3D

Lateral capacities of a single pile (CALCULATED BY DRAIN3D)						
	First Yielding Capacity (kips)			Ultimate Capacity(kips)		
Head Rigidity	Quasi-static	Quick	Cyclic	Quasi-static	Quick	Cyclic
Fixed Head	512.6	608.8	412.7	765.1	895.3	645.2
Free head	414.8	472.4	351.4	488.5	536.8	400.2
Grouted	479.5	644.6	452.8	765.1	895.3	640.8
Non-grouted	643.4	725.2	553.6	765.1	895.3	645.2

Table 3.5 Static ultimate capacities calculated by ULSLEA

Static ultimate capacity of a single pile (CALCULATED BY ULSLEA)	
Fixed Head	Static ultimate Capacity(kips)
ULSLEA 3.0 (linearly increasing S_u)	793.0
ULSLEA phase IV(layered soils)	909.5

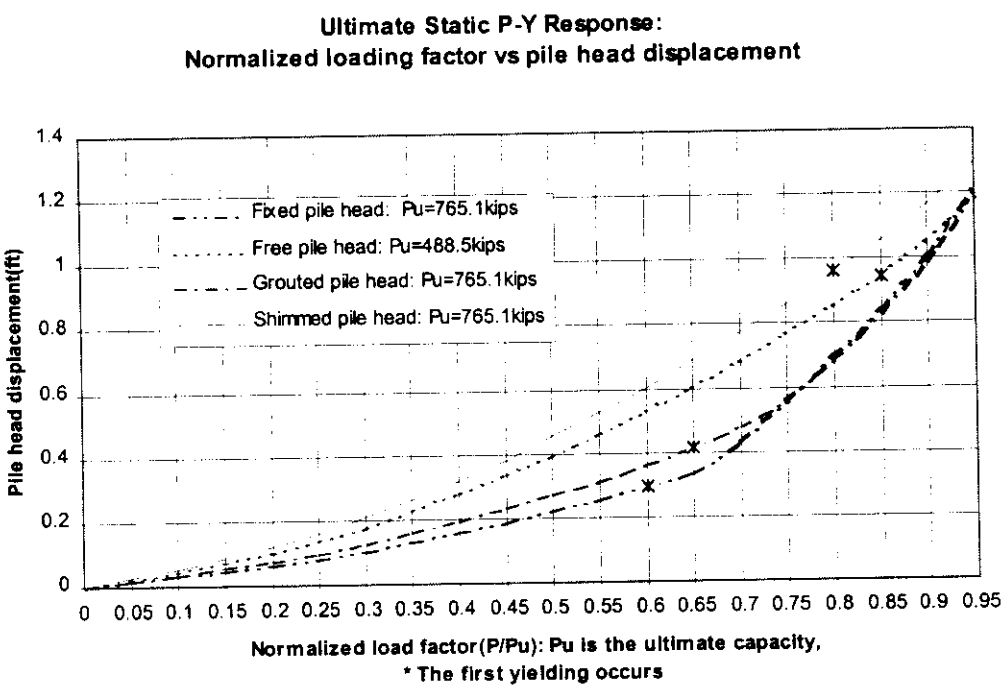

Figure 3.13 Displacement-loading relationship for static loading

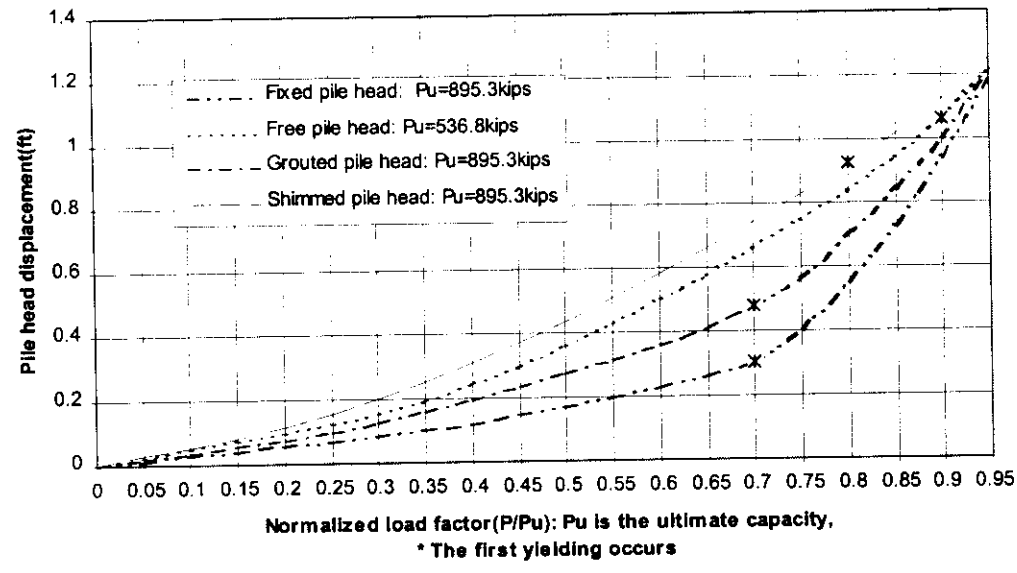

Figure 3.14 Displacement-loading relationship for fast loading

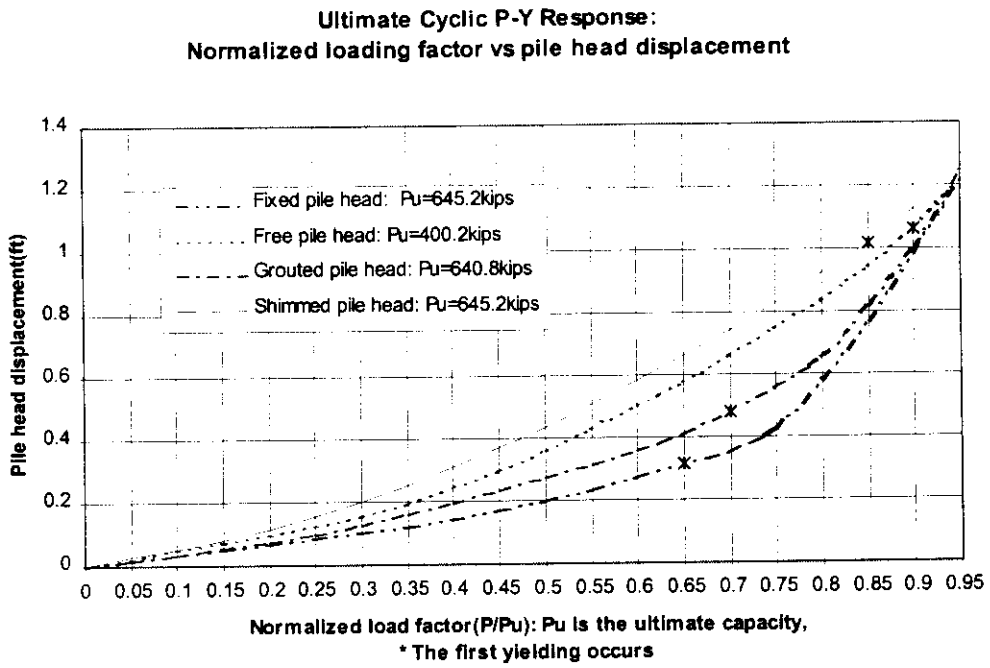

Figure 3.15 Displacement-loading relationship for cyclic loading

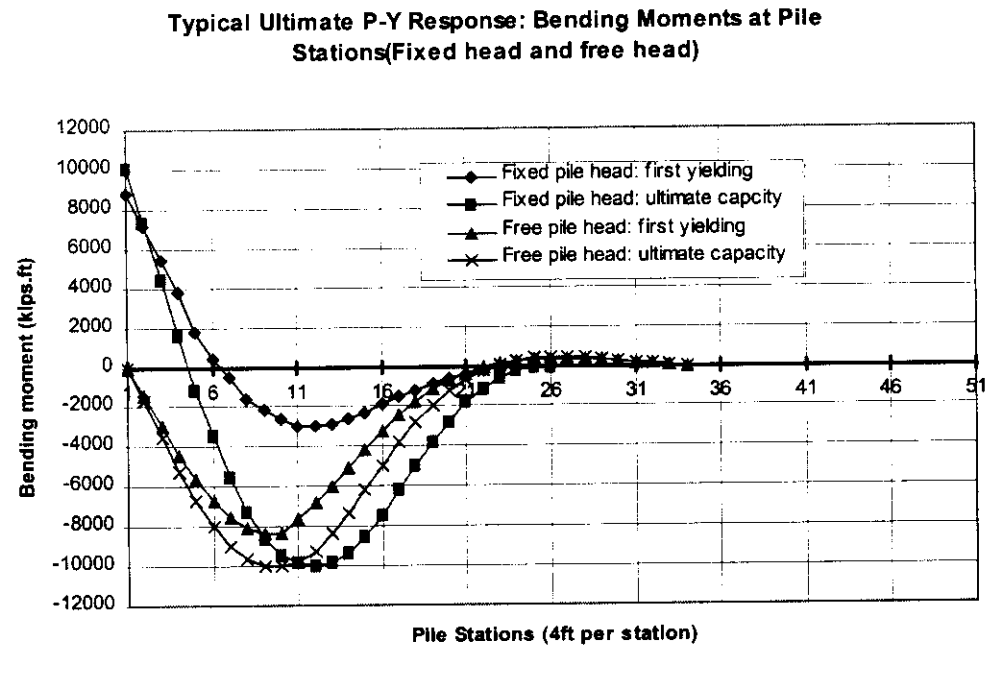

Figure 3.16 Bending moments at ultimate state (fixed and free pile head)

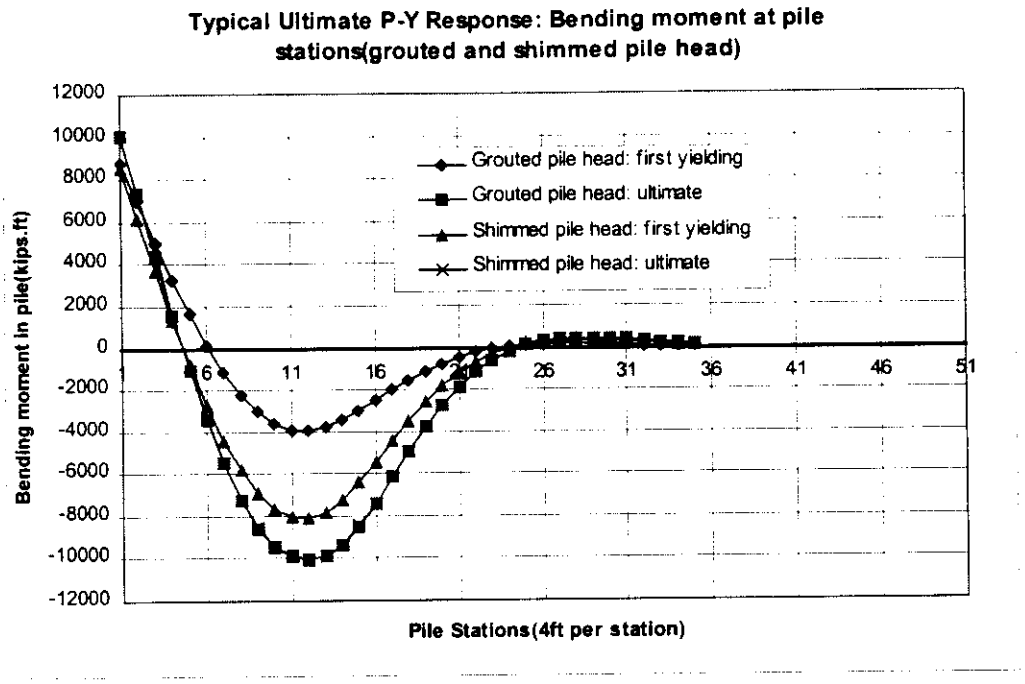

Figure 3.17 Bending moments at the ultimate state (grouted and shimmed pile head)

3.3.5 Summary

Tang(1990) performed a systematic reliability analysis of the lateral response of the offshore pile foundation. He defined three performance criteria for laterally loaded pile. Namely, they are the displacement mode (excessive displacement at pile head), the damage (first yielding) mode, and the collapse (ultimate yielding) mode. His analysis assumed an elastic pile, thus they are valid only up to first yielding. This report extends the analysis scope to the plastic range. The analysis results have demonstrated that the three failure modes are inherently related.

As to the displacement criteria, a surprising conclusion drawn from the analysis results in the Bay of Campeche is that there exists a maximum pile head displacement for the pile

under study. Given the pile configuration and soil characteristics in the area, the pile-soil system in this study has maximum displacements ranging from 1.1 feet to 1.3 feet for different pile head rigidities and loading patterns. The range is very narrow considering that there are large variation in pile head rigidities and loading patterns. So, it can be concluded that the pile will be doomed to fail if this maximum displacement is exceeded. This concedes with the empirical displacement criteria that the maximum pile head displacement is 1 foot to maintain the serviceability of the platform systems. More case study of different pile configuration and soil profiles will be conducted to see whether the above conclusion is generally applicable.

The displacement criteria are related to the pile head rigidity. The pile rigidity greatly influences the damage criteria. When the initial yielding occurs, the lateral loading and the pile head displacement at that point are quite different for different pile head rigidities. For the large pile head rigidity, the first yielding occurs earlier during the loading process. The displacement at the point of first yielding is relatively small. But the pile has large porting of reserve strength. The pile with small head rigidity is the contrary case. The displacement at the first yielding is relatively large. The first yielding occurs later. But this kind of pile has small reserve strength. In one word, the more rigid piles are prune to suffer permanent damage, but not easy to collapse, while the more flexible piles can stand large loading without suffering permanent damage, but tend to collapse quickly after the occurrence of the first yielding.

The collapse criteria is amazing the same for the restrained pile head, no matter how large is this restrain. The ultimate lateral capacities of the pile are almost the same. The ultimate displacements are almost the same too. The free pile head case is an exception. But this case is just a sensitivity study, which can not and shall not be achieved in field.

The bending moment distribution has typical patterns for the cases of first yielding and ultimate collapse. Such typical patterns obtained by Drain3D are plotted in Fig. 3.16 and 3.17. Note that the bending moment distributions at collapse are the same for restrained pile head except the positions of the second plastic hinges. For different pile head restrain and loading pattern, the positions of the second plastic hinges vary from 11^{th} pile node to 13th pile node, i.e., 44 to 52 feet below the mudline. This value is comparable with the prediction of ULSLEA, which is 39 feet for the fixed pile head.

As to the loading rate effects, the increase in the strength and stiffness of the soil results in an increase in the first yielding and ultimate collapse capacities compared with the static capacities. The soils provide larger supporting to the pile. More lateral loading will be transferred to soils. Again, no matter how large is the pile head restrain for this case, the ultimate capacities keeps the same. This implies that the increase in the soil resistance is not large enough. After the formation of the first plastic hinge in the pile, the pile stiffness drops drastically. The boundary condition of the head restrain becomes less important. The pile can not take as much loading as before. But the increase in soil strength by loading rate effect is not strong to take the additional loading. This is the reason why the ultimate collapse states are similar for different cases of the pile head

rigidity. The collapse failure mode of the laterally loaded pile involves mainly yielding of the pile itself instead of the soil, the loading rate effect is not as important as for the axial pile capacity.

As to cyclic degradation, the soils can only provide the residue resistance to the pile after they are fully degraded. The typical value for residue resistance of the soils in the Bay of Campeche is 70-80%. The cyclic first yielding and ultimate collapse capacity suffer a decrease. Both approaches of loading time-history in SPASM and the equivalent cyclic p-y curves in Drain3D produce results with good agreement. They capture the lower bound of the residual soil resistance that can be developed during the cyclic degradation. The lower bound capacities of pile-soil system under cyclic loading are roughly 65-80% of the static capacities.

3.4 Axial Pile Response

The analysis of the axial response of a single pile has the same framework as that of the lateral response. Drain3D and ULSLEA/TOPCAT are used to evaluate the capacities of the pile-soil system. ULSLEA/TOPCAT calculates the static ultimate axial capacity of the pile-soil system. Drain3D calculates the static and dynamic response of the pile-soil system.

Unlike the lateral response of the pile that has three major failure modes, the axial response of the pile-soil system is mainly determined by the soil resistance. It has only one major failure mode, i.e., failure of the soil resistance. The platform pile itself under

normal axial loading very seldom reach the steel plastic range, thus never buckle or collapse due to axial loading. It is the failure of the soils that causes the excessive displacement of pile head, thus causes the failure of the whole pile-soil system.

3.4.1 Pile Configurations and Soil Properties

The pile and soil properties are the same as those in the lateral analysis. The decomposition process of the discrete pile-soil Winkler model keeps the same. The positions of the nodes and the lengths of the pile segments are not changed. As the axial loading is transferred from the jacket, the restrain at the pile is not a factor in consideration, unlike what was done in the lateral analysis.

The basic soil profile is the same as that in the lateral analysis. Based on this backbone profile, the soil profile for the case of fast loading is modified. As the axial pile response is more sensitive to the loading rate effect than the lateral response, special care is taken to warrant this effect is reflected correctly in the modified t-z and q-z curves. This approach will be detailed in the following section.

As to the construction of the t-z and q-z curves, this study follows the API guideline, with a little modification. The construction process is detailed as follows:

T-Z curves

The unit ultimate friction for each layer of soils can be calculated using the formulae documented in section 3.2. The displacement (z_{max}) at which the ultimate friction

capacity is mobilized is a function of soil stress-strain behavior, stress history, pipe installation method, pile load sequence and other factors. In this study, z_{max} is taken to be 0.01D, according to the recommendation of the guideline. The shapes of the t-z curves at displacements greater than z_{max} as shown in Figure 3.18 are carefully considered. There is no definite data available about the values of the residual adhesion ratio t_{res}/t_{max} in the Bay of Campeche. Also this parameter involves large uncertainties for soils in field. So two cases are studied, one with the displacement softening after the peak friction is mobilized, the other without displacement softening. Usually, the value of t_{res}/t_{max} can range from 0.70 to 0.90. The mean value 0.80 is chosen to use in the case of softening. This is regarded as the lower bound of the unit ultimate side friction. The case without displacement softening is regarded as the upper bound of the unit ultimate side friction. The values of z/D and t/t_{max} used in this study are listed in Table 3.6. The shape of the t-z curve is shown in Figure 3.18.

Table 3.6 Coordinates of control points on t-z curves

z/D	t/t_{max}
.0016	0.30
.0031	0.50
.0057	0.75
.0080	0.90
.0100	1.00
.0200	0.80(or 1.00)
∞	0.80(or 1.00)

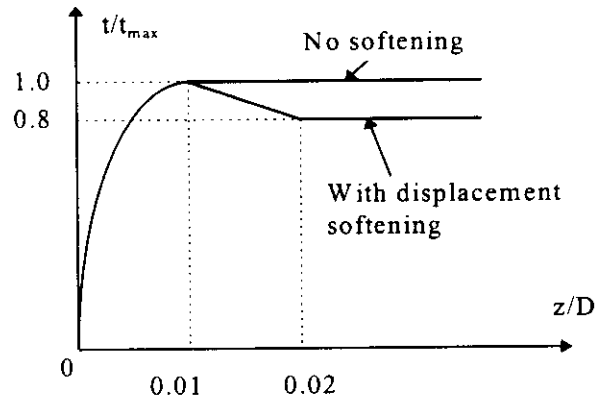

Figure 3.18 Typical t-z curves

Where,

z = local pile deflection, in. (mm)

D = pile diameter, in. (Mm)

t = mobilized soil pile adhesion, lb/ft^2 (kPa)

t_{max}= maximum soil pile adhesion or unit skin fraction capacity computed according to the API method described in Section 3.2, lb/ft^2 (kPa)

Q-Z Curve

The end bearing or tip load capacity Q_p can determined by equations described in Sections 3.2: $q=9*S_u$, S_u is the undrained shear strength. However, relatively large pile tip movements are required to mobilize the full end bearing resistance. A pile tip displacement up to 10 percent of the pile diameter may be required for full mobilization in clay soils. And compared with the side friction capacity, the ultimate bearing capacity is relatively small. The values of Q/Q_p and z/D are listed in Table 3.7. The shape of the q-z curve is shown in Figure 3.19.

Table 3.7 Coordinates of control points on the q-z curve

z/D	Q/Q_p
.002	0.25
.013	0.50
.042	0.75
.073	0.90
.100	1.00
∞	1.00

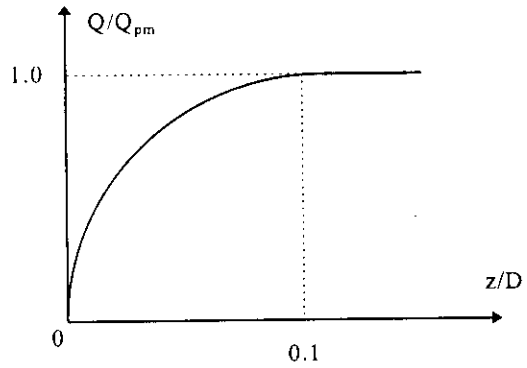

Figure 3.19 Typical q-z curve

where:

z = Axial tip deflection, in. (mm)

D = pile diameter, in. (mm)

Q = mobilized end bearing, lb (KN)

Q_p = total end bearing, lb (KN),computed according to Section 3.2

3.4.2 Drain3D and ULSLEA/TOPCAT models

Similar to the description in the last section, the Drain3D axial pile response model is a completely new analysis model. The idea is to simulate the response of pile-soil system to loading by an equivalent "solid" structure, i.e., a truss frame consists of steel column and soil supporting beam. The elements used in this Drain3D model are of type 1, type 4, and type 15. An illustration of such a truss frame is shown in Figure 3.20. The details of the node connections and sub-element configurations are also shown in Figure 3.12. Note that the axial soil beams can be actually regarded as being plugged in the steel pile. They are connected at pile nodes. The loading is allocated to pile and soil beams at these nodes. Since there are significant displacement softening for the axial response, the "rigid bars" are also added to each soil beams to prevent them from buckling before the ultimate soil friction capacity is mobilized. The soil beams simulating the t-z springs are 2 feet long. This length is chosen so that the largest strain occurs in the bar is less than 10% when it yields or reaches the residual resistance. For the same reason, the soil beams simulating the q-z spring have a length of 4 feet. Just as in the lateral analysis, the soil beams are assigned to have zero resistance to tension. There are a pair of such soil beams with opposite orientations at each pile, one resisting the compression loading, the other resisting the tension loading.

The ULSLEA/TOPCAT can only calculate the static ultimate capacity of the pile-soil system. It assumes a rigid pile. It also assumes that the maximum end bearing and side friction are mobilized at the same time. These assumptions greatly simplify the approach, but meanwhile, does not loss control of the major factors influencing the axial ultimate

capacity. ULSLEA/TOPCAT can not provide the information about the pile head displacement. The calculation method has been stated in section 3.2. The layered soil calculation is used. The total pile-soil system capacity is obtained by integration of the unit friction along the pile length. The results of ULSLEA/TOPCAT are detailed in the following section.

3.4.3 Axial Response of a Pile to the Static Loading

The axial response of the pile is calculated by Drain3D model. The pile head displacement-axial loading relationship is obtained and plotted as a graph. The prediction of axial ultimate capacity by different calculation method is listed in a table for comparison.

Ultimate capacity predicted by DRAIN3D

For static loading, two cases are studied by Drain3D model. The first analysis considers the displacement softening after the peak friction resistance. The residual friction resistance is 80% of the peak value. The second one does not consider this softening. The two cases define a possible range of the static axial ultimate capacity. The capacity obtained by the first case is the lower bound. The ultimate capacity of the first case is around 80% of the second case. The second one is the upper bound. The results are listed in Table 3.8. The displacement-loading relationship is also obtained. This relationship is plotted in Figure 3.20. It can be easily seen that the major portion of the axial capacity is contributed to side friction resistance. The end bearing is not very important. After the failure has occurred in all the t-z springs, The loading is transferred to the q-z springs.

And the displacement increases drastically. For the pile-soil system with this configuration, there exists a maximum value for pile head displacement. Considering the fact that the end bearing q-z springs will fail as the pile tip displacement exceeds 0.1D=0.4ft, the maximum pile head displacement is around 4.5ft.

Correlation with ULSLEA/TOPCAT and API guidelines

The static ultimate axial capacity can be calculated by ULSLEA/TOPCAT program. An estimation of this capacity can also be made following the API guidelines. The calculation methods have been detailed in section 3.2.

The comparisons of all these results are listed in Table 3.8. All the calculated capacities are pretty close. A good agreement between different calculation methods is achieved.

Table 3.8 Predictions of axial capacities

Axial capacities of a single pile (Calculated by DRAIN3D, ULSLEA and API Guideline)		
	Axial ultimate Capacity(kips)	
Calculation Methods	Static	Quick
Drain3D without displacement softening	3787.2	6430.3
Drain3D with displacement softening	3108.7	5600.8
ULSLEA(layered soils)	3102.8	non
API calculation method	3389.5	non

One thing shall be made clear is that the ULSLEA/TOPCAT result is obtained by assign maximum friction factors in Table 3.1. The capacity in Table 3.8 is possible maximum

that can be predicted by ULSLEA/TOPCAT. But the ULSLEA/TOPCAT capacity value is still the smallest one. So it seems that ULSLEA/TOPCAT under-estimated the axial ultimate pile capacity. The reason can be traced to the method of determining the side friction factor. In ULSLEA/TOPCAT, the friction factor is a function of the average undrained shear strength (Table 3.1). While the API guideline takes an effective overburden pressure approach which is better in predicting the friction resistance (Tang, 1988). Drain3D also takes this way to predict the ultimate capacity. Anyway, the ULSLEA results are conservative, and tend to be on the safe side if it's predicted capacities are used in practical design.

3.4.4 Axial Response of a Pile to the Dynamic Loading

Two dynamic responses are studied: responses to the fast loading and to the cyclic loading. The fast loading increases the strength and stiffness of the soils thus increases the ultimate capacity of the pile-soil system. The cyclic loading just do the opposite things.

Sully, et al (1994) defined an approach to estimate the effective axial dynamic load carrying capacity based on the static axial capacity:

$$R_d = R_s \bullet \beta_c \bullet \beta_r \qquad 3.20$$

Where R_s is the static capacity; R_d is the dynamic capacity; β_c reflects the cyclic loading effect; and β_r reflects the loading rate effect. The dynamic analysis in this study is trying to find the characteristics of β_c and β_r.

Fast loading

For fast loading, the loading rate effect is obvious. There are presently two ways to reflect these kinds of effects. The first is incorporate dynamic effects into the *t-z* and *q-z* characterizations. This was an implicit way to incorporate the effects. The second way was to apply a velocity-dependent strain-rate correction to the static backbone *t-z* and *q-z* curves.

Using the parameter β_r is the second approach. β_r is larger than 1 for fast loading. The dynamic capacity for fast loading is larger than the static capacity. For normally consolidated, moderate plasticity clays, r=0.10 to 0.20. The study of the available laboratory test data on the Bay of Campeche cohesive soils indicates that the r value for the soils under study can be taken as 0.15. If the static loading rate of the pile is 24 hours and the average loading rate from storm waves is 3 seconds, The β_r value turns out to be 1.67.

The Drain3D take the similar approach. The static backbone t-z and q-z curves were modified by a factor of 1.5, just as how the p-y curves were modified in lateral analysis. The soil beams' properties are modified according to the new t-z and q-z curves. The "concrete" strain-stress relationships for the material of the soil beams are then corrected for the fast loading. The results of the time-history of the pile-soil system response are plotted in Fig. 3.21. Compared with the static response, the ultimate capacity for fast loading is about 1.7-1.8 times the static ultimate capacity, which is comparable with the

β_r value. The increase in ultimate capacity is a little higher than the increase of resistance in t-z and q-z curves. This is due to the viscous damping at the high loading rates.

The above results are quite reasonable. The loading effects is due to the viscous behavior of the soils, that is, their strength depends upon the rate at which they are sheared. This behavior extends to the observed capacity of piles installed in clays. The ultimate capacity of pile in clays reportedly increases between 5 and 20 percent for each order of magnitude increase in loading rate. In the absence of soil strength degradation due to load cycling, axial capacities of piles in clay that are loaded by storm waves could be 30 to 80 percent greater than capacities calculated using static design procedures (Bea, 1980). The results of this study provide more support to this argument.

Cyclic loading

The cyclic loading analysis needs the soil supporting beams exhibit strength degradation behavior. Element type 15 in Drain3D does have a degradation mechanism in element stiffness and strength. However, a cyclic model by this way doesn't work well in simulating the pile-soil response. The degradation mechanism is originally designed to reflect the "pull-out" bar degradation in the re-enforced concrete. The degradation is concentrated at the connection between elements. The degradation process is a function of the element's accumulated plastic displacement. It does not fit the soil degradation process defined by Matlock(1978). By now, the Drain3D model has not developed to be a valid analysis tool with respect to the cyclic axial loading yet. A new, more specific element is needed to simulate the soil degradation. Although the model is not good

enough to do the detailed analysis, reviewing of the related research can lead to some valuable general comments about the axial cyclic response problem.

Existing experimental and analytical programs show that the cyclic pile problem is complex. The recent research efforts have identified several factors that influence cyclic axial pile performance, including:

- static capacity;
- the nature of the cycling, including the magnitude of the sustained and cyclic load components and whether the pile is cycled using load control or displacement control;
- viscous soil behavior (rate effects);
- displacement softening behavior of soil resistance-vs.-pile displacement (t-z) relations;
- the stiffness of the pile relative to the soil; and
- the number of cycles applied at each given load level

Each of these factors is important, and should be considered when assessing the likely behavior of a pile under storm loading.

Based on the research works of Bea (1992), and Clukey (1990), cyclic axial pile response has its' unique patterns. The cyclic loading effect in equation (4.1) can be estimated by:

$$\beta_c = 1 - \Delta(1-\delta) \qquad 3.21$$

where Δ = the ratio of percentage change in soil strength to percentage change in soil stiffness; and δ = the degradation index:

$$\delta = N^{t} = \frac{Gn}{G_{1}} \qquad 3.22$$

where N = the number of cycles of peak strain (fully reversing harmonic straining); t = the degradation parameter (function of peak strain and soil); and G = the shear modulus at $N = 1$ and n cycles. β_c is the ratio of the capacity of the pile after design cyclic loading to the static capacity. The cyclic-loading factor is generally less than unity and can be based on results of laboratory cyclic or model and prototype pile tests. For a moderate-plasticity, normally consolidated clay, estimates of $\Delta = 0.5$, $t = 0.1$ (0.1% cyclic shear strain), $N = 10$ (equivalent number of cycles of design loading) results in $\beta c = 0.9$.

The cyclic degradation mechanism for axial response can be formulated in a similar way as that used in the SPASM lateral analysis (Bea, 1992; Matlock, 1980): For small levels of strain, the degradation index is reasonably linearly related to the number of cycles of the strain. For high levels of strain (greater than 1-2%), which is the case for near-field soils, the degradation factor was used with a specified residual capacity. The shaft resistance at cycle N, t_n, was computed as:

$$t_{N} = \delta\left(t_{N} - t_{res}\right) + t_{res} \qquad 3.23$$

where t_{res} = the residual level of capacity (e. g. $_{,tres} \approx t$ remolded). This is a modified from of the model proposed by Matlock and Foo (1979) in which:

$\delta = (1 - \lambda)$

where λ = a model parameter that is used to fit measured data from soil tests or model pile tests. The minimum degradation parameter, δ_{min} was taken to be the reciprocal of the clay sensitivity (δ_{min} = 0.33 - 0.25). This degradation mechanism should be incorporated into a new Drain3D model to accurately simulate the soil behavior under cyclic loading.

The degree to which cyclic loading degrades static skin friction depends upon the relative magnitudes of the sustained and cyclic load components and on whether the cycling is with respect to pile head loads or to pilehead displacements (load or displacement control). With all else being equal, damage to pile performance generally decreases either as:

- the magnitude of cyclic loads, as a fraction of ultimate pile capacity, decreases, or
- the amplitude of imposed cyclic displacements decreases.

Strictly speaking, the local nature of the cycling and the resulting damage must be evaluated at each point along the pile. This is because pile-soil relative stiffness effects reduce the correspondence between cyclic pilehead loads and the resulting soil stresses. For example, stress reversals can occur in the soil near the tops of long piles that are subjected to wholly compressive or tensile cyclic loads.

One-way cycling in clays without local soil shear stress reversals normally causes little reduction in peak skin friction; damage from such cycling is manifested predominately in accumulated displacements. Piles in firm to hard clays reportedly have resisted several

hundred one-way load cycles when the peak pile load was less than 0.75 - 0.80 static capacity.

Two-way cycling, i.e., subjecting the soil around a pile to both positive and negative shearing stresses, is much more damaging than one-way cycling. Failure due to increased displacements reportedly has occurred during symmetric two-way loading tests of stiff piles. Large amplitude two-way displacement-controlled cycling can be the most damaging of all. It was found in one case the skin friction is reduced to about thirty percent of the undegraded static skin friction. The skin friction that is lost during two-way cycling in non-strain-softening clays generally is recoverable by soil reconsolidation after cycling. This suggests that frictional resistance that is lost in such soils during a major storm probably can be substantially reestablished before another major storm occurs. However, some results in clays with displacement-softening t-z behavior show incomplete strength regain after cycling. It cam be inferred from this collective experience that a foundation's survivability through multiple design storm perhaps does not need to be investigated unless the supporting clay exhibits strain softening behavior.

The stiffness of a pile relative to the soil in which it is embedded can influence the pile's cyclic performance substantially. Considering the following special case, an infinitely stiff pile that is subjected to one-way cyclic pile head loads will induce relatively undamaging one-way stress cycling along its entire length. On the contrary, a pile with a finite stiffness that is loaded with one-way cycles can subject the soil along a substantial

portion of its length to damaging two-way cycles. The second pile will have a lower static capacity after cycling than will the first pile.

One thing should be emphasized that the foregoing comments may not be regarded as general. They are appropriate for the particular pile, soil, and loading conditions evaluated in the analyses. More comprehensive analyses of the dynamic response characteristics of offshore piles embedded in marine soils and subjected to realistic characterizations of marine-structure pile loadings ate needed to permit development of general engineering guidelines for consideration of dynamic cyclic-loading effects on piles.

3.5 Summary and Conclusions of Pile Dynamic Response Analysis

3.5.1 Summary

A systematic analysis of the offshore pile foundation response and its ultimate characteristics has been finished. This research is a part of the effort to develop design and re-qualification criteria for PEMEX and IMP. This research focuses the study on the behavior of a single pile driven into soft clays. This research based the study on the oceanographic, geotechnic and in-situ platform information provided by PEMEX and IMP.

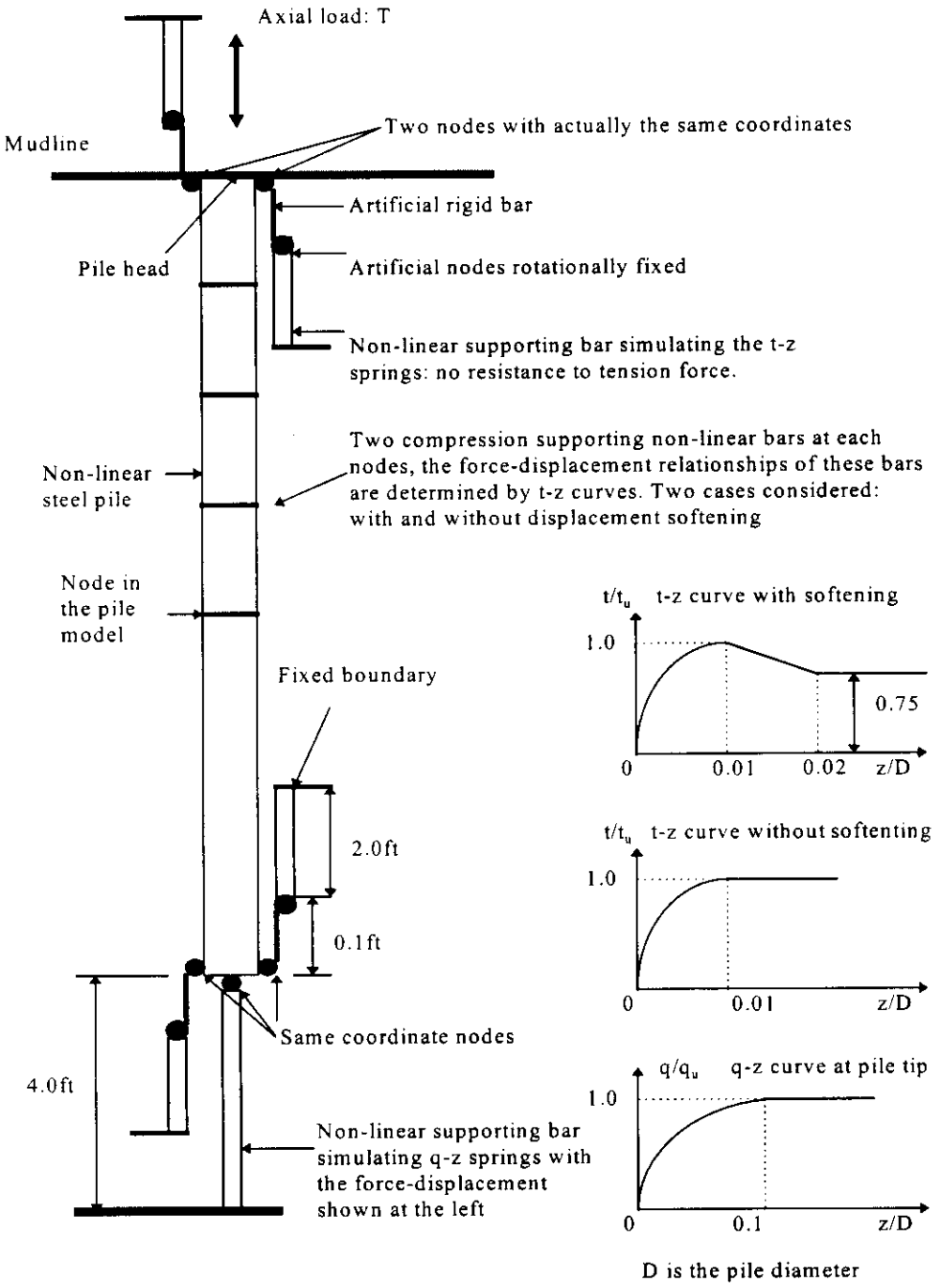

Figure 3.20 Equivalent truss frame simulating the axial response of the pile-soil system

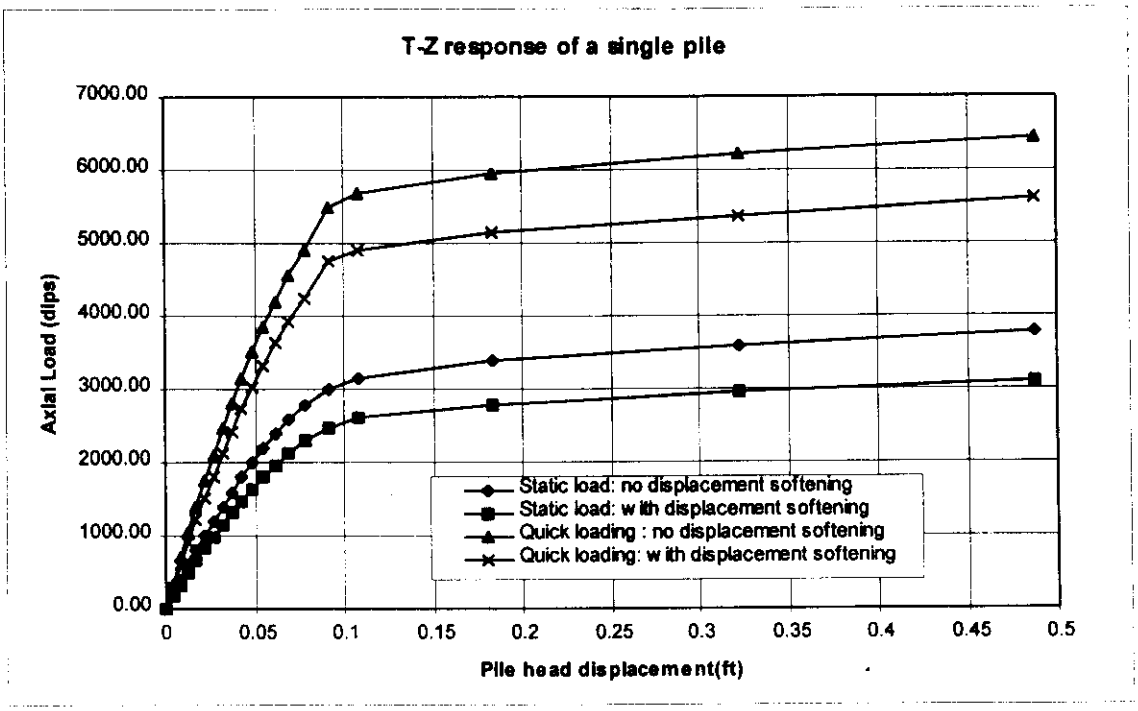

Figure 3.21 Pile head displacement - axial load relationship for static and fast loading

There are mainly three computers codes used in the analysis: Drain3D, SPASM and ULSLEA/TOPCAT. Drain3D model is a new pile analysis tool. It extends the analysis scope to non-linear steel pile and non-linear-hysteretic soil supporting. It can handle both lateral and axial response of the single pile. It can calculate the dynamic response of the pile by a time-history approach, either displacement control or load control. The SPASM is a specific pile analysis tool for lateral loading. It assumes an elastic pile. It can couple the complicated interaction between the linear pile and the hysteretic soil springs. ULSLEA/TOPCAT is a simplified ultimate state analysis tool. It can give very good estimation of the lateral and axial ultimate capacity of a single pile, although it has a very simple approach. Using these analysis tools, lateral loading and axial loading analyses are performed.

The lateral analysis includes a set of standard cases. The loading patterns, soil characteristics, and pile configuration are systematically changed to reflect the effects of cyclic loading, fast loading and the ultimate state properties for different combination of all these variables. It is intended to capture the impacts on the pile response and ultimate capacity by the natural variation. The results from different analysis tools are compared. Valuable conclusion about the response and ultimate state of the laterally loaded piles are obtained.

The axial analysis takes the similar framework as the lateral analysis. The static and fast loading cases are successfully studied. The loading rate effect has been identified. The validity of the simplified ULSLEA/TOPCAT program has been proved. The possible range of the axial ultimate capacity is defined based on the variation in the residual resistance after the peak value. A cyclic axial model has been built. Although the simulation of the pile-soil response is not as good as expected, a study of the features of the cyclic degradation, cyclic loading pattern, relative pile stiffness, etc., leads to some general comments on the cyclic axial pile response problem.

3.5.2 Conclusion

Based on the analysis results, some useful conclusions can be drawn:

- For lateral loaded pile, three failure modes exist: excessive pile head displacement; permanent damage to the pile; and ultimate collapse.

- For the pile configuration under study, pile rigidity is not an important factor influencing the ultimate capacity, all shimmed, grouted, and fixed pile heads have the similar lateral ultimate capacity. Free pile head is an exception.
- For the pile configuration under study, pile rigidity is an important factor influence the first yielding capacity, and the reserve strength of the pile. Stiff pile head is prune to suffer permanent damage but has large reserve strength. Flexible pile head is not easy to yield, but has little robustness.
- For the pile configuration under study, there exists a maximum later pile head displacement. The pile is doomed to fail if the pile head displacement exceeds this value.
- The cyclic degradation in the Bay of Campeche will cause 20-30% loss of static lateral capacities, both first yielding capacity and ultimate capacity.
- The loading rate effect will cause around 20% increase in lateral dynamic capacity with respect to the static capacity.
- In practice, ULSLEA/TOPCAT has good validity in predicting the ultimate capacities of the platforms.
- For the pile-soil system under study, the axial loading rate effect increases the dynamic capacity by 70-80% with respect to the static axial capacity.
- The end bearing capacity is not as important as the side friction for the axially loaded piles. For the pile configuration under study, the maximum pile head displacement is a little larger than 10% of the pile diameter.
- The displacement softening occurring during the axial loading process decreases the ultimate axial capacity by around 20%.

- For the case of axial loading, ULSLEA/TOPCAT capture the lower bound of the ultimate capacity, thus is conservative in practice.

Reference

Aaghaakouchak, A. A., Asgaroan, B.(1996), "*Dynamic Characteristics of a Jacket Type Offshore Structure Considering Non-Linear Behavior of Pile Foundations*", 1996 OMAE--Volume 1--Part A, *Offshore Technology*, ASME 1996.

Aggarwal, R. K., Litton, R. W., Cornell, C. A., Tang, W. H., Chen, J. H., Muff, J. D., "*Development of Pile Foundation Bias Factors Using Observed Behavior of Platform During Hurricane Andrew*", *Proceedings of Offshore Technology Conference*, OTC 8078.

American Petroleum Institute, API. *Recommended Practice for Planning, Designing and Constructing Fixed Offshore Platforms.* API Recommended Practice 2A (RP 2A)-LRFD. 20, August, 1993, Dallas, Texas.

Arnoid, P.(1973), "Finite Element Analysis -- A Basis for Sea-Floor Soil Movement Design Criteria", *Proceedings of the Offshore Technology Conference,* OTC 1900, Society of Petroleum Engineers, Richardson, TX.

Barltrop, N. D. P., and Adams A. J., *Dynamics of Fixed Marine Structures*, Third Edition (1991), The Marine Technology Directorate Limited.

Bea, R.G., Audibert, J.M.E., and Dover, A. R. (1980), "Dynamic Response of Laterally and Axially loaded Piles", Proceedings, 12th Annual Offshore Technology Conference, Paper OTC 3749, Houston (May, 1980) Vol. II, 129-139

Bea, R. G (1992)., "Analysis of Tension leg Platform Pile Foundations for Dynamic Loading", *Geotechnical News--Newsletter of the North American Geotechnical Community*, Volume 10, Number 2, June, 1992.

Bea, R. G. (1984), "Dynamic Response of Marine Foundation", *Proceedings of Ocean Structural Dynamics Symposium*, Oregon State University, Corvallis, Oregon, September, 1984.

Bea, R. G.(1994), *Evaluation of the Reliability of a Conventional Platform Installed in South Pass Block 47.*

Bea, R. G. , Litton, R. W. and Chang, J. Y.(1984), "A Specialized Design and Research Tool for the Modeling of Near-Field Pile-Soil Interactions", *Proceedings of Offshore Technology Conference*, OTC 4806.

Bea, R. G. (1992), "Pile Capacity for Axial Cyclic Loading", *Journal of Geotechnical Engineering*, Vol. 118, No. 1, January, 1992.

Bea, R. G. (1997), "Risk Based Hurricane and Earthquake Criteria for Design and Requalification of Platforms in the Bay of Campeche." Report to Petroleo Mexicanos, September 1997.

Bea R. G.(1994), Evaluation of the Reliability of a Conventional Platform Installed in South Pass Block 47. Department of Civil Engineering and Department of Naval Architecture & Offshore Engineering

Bea, R. G. (1975). "Gulf of Mexico Hurricane Wave Heights," Journal of Petroleum Technology, Society of Petroleum Engineers, Richardson, TX.

Bea, R. G. (1983). "Gulf of Mexico Shallow-Water Wave Heights and Forces," Proceedings of the Offshore Technology Conference, OTC 4586, Society of Petroleum Engineers, Richardson, TX.

Bea, R. G. (1988a). "*Tropical Cyclone parameters for Goodwyn Substructure Environmental Criteria: Maximum Wave Heights and Periods*", Report to Woodside Offshore Petroleum Ltd., Perth, Western Australia, Department of Civil Engineering, University of California at Berkeley.

Bea, R. G. (1988b). "*Review of the Ocean Engineering Group's Definition of Environmental Design Criteria for Goodwyn 'A' Platform*", Report to Woodside Offshore Petroleum Ltd., Perth, Western Australia., Department of Civil Engineering, University of California at Berkeley.

Bea, R. G. (1990), "Effects of Water Wave Kinematics Uncertainty on Design Criteria for Offshore Structures," *Water Wave Kinematics*, A. Torum and O. T. Gudmestad (Editors), Kluwer Academic Publishers, London, UK.

Bea, R. G.(1991). "*Loading and load Effects Uncertainties*", Verification Program for CSA Code for the Design, Construction, and Installation of Fixed Offshore Structures Project No. D-3, Report to the Canadian Standards Association, Calgary, Canada, Department of Civil Engineering, University of California at Berkeley.

Bea, R. G. (1996). "*Evaluation of the Reliability of a Conventional Platform Sited in South Pass Block 47 of the Mississippi River Delta*," Proceedings of the Offshore Technology Conference, OTC 8305, Society of Petroleum Engineers, Richardson, TX.

Bea, R. G. ,Audibert, J. M. (1980). "Offshore Platforms and Pipelines on Mississippi River Delta, *Journal of Geotechnical Engineering*, American Society of Civil Engineers, New York, NY.

Bea, R. G., and Aurora, R. P.,(1981). "A simplified Evaluation of Seafloor Stability," *Proceedings of the Offshore Technology Conference*, OTC 39975, Society of Petroleum Engineers, New York, NY.

Bea, R. G., Wright, S W., Sircar, P., Niedorda, A. W. (1983). "Wave-Induced Slides in South Pass Block 70, Mississippi Delta, *Journal of Geotechnical Engineering*, American Society of Civil Engineers, New York, NY.

Bea, R. G., Pawsey, S. F., and Litton, A. W. (1988). "Measured and Predicted Wave Forces in Offshore Structures," Proceedings of the Offshore Technology Conference, OTC 5787, Society of Petroleum Engineers, Richardson, TX.

Bea, R. G., Lee, G. C., and Moore, G. H. (1991). "Reliability Based Design Criteria for Freeport McMoRan Main Pass Block 299 Sulphur Mine Platforms," *Proceeding of the Offshore Technology Conference*, OTC 6663, Society of Petroleum Engineers, Rochardson, TX.

Budkowaka, B. B. and E. Cean (1996), "Comparative Sensitivity Analysis of Laterally Loaded Piles", *Proceedings of the Sixth-International Offshore and Polar Engineering Conference*, Los Angeles, May, 1996.

Clukey, E. C., Maller, A. V., Murff, J. D., Goodwin, R, H., Miller, M. C., and Ebelhar, R. J.(1990). "Wave Attenuation, Mudslide, and Structural Analyses for Mississippi Delta/Main Pass Caisson, *Transactions of the American Society of Mechanical Engineers*, Vol. 112, New York, NY.

Clukey, E. C., Maller, A. V., Murff, J. D., Miller, M. C., Goodwin, R, H, and Ebelhar, R. J., "Wave Attenuation, Mudslide, and Structural Analyses for Main Pass/Mississippi Delta Caisson.". *Proceedings of the Seventh International Conference on Offshore Mechanics and Arctic Engineering*, Houston, TX.

Clukey,E. C., Jackson, C. R.,Vermersch, J. A.,Koch, S. P., and Lamb W. C.(1989), "Natural Densification by Wave Action of Sand Surrounding a Buried Offshore Pipeline", *Proceedings of the Offshore Technology Conference*, OTC 6151. Society of Petroleum Engineers, Richardson, TX.

Coleman, J. M., Suhayda, J. N., and Dawson T. H. , "Determination of Elastic Shear Modulus of Marine Sediments from Wave Theory and Field Measurements".

Dawson, T. H., Suhayda, J. N., and Coleman,J. M.(1981), "Correlation of Field Measurements with Elastic Theory of Sea-Floor Response to Surface Waves", *Proceedings of the Offshore Technology Conference*, Society of Petroleum Engineers, Richardson, TX.

Dunnavant, T. W., Clay, E. C, Murff, J. D.(1990), "Effects of Cyclic Loading and Pile Flexibilities in Clay", *Proceedings of Offshore Technology Conference*, OTC 6378.

Earth Mechanics, Inc., "Dynamic Soil-Pile Interaction Analysis, Group Va Sites Borings YAXILTUM-101, YAXILTUM-1, IB-102, CEEH-101, Moan-1, Tabay-1 and Kayab-1,

Bay of Campeche, Mexico", Report to Fugro-McClelland Marine Geosciences, Inc, May, 1994.

Emrich, W. J. , "Performance Study of Sampler for Deep-Penetration Marine Borings", Sampling of Soil and Rock.

Folse, M. D. "Reliability Analysis for Laterally Loaded Piles", *Journal of Structural Engineering*, ASCE .

Forristall,G. Z.,Reece, M. A., Thro, M. E., Ward, E. G.,Doyle, E. H., and Hamilton, R. C.(1980), "Measurements of Sea Wave Attenuation Due to Deformable Bottoms", Preprint of Paper to be Presented at the ASCE Fall Convention.

Forristall, G. Z. and Reece, A. M. (1985). "Measurements of Wave Attenuation Due to a Soft Bottom: the SWAMP Experiment", Journal of Geophysical Research, Vol. 90, American Geophysical Union, New York, NY.

Forristall, G. Z., Doule, E. H., Silva, W., Moriwaki, Y.(1987). "Verification of A Soil Wave Interaction Model(SWIM)", Paper Prepared for Publication, Shell Development Co., Houston, NY

Forristall, G. Z., Reece, A. M., Thro, M. E,, Ward, E. G. Doylem E. H., and Hamiltin, R. C., (1980). "Sea Wave Attenuation Due to Deformable Bottoms." {reprint 80-536, American Society of Civil Engineers Convention and Exposition, Miami, FL.

Fugro Gulf, Inc., (1979), "Investigacion Geotecnica en la Localizacion, ABKATUN-4, Bahia de Campeche", Septiember, Mexico D. F.

Fugro Gulf, Inc., (1981), "Inverstigacion Geotecnica en la Localizacion Pol-79 en Bahia de Campeche", Reporte Final No. 17, Junio, Mexico D. F.

Fugro Gulf, Inc., (1979). "Investigacion Geotecnica y Consideraciones Para la Cimentacion en el Sitio KU-57 en Bahia de Campeche", Diciembre, Mexico D. F.

Fugro-McClelland Marine Geoscinces, Inc., "Criterios para Diseno Estatico Informacion Prelimlnar Para Diseno de Pilotes", Investigacion Geotecnica Sondeo: AKAL-T-J Bahia de Campeche, Mexico", Reporte Preliminar Numero 0201-2927-16, Julio, Houston, Texas.

Fugro-McClelland Marine Geoscinces, Inc.(1996), "Reporte Final Investigacion Geotecnica , Sondeo AKAL-T-J Bahia de Campeche, Mexico, Volumen I", Reporte Numero 0201-2927-16, Octubre.

Fugro-McClelland Marine Geoscinces, Inc.(1996), "Reporte Final Investigacion Geotecnica , Sondeo AKAL-T-J Bahia de Campeche, Mexico, Volumen II", Reporte Numero 0201-2927-16, Octubre.

Fugro-McClelland Marine Geoscinces, Inc. "Evaluacion Ingenieril-Geologica Area Kuts, AKAL-L-KL y AKAL-T-J Bahia de Campeche, Mexico", Reporte Numero 0201-2926-24, Agosto, Houston, Texas.

Fugro-McClelland Marine Geoscinces, Inc. (1996), "Reporte Final Investigacion Geotecnica Sondeo POOl-TF Bahia de Campeche, Mexico", Reporte No.: 0201-2927-2, Septiembre, Houston, Texas.

Fugro-MccCclelland Marine Geoscinces, Inc. (1996), "Reporte Final Investigacion Geotecnica Sondeo Che-1 Bahia de Campeche, Mexico", Reporte No.: 0201-2927-23, Noviembre, Houston, Texas.

Fugro-MccCclelland Marine Geoscinces, Inc.(1993), " Static Design Criteria Geotevhnical Investigation Boring CHA-1 Bay of Campeche, Mexico", Report No. 00201-2131-4, October, Houston, Texas.

Fugro-MccCclelland Marine Geoscinces, Inc.(1994), " Static Design Criteria Geotevhnical Investigation Boring OCH-TA Bay of Campeche, Mexico", Report No.0201-2336-7, May, Houston, Taxas.

Fugro-MccCclelland Marine Geoscinces, Inc.(1994), "Dynamic Disign Criteria For Earthquake Loading Conditions Boring UECH-TB Bay of Campeche, Mexico", Report No. 0201-2336-6D, August , Houston, Texas.

Fugro-MccCclelland Marine Geoscinces, Inc.(1994), "Static Design Criteria Geotechnical Investigation Boring TARATUNICH-TF Bay of Campeche, Mexico", Report No.0201-2336-5, May, Houston, Texas.

Fugro-MccCclelland Marine Geoscinces, Inc.(1994), "Dynamic Design Criteria For Earthquake Loading Conditions Boring TARATUNICH-TF Bay of Campeche, Mexico", Report No.0201-2336-5D, August, Houston, Texas.

Gu, G. Z., and Thompson, G. R. (1995). "Wave Induced Mudslide Analyses for Offshore Structure, Design," Mobil Research and Development Corporation Paper, Dallas, TX.

Gade,H. G.(1958), "Effects of A Nonrigid, Impermeable Bottom on Plane Surface Waves in Shallow Water", *Journal of Marine Research, Vol. 16,* Bingham Oceanographic Laboratory, Yale University.

Heideman, J. C., and Weaver, T. O. (1992). "Static Wave Force Procedure for Platform Design," Civil Engineering in the Oceans V, Proceedings of the International Conference, American Society of Civil Engineers, New York, NY.

Kraft, L. M., and Ploessel M. R., "Stability of Submarine Slopes", *Environmental Factors*.

Kraft, L. M., Helfrich, S. C., Suhayda, J. N., Marin, J. E. (1985). "Soil Response to Ocean Waves," *Marine Geotechnology*, Vol. 9, Crane, Russak & Col, Inc., UK.

Kraft, L. M., Suhayda, J. N., Helfrich, S., C., and Marin, J. E. (1985). "Ocean Wave Attenuation Due to Soft Seafloor Sediments," *Marine Geotechnology*, Vol. 9, Crane, Russak & Col, Inc., UK.

Kraft, L. M., Cox, W. R., Verner, E. A. (1981), "Pile Load Tests: Cyclic Loads and Varying Load Rates", Journal of the *Geotechnical Engineering Division, Proceedings of the American Society of Civil Engineers*, ASCE, Vol.107, No. GT1, January, 1981.

Kraft, L. M., Forht, J. A., Amerasinghe, S.F. (1981), "Friction Capacity of Pile Driven into Clay", *Journal of the Geotechnical Engineering Division, Proceedings of the American Sociey of Civil Engineers*, ASCE, Vol.107, No. GT11, November, 1981.

Kriebel, D. L., Berek, E. P., Chakrabarti, S. K., and Waters, J. K. (1997). "Wave-Current Loading on a Shallow Water Caisson ; An Evaluation of the API Recommended Practice," Paper Submitted for Publication in the Journal of Waterway, Port, Coastal, and Ocean Engineering, American Society of Civil Engineers, Manuscript 0145938-WW, July, New York, NY.

Lok, T. M. and Pestana, J. M.(1996), "Numerical Modeling of the Seismic Response of Single Piles in a Soft Clay Deposit".

Matlock, H. and Foo, S. H. C. (1978), "Simulation of Lateral Pile Behavior Under Earthquake Motion", A Report to Chevron oil Field Research Company, La Habra, California, on Research Performed at the University of Texas at Austin, Department of Civil Engineering.

Matlock, H. (1970), "Correlation for Design of Laterally Loaded Piles in Soft Clay", *Proceedings of Offshore Technology Conference*, OTC 1204.

Matlock, H., Foo, S. H. C., "Axial analysis of piles using a hysteretic and degrading soil model", *Numerical methods in Offshore Piling* (1980).

Matlock, H., Foo, S. H. C., Tsai, C. F.(1979), *SPASM 8 , A Dynamic Beam-Column Program for Seismic Pile Analysis With Support Motion.*

Matlock, H. , Ingram, W. B. , Kelley, A. E. and Bogard, D(1980), "Field Tests of the Lateral-Load Behavior of Pile Groups in Soft Clay", *Proceedings of 12-th Offshore Technology Conference*, OTC 3871.

McCLelland Engineers, Inc., Geotechnical Consultants (1975), "Bottom Stability and Foundation Design Study , Block 109, West Delta Area", Report to Texaco Inc., November, New Orleans, LA.

McClelland Engineers, Inc. Geotechnical Consultants(1979), "Geotechnical Investigation Potroleos Mexicanos Boring AKAL-O Bay of Campeche", Report to Proyectos Marinos, S. C. Mexico City, Mexico. February, Houston, TX.

McClelland Engineers, Inc., Geotechnical Consultants(1978),"Bottom Stability and Foundation Disign Study Block 57, South Pass Area", *McClelland Engineers*, Volume II, New Orleans, LA.

McClelland Engineers, Inc., Geotechnical Consultants (1977), "Bottom Stability and Foundation Design Study , Block 57, South Pass Area", *McClellant Engineers*, Volume III, March, New Orleans, LA.

McClelland, B. and Focht, Jr. J. A. (1958), "Soil Modulus of Laterally Loaded Piles", Transactions, ASCE, Vol. 123, Paper No. 2954.

Meyer, P. L., Holmquist, D. V. And Matlock, H., "Computer Predictions for Axially-loaded Piles with Nonlinear Supports", *Proceedings of Offshore Technology Conference*(May, 1975), OTC 2186.

Molina, C. V., Modelado Del Comportamiento De Pilotes De Friccion Bajo Carga Axial Eststica y Ciclica. Tesis Presentada a la Division de Estudios de Posgado de la, Facultad de Ingenieria de la Universidad Nacional Autonoma de Mexico.

Mortazavi, M., and Bea, R.G. (1996), "Screening Methodologies for use in platform assessments and requalifications", final project report, Marine Technology and Management group, Dept. of Civil Engineering, University of California, Berkeley, Jan., 1996.

Oceanweather Inc. (1996a), "Final Report, Update of Meteorological and Oceanographic Hindcast Data and Normals and Extremes Bay of Campeche", Report to Brown and Root International Inc. Cos Cob, CT.

Oceanweather Inc. (1996b), "Final Report, Hurricane Roxanne/1996 Hindcast Study", Report to Brown and Root International Inc. Cos Cob, CT.

Oceanweather Inc. (1996c), "Interim Report Preliminary Estimate of Impact of Hurricane Roxanne on Bay of Campeche Metocean Extremes", Report to Brown and Root International Inc. Cos Cob, CT.

Poulos, H. G.(1981), "Cyclic Axial Response of Single Pile", Journal of the Geotechnical Engineering Division, *Proceedings of the American Society of Civil Engineers*, ASCE, Vol.107,No. GT1.

Prakash, V., Powell, G. H., Campbell, S., Drain-2DX Base Program Description and User Guide. Version 1.10, November 1993.

Prakash, V., Powell, G. H., Campbell, S., Inelastic Truss Bar Element (Type 01) For Drain-2DX (Element Description and User Guide), Version 1.10, December 1993.

Powell, G. H., Campbell, S., (1993), Drain-3DX Element Description and User Guide For Element Type 01, Type 04, Type 05, Type08, Type09, Type15,and Type17, Version 1.10.

Prakash, V., Powell, G. H., Campbell, S., (1993), Drain-3DX Base Program Description and User Guide, Version 1.10.

Quiros, G. W. , Asce, A. M. , Young, A. G., Pelletier, J. H. , Chan, J. H-C, "Shear Strength Interpretation For Gulf of Mexico Clays", *Offshore Engineering Practice*,

Reese, L. C. ,Cox, W. R.and Koop, F. D.(1974) , "Analysis of Laterally Loaded Piles in Sand", *Proceedings of 6-th Annual Offshore Technology Conference*, OTC 2080.

Ruiz, S. E., (1984), "Reliability Index for Offshore Subjected to Bending", *Structural Safety*, Vol. 2, 1984.

Ruiz, S. E., (1986), "Non-Dimensional Probabilistic Coefficients for Laterally Loaded Piles", *Structural Safety*, Vol. 4,1986.

Ruiz, S. E., "Uncertainty About p-y Curves for Piles in Soft Clay", *Journal of Geotechnical Engineering*, ASCE, Vol. 112, No. 6.

Schapery, R. A., and Dunlap, W A. (1977). "Wave-Sea Bottom Interaction Study," Texas engineering Experiment Station Technical Bulletin, Texas A & M University, College Station, TX.

Schapery, R. A., and Dunlap, W. A. (1978). "Prediction of Storm-Induced Sea Bottom Movement and platform Forces," *Proceedings of the Offshore Technology Conference*, OTC 3259, Society of Petroleum Engineers, Richardson, TX.

Singh, Gurdev, Lai, W. T. , Das, Braja, M.(1996), "Sensitivity of Probabilistic Pile Design to Various Uncertainties", *Proceedings of the Sixth-International Offshore and Polar Engineering Conference*, Los Angeles, May, 1996.

Shamsher Prakasher, Sanjeev Kumar(1996), "Analysis of Pile Supported Offshore Structures Under Wave Loading", *Proceedings of the Sixth-International Offshore and Polar Engineering Conference*, Los Angeles, May, 1996.

S. Narasimha Rao and V. G. S. T. Ramakrishna(1996), "Behavior of Laterally loaded Model Pile Group in Clay", *Proceedings of the Sixth-International Offshore and Polar Engineering Conference*, Los Angeles, May, 1996.

Stear, D. James, (1997) "Screening Methodologies for Use in Platform Assessments and Requalifications", Project Progress Report 9, Report to Project Sponsors, UC Berkeley, October 31, 1997.

Stear, D. James, Mortazavi, M., and Bea, R. G., (1996), "Manual of Operation, ULSLEA", Marine Technology and Management Group, Dept. of Civil and environmental Engineering, Unversity of California at Berkeley, January, 1996.

Suhayda, J. N. (1996). "Oceanographic Design Data for South Pass Area Block 47," *Proceedings of the Offshore Technology Conference*, OTC 7952, Society of Petroleum Engineers, Richardson, TX.

Suhayda, J. N., (1977). "Surface Waves and Bottom Sediment Response," Marine Slope Stability, *Marine Geotechnology*, Vol. 2, Crane, Russak & Co, Inc., UK.

Suhayda, J. N., (1997), "Wave/Sea Bottom Interaction Effects", Report to PEMEX and IMP and Brown and Root International Inc., July, 1997.

Sullivan, W. R., Reese, L. C. and Fenske, C. W.(1980), "Unified Method for Analysis of Laterally Loaded Piles on Clay", *Numerical Methods in Offshore Piling*, Institution of Civil Engineering's, London, England.

Sully, J. P., Paga, M., Bea, R., Gajardo, E., Gonzalez, R., and Fernandez, A. F., (1994), "Aspects of Pile Design for Cyclic and Dynamic Loading With Reference to API Conditions for Offshore Structures", *Proceedings International Conference on Design of Pile Foundations for Dynamic Loadings*, American Society of Civil Engineering, New York, NY.

Tang, W. H. (1988), "Offshore Axial Pile Design Reliability", Research Report for Project PRAC 86-298.

Tang, W., H and Gilbert, R., B.(1990), "Offshore Lateral Pile Design Reliability", Research Report to Project PRAC 87-29.

Tubman, M. W., and Suhayda, J. N., (1976). "Wave Action and Bottom Movements in Fine Sediments," *Proceedings 15th Coastal Engineering Conference*, Honolulu, American Society of Civil Engineers, New York, NY.

Wang, S. , Kuter, B. L. , Jacob Chacko, M. and Wilson, D. W.(1996), "Nonlinear Seismic Soil-Structure Interaction".

Yamamoto(1978),"Sea Bed Instability From Waves", *Proceedings of Offshore Technology Conference*, OTC 3262, Society of Petroleum Engineers, Richardson, TX.

Young, A. G., Quiros, G. W. and Ehlers, C. J.(1983), "Effects of Offshore Sampling and Testing on Undrained Soil Shear Strength", *Proceedings of Offshore Technology Conference*. OTC 4465.

Zhaohui Jin and Bea, R. G. (1997), "Analysis of Wave Attenuation in the Bay of Campeche", report to PEMEX and IMP, Marine Technology & Management Group, Dept. of Civil & Environmental Engineering, University of California at Berkeley, August 1997.

Zhaohui Jin and Bea, R. G. (1997), "Dynamic Response of a Single Pile to the lateral Loading", report to PEMEX and IMP, Marine Technology & Management Group, Dept. of Civil & Environmental Engineering, University of California at Berkeley, August 1997.

Zhaohui Jin and Bea, R. G. (1997), "Analysis of Wave Decay Characteristics", report to PEMEX and IMP, Marine Technology & Management Group, Dept. of Civil & Environmental Engineering, University of California at Berkeley, December 1997.

Zhaohui Jin and Bea, R. G. (1997), "Dynamic Lateral and Axial Loading Capacities of Piles in the Bay of Campeche", report to PEMEX and IMP, Marine Technology & Management Group, Dept. of Civil & Environmental Engineering, University of California at Berkeley, December 1997.